PERSONAL HAND-HELD COMMUNICATIONS VIA L-BAND CDMA-BASED GEOSTATIONARY BEAMFORMING SATELLITES

by

Joubin Karimi

A thesis submitted to the
Department of Electrical and Computer Engineering
in conformity with the requirements
for the degree of Master of Science (Engineering)

Queen's University
Kingston, Ontario, Canada
April 1996

Abstract

In recent years, the demand for wireless communications around the world has been phenomenal, as personal communications has become an integral part of modern life. In North America alone, the number of cellular users has already exceeded the projected numbers expected to be reached by the year 2000. Cellular systems, however, are not expected to provide services for rural and suburban areas due to the potentially fewer number of subscribers compared with urban areas. Satellite communications has therefore emerged as a viable solution for personal communications in areas with low population density. The future of personal mobile satellite communications services depends critically on achieving maximum rural and suburban coverage at minimum payload cost. The goal of this thesis is to investigate the feasiblilty of utilizing a CDMA-based, L-band, geostationary satellite to provide personal hand-held communications in sparsely populated areas.

To extend coverage of terrestrial cellular communication systems in the southern half of Canada, a CDMA-based geostationary satellite with on-board processing is proposed. The satellite transmits and receives signals at L-band frequencies. For compatibility with the terrestrial CDMA standard, the communication model is based on the IS-95 standard. Coast to coast coverage of the provinces is accomplished by five spot beams with each beam treated as a separate cell. The satellite employs two multiple-beam parabolic antennas of 8.3 and 6.7 meters in diameter for the uplink and downlink, respectively. The system uses a bandwidth of 4.9 MHz on each link. Handsets are assumed to perform at a no more than 600 mW average power. Due to the existence of a pilot channel on the downlink, the reception is assumed to

be coherent. For the uplink, however, both coherent and non-coherent cases are considered. For the non-coherent case, similar to IS-95, the uplink employs 64-ary orthogonal modulation. A soft-decision Viterbi decoding scheme is presented for the non-coherent receiver. Link budget analyses are performed and the maximum allowable number of simultaneous users in the system is determined for various cases. Due to the handset's antenna gain and power limitations, the uplink capacity is proven to be more difficult to improve than the downlink capacity.

The use of on-board array signal processing to improve the uplink performance is also investigated and a novel beamforming technique is introduced. The proposed approach involves on-board antenna array signal processing of multiple feeds in a parabolic reflector antenna. Knowledge of user location is not required; code division multiple access (CDMA) signaling provides an estimate of each mobile's steering vector. A new single-beam-per-user beamforming network is described that is able to provide nearly uniform Canadian coverage using only a five-element antenna array. It is shown that link margins are typically increased from a minimum requirement of 5.25 dB to around 7.5 dB in border areas compared to a conventional isolated beam system.

TO MY AUNTS AND THEIR FAMILIES
FOR THEIR FORTITUDE AND SACRIFICE

Acknowledgements

I would like to thank my thesis supervisors, Dr. Peter J. McLane and Dr. Steven D. Blostein, for their advice, help and encouragement, without which the accomplishment of this work would have been impossible. Tracey Nairn and Chris Bardon of the TRIO office are thanked for their assistance and help and for putting up with my unending requests. I am also grateful to the Communication Institute for Telecommunications Research for their financial support.

Special thanks to Mark Earnshaw for proofreading this thesis and for his generous help and assistance over the years.

Many thanks go to Oguz Sunay, David Pauluzzi, Xiaohong Wang, and Paul Wareham for their friendship and the aid they provided.

To my labmates and all my friends who made my experience at Queen's exciting and enjoyable.

Finally, to my parents and my brother for their loving support and encouragement throughout my life.

Contents

List of Tables

List of Figures

Summary of Notation

Abbreviations

AMSC - American Mobile Satellite Corporation

AWGN - additive white Gaussian noise

BER - bit error rate

BPSK - binary phase shift keying

CDMA - code division multiple access

cdf - cumulative distribution function

dB - decibel

deg. - degrees

DS - direct sequence

E{} - expected value

EIRP -equivalent isotropic radiated power

FCC - Federal Communications Commission

FDMA - frequency division multiple access

FH - frequency hopping

GEO - geostationary earth orbit

HPA - high power amplifier

IS-95 - terrestrial CDMA standard

LEO - low earth orbit

MEO - medium earth orbit

pdf - probability distribution function

PLMN - public land mobile network

PN - peusdo random

PSTN - public switched telephone network

Re{} - real part

RF - radio frequency

SINR - signal-to-interference-noise ratio

SNR - signal-to-noise ratio

SS - spread spectrum

TDM - time division multiplexing

TDMA - time division multiple access

TH - time hopping

Symbols, Variables, and Functions

α_n - angle between the direction of mobile movement and the incident wave

β - angle subtended by the satellite at two arbitrary users on earth

γ_s - polar angle describing the location of an arbitrary feed

$\Delta\lambda$ - difference in longitude between an arbitrary user at E and the subsatellite point

Γ - signal attenuation due to fading on the downlink

ϵ -distance of an arbitrary feed from the focal point of the parabola

η - total aperture efficiency

η_i - illumination efficiency

η_s - spillover efficiency

$\eta_\circ$ - losses due to antenna surface errors

$\theta_{3\text{dB}}$ - 3 dB beamwidth angle subtended by the reflector antenna

θ_b - angle an arbitrary user makes with the antenna beam boresight

θ_e - elevation angle of an arbitrary user at E

θ_i - angle an arbitrary signal incident upon the satellite makes with the z-axis

θ_n - angle the furthest beam boresight makes with the on-focus beam boresight

λ - signal wavelength

λ_d - downlink wavelength

λ_{in} - interleaving depth

λ_u - uplink wavelength

σ_N^2 - variance of the noise term N_j in the non-coherent receiver

σ_I^2 - variance of the interference term I_j in the non-coherent receiver

τ - dummy variable

τ_i - channel delay for the i^{th} user

$\tau_i^{(h)}$ - channel delay for the i^{th} user in beam (h)

ϕ_A - latitude of an arbitrary user at A

ϕ_B - latitude of an arbitrary user at B

ϕ_g - latitude of an arbitrary user at E

Ψ - signal attenuation due to fading on the uplink

A_{eff} - effective antenna area

A_i - array response vector for the i^{th} user

$A_i^{(n)}$ - phase component of the received electric field from the i^{th} user by feed (n)

$b_i(t)$ - modulating signal of the i^{th} user (uplink)

$b_j^k(t)$ - data symbol transmitted for user j in beam (k) (downlink)

B - signal bandwidth

B_u - beam deviation factor

$c_i(t)$ - i^{th} user PN code

$c^k(t)$ - PN code for users in beam (k) (downlink)

C - received carrier power

C_k - Rician fading channel gain

d_A - distance from the satellite to an arbitrary user at A

d_B - distance from the satellite to an arbitrary user at B

$d_i(t)$ - i^{th} user modulating signal

d_{TR} - distance between transmitting and receiving antennas

d_u - distance from the satellite to an arbitrary user at E

D - parent reflector diameter (offset paraboloid)

D_1 - reflector diameter

E - arbitrary user location

$E(\theta_i, \phi_i)$ - received antenna electric field as a function of the user location

$E_n(\theta_i, \phi_i)$ - normalized antenna electric field

E_b - energy per received data bit

E_f - effective aperture distribution

E_s - energy per data symbol

E_w - energy per Walsh symbol

f_H - frequency hop rate in FH-SS

$f_m(U_j)$ - pdf of the envelope detector output for the matched filter corresponding to the correct Walsh symbol

$f_{nm}(U_k)$ - pdf of the envelope detector output for the k^{th} matched filter not corresponding to the correct Walsh symbol

fad_{down} - fading margin on the downlink

fad_{up} - fading margin on the uplink

f_D - normalized Doppler frequency

f_s - data symbol rate

F_r - radiation pattern of a rotationally symmetric feed

F - focal length of the reflector

$g(\theta_b)$ - normalized far-field satellite antenna gain pattern

$G(\theta_b)$ - overall satellite antenna gain pattern

G_{max} - antenna gain in the direction of maximum radiation

G_{nu} - satellite antenna gain in the direction of the desired user by feed(n) (downlink)

G_u - user antenna gain

G_{un} - satellite antenna gain in the direction of the desired user by feed(n) (uplink)

G_T - transmitting antenna gain

G_R - receiving antenna gain

GL - loss in gain in the farthest beam

h - vertical distance between the focus of the parabola and the centre of the dish

$h_\circ$ - orbital altitude

$I_\circ$ - interference spectral density for the non-coherent receiver

$I^{(i)}$ - interference spectral density due to the i^{th} user

I_{down} - interference spectral density on the downlink

$I_{zb}()$ - 0th-order modified Bessel function

I_j - multiple access interference term for the j^{th} matched filter

I_L - $L \times L$ identity matrix

I_t - total interference spectral density

I_{up} - interference spectral density on the uplink

IN - total interference-noise spectral density

$J_1()$ - first order Bessel function

$J_2()$ - second order Bessel function

k - Boltzman's constant

K_s - receiver sampling index

K - K-factor

L - quantization level

L_{at} - atmospheric loss

$L_j(t)$ - Walsh code assigned to user j (downlink)

L_u - free space loss for an arbitrary user

m_i - desired signal term in v_i

M - total number of active users in the system

M_k - number of active users in beam (k)

M_s - number of Walsh symbols

MAI - multiple access interference term in the beamforming receiver

$n(t)$ - white Gaussian noise signal

n_v - thermal noise vector

N - number of spotbeams

$N_\circ$ - noise spectral density

N_j - thermal noise term for the j^{th} matched filter

$N(t)$ - complex representation of AWGN

$N(T_s)$ - thermal noise term in the beamforming receiver

P_i - received signal power from the i^{th} user

$P_i^{(h)}$ - power received from the i^{th} user by feed (h) (uplink)

$P_i^{(k)}$ - signal power received by the desired user i in beam (k) (downlink)

$P_{ij}^{(k)}$ - power intercepted by the user i, intended for user j in beam (k) (downlink)

P_M - probability of Walsh symbol error

P_{nu} - satellite output power for the desired user

P_s - desired signal power

P_T - transmitting antenna power

P_u - power transmitted by the desired user

q - constant that satisfies sidelobe requirements of the satellite antenna gain pattern

Q - multiple access interference plus noise term in the beamforming receiver

$r(t)$ - total received signal

$r^{(h)}(t)$ - total signal received by feed (h) (uplink)

$r_i(t)$ - received signal from the i^{th} user

$r_i^h(t)$ - total received signal by the desired user i in beam (h) (downlink)

R_A - receiving antenna

R_E - radius of the earth

R_{NI} - covariance matrix of Q

$R_{pn}(\tau)$ - PN code autocorrelation function evaluated at τ

$R_{v_1 v_1}$ - post-despreading covariance matrix for the desired user

$\hat{R}_{v_1 v_1}$ - estimate for $R_{v_1 v_1}$

R_{xx} - pre-despreading covariance matrix in the beamforming receiver

$\hat{R}_{xx}$ - estimate for R_{xx}

$s_i(t)$ - i^{th} user transmitter output

S_E - subsatellite point

SL - amount in dB by which the first sidelobe is below the maximum antenna gain

$\text{SINR}_{\text{down}}$ - received SINR on the downlink (no fading)

SINR_{fad} - received SINR (with fading)

SINR_{up} - received SINR on the uplink (no fading)

T - tilt angle at the satellite

T_A - transmitting antenna

T_b - data bit duration

T_c - PN code chip rate

T_i - noise temperature at the receiver input

T_s - data symbol duration (encoded data)

T_w - Walsh symbol duration

$u_b(t)$ - square pulse with unit magnitude and direction T_s

$u_c(t)$ - square pulse with unit magnitude and direction T_c

U_m - envelope detector output for the m^{th} matched filter

v_c - speed of light

v_i - input vector to the i^{th} user beamforming network

v_b - mobile speed

VA - voice activity factor

$w_\circ$ - carrier frequency

w_i - complex weight vector for the i^{th} user

W_M - m^{th} Walsh symbol

W_s - CDMA system bandwidth

$x_{k,opt}$ - k^{th} representation level in the Lloyd-max quantizer

$x(t)$ - total received signal by the beamforming receiver

$y_{k,opt}$ - k^{th} decision level in the Lloyd-max quantizer

z_i - receiver output for the i^{th} user

Chapter 1

Introduction

1.1 Introduction

In recent years, there has been a great interest in the provision of personal hand-held communications via satellites. After more than a quarter century of satellite communications development and operation, it is only recently that the inherent potential of satellites in mobile communications is unfolding. The ever growing mobility of people and the demands of modern life, both professional and personal, have prompted a need for personal communications for anyone, anywhere, at any time. This calls for advanced personal communication systems that go beyond cellular service. Cellular systems around the world predominantly serve highly populated areas and are not expected to provide coverage for rural areas. Meanwhile, the majority of Earth's population still lacks access to even basic telephone service; access it needs to develop socially and economically. Even in the United States it is estimated that 35% of the population would not be serviced by terrestrial cellular systems. Satellite-based mobile communications promises to provide convenient, effective and consistent personal hand-held communications. For the last five years, mobile satellite activities have exceeded those of the last thirty years. Much attention has been given to the design of global systems providing communications via hand-held terminals, and operating in both satellite and cellular modes to respond to the the growing demands for voice, message, paging and data communications.

Currently, satellite service for hand-held users is not available. However, there are two major providers of mobile satellite services. Inmarsat, with two geostationary (GEO) satellites, provides worldwide voice, data, telex, and facsimile services, and AMSC, with its long awaited GEO satellite MSAT, provides similar services for North America [51]. The potential market for personal hand-held communications via satellite systems has triggered several major proposals for global coverage [51]. The United States Federal Communications Commission (FCC) announced its licensing decision on Jan 31, 1995, regarding satellite systems geared for wireless personal communications systems. Of the six proposals submitted, the FCC selected the three following systems: Motorola's Iridium, Qualcomm's Globalstar, and TRW's Odyssey. While Iridium and Globalstar consist of constellations of satellites (66 and 48 respectively) in low earth orbits (LEO), Odyssey employs satellites (12) in medium earth orbits (MEO). Globalstar and Odyssey are alike in that both use code division multiple access (CDMA), whereas Iridium uses frequency division multiple access (FDMA) on the uplink and time division multiplexing (TDM) on the downlink. All three are promising to have satellites in service by the year 2000.

GEO satellites have been in use since early 1960s, and due to design maturity there is minimum technology risk involved as compared with LEO and MEO satellites. Also, in order to provide global coverage, only 3 GEO satellites are needed. This will eliminate complex tasks such as constellation control operation and satellite deployment. Since far fewer satellites are needed in a global GEO system, satellites can be built with on-board processing capabilities, thereby eliminating the need for ground operations for communications network management. A disadvantage with GEO is the large propagation delay due to the great orbit distance. The altitude of a GEO orbit is 35,786 km, compared to $<$ 1,500 km for LEO and between 5,000 km to 13,000 km for MEO. The path loss incurred on the signals due to this large distance significantly reduces the received power at both user and satellite. Another problem is the lack of coverage at far northern and southern latitudes, which suggests that the practical operating limits are latitudes below 75°.

As can be seen, LEO and MEO are the orbits of choice in the above proposed systems and have been the focus of numerous research and studies in recent years [24] [11] [15]. On the other hand, not much attention has been given to GEO satellites to provide hand-held communications, and this has motivated our study. The goal of this thesis is to investigate the feasibility of utilizing a CDMA-based geostationary satellite to provide hand-held communications for users in rural and suburban areas in the southern half of Canada. The southern half of Canada was chosen since at higher latitudes geostationary satellites will not be able to provide consistent service due to lower elevation angles. In this study, only voice communications is being investigated. CDMA has been chosen in order for the system to be compatible with the existing terrestrial IS-95 standard for dual mode operation [19]. The handset envisioned will first attempt to provide connection through existing terrestrial service. If such service is absent or interrupted, the handset will link the subscriber directly to the satellite. Most of the users are expected to be in rural areas since cellular service is available in almost all urban areas in Canada. L-band frequencies have been considered for both user-to-satellite (uplink) and satellite-to-user (downlink) links. The space segment consists of an on-board processing GEO satellite equipped with two reflector antennas, one for uplink and one for downlink. Link budget analyses are performed to investigate the system capacity for 4.9 MHz and 9.8 MHz system bandwidths. Finally, on-board satellite digital beamforming is investigated to provide interference cancellation on the uplink and improve the system performance.

1.2 Summary of Contributions

This thesis makes the following contributions:

1. A CDMA-based L-band geostationary satellite system is proposed to provide personal communications via hand-held terminals for users in the southern half of Canada. This involves the design of two reflector antennas, a link budget analysis, capacity estimations, and an overall performance evaluation for users

in various parts of the coverage area.

2. Coherent and non-coherent uplink receivers are compared, and a new soft-decision Viterbi decoding technique for the non-coherent receiver employing 64-ary orthogonal modulation is introduced. It has recently come to our attention that a similar decoding scheme with similar results appeared in a recent issue of the *IEEE Transactions on Communications* [5].

3. A novel beamforming technique is proposed which involves antenna array signal processing of multiple feeds in a parabolic reflector and provides performance improvement through interference cancellation. We have shown that for satellite communications, the approach to antenna array processing must be adapted from terrestrial cellular systems which employ omni-directional antennas [35].

1.3 Thesis Outline

In Chapter 2, background material on spread spectrum communications, satellite link budget analysis, earth-satellite geometry and reflector antenna design is presented. In Chapter 3, the system communication model is presented. Reflector antennas are designed and the system coverage area is defined. Coherent demodulation is assumed for both uplink and downlink receivers. The system capacity is determined for a CDMA bandwidth of 4.9 MHz. A possible CDMA/FDMA system with a bandwidth of 9.8 MHz is investigated and compared with a CDMA system of 9.8 MHz bandwidth. System performance over AWGN and Rician fading channels for users in the coverage area is determined through a link budget analysis and computer simulations. In Chapter 4, a non-coherent uplink transmission for the system presented in Chapter 3 is considered. The uplink employs 64-ary orthogonal modulation. Hard-decision Viterbi decoding is compared with a new soft-decision Viterbi decoding scheme, and the system performance in AWGN and Rician fading scenarios is discussed. In Chapter 5, adaptive array signal processing is added to the uplink reflector antenna designed in Chapter 3, and the coherent uplink system performance is re-evaluated. System

performance for both an optimum and a sub-optimum beamforming technique is determined and compared with that of the non-beamforming receiver. Performance results are obtained for uniform and non-uniform user distributions in the coverage area. In Chapter 5, a more accurate approximation, as compared to Chapters 3 and 4, is used to determine the received signal-to-interference-noise ratio. Finally, in Chapter 6 a summary of results in the previous sections is presented and a few suggestions for future work are given.

Chapter 2

Background

2.1 Introduction

This chapter gives a brief review of the basic equations and principles used in this thesis. In Section 2.2, the spread spectrum concept and the multiple access technique used are reviewed. In Section 2.3 the satellite link budget analysis is described. Section 2.4 gives relevant earth-satellite geometry, and finally, Section 2.5 discusses satellite antenna design and performance.

2.2 Spread Spectrum

It was in the mid-1950s that the first spread spectrum (SS) systems were developed. In those days, however, spread spectrum technology was dedicated solely to military applications. Spread spectrum was of interest due to its antijamming capabilities and low probability of interception by the unintended user. In recent years, spread spectrum has received a significant amount of attention for its commercial applications [12][21]. Much of the research has been devoted to the study of spread spectrum multiple access techniques for use in personal communication systems. In Section 2.2.1, the basic principles and theory behind spread spectrum are discussed. Sections 2.2.2 and 2.2.3 describe the *direct sequence* signal spreading and the *code division multiple access* techniques respectively.

2.2.1 Spread Spectrum Theory

Spread spectrum communication is signified by a transmission that occupies a significantly larger bandwidth than the minimum required for the transmission of the baseband signal itself. In other words, a signal with a bandwidth of B is transmitted in a bandwidth W_s which is much larger than B. The increase in bandwidth is accomplished by modulating the signal by a larger bandwidth pseudo-random code with a flat spectrum, which is independent of the data signal. Considering that the total power transmitted by the spread spectrum signal is equal to the original data signal power, the power spectral density of the spread spectrum signal would be B/W_s of that of the original signal. Thus, the power is spread over a large bandwidth, and this makes the SS signal appear as random noise to the other signals in the same band.

Some of the advantages of spread spectrum are listed below.

- Service can be provided to multiple users sharing the same frequency and time slots in a channel.
- It is difficult for an unauthorized user to detect the presence of the signal.
- The effects of intentional jamming can be significantly reduced.
- The detrimental effects of multipath fading can be reduced.

There are 3 popular signal spreading schemes:

- Direct Sequence (DS-SS)
- Frequency Hopping (FH-SS)
- Time Hopping (TH-SS)

In direct sequence spreading, the information-bearing signal is modulated by standard techniques and then is multiplied by a higher frequency pseudo-random code (PN). Direct sequence spreading is described in further detail in Section 2.2.2. In

frequency hopping, the centre frequency of the modulated signal is changed every T_H seconds resulting in a hop rate of $f_H = 1/T_H$ hops/s. The frequency hopping pattern is driven using a pseudo-random code. Finally, in the time hopping spread spectrum, bursts of signals are initiated at pseudo-random times. In all of the above schemes, the spread spectrum signals appear as wideband noise to other users.

A PN code consists of a sequence of 1's and -1's (or zeros) called chips, which exhibit certain statistical properties [36] [41]. Pseudo-random codes are periodic, where a period is defined by the number of chips contained in one complete symbol duration. The codes are generated with very long periods and are difficult to reconstruct from a short segment. The autocorrelation function of a long PN sequence evaluated at τ can be approximated by [46]:

$$R_{pn}(\tau) = \begin{cases} 1 - \frac{|\tau|}{T_c} & |\tau| \leq T_c \\ 0 & \text{elsewhere} \end{cases} \tag{2.1}$$

where T_c is the chip duration.

Among the three spreading techniques, direct sequence is most widely used in personal communication systems. Section 2.2.2 describes DS-SS in further detail.

2.2.2 Direct Sequence Spread Spectrum

In this section, we review and analyze a simple DS-SS transmitter and receiver model.

2.2.2.1 DS Transmitter

Figure 2.1 shows a basic DS-SS transmitter model. The output of the transmitter for user i is given by

$$s_i(t) = \sqrt{2P_i}\, d_i(t) c_i(t) \cos w_o t \tag{2.2}$$

where $d_i(t)$ is the data modulation signal of duration T_b, $c_i(t)$ is the PN sequence with a chip duration of T_c (where $T_b \gg T_c$), P_i is the signal power, and w_o is the carrier frequency. Binary phase shift keying is used for $d_i(t)$. For simplicity, all data bits

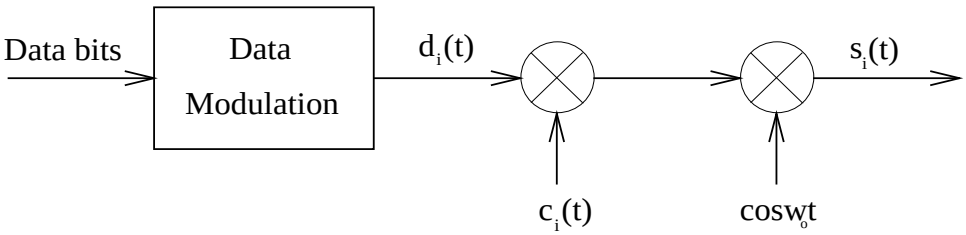

Figure 2.1: DS-SS Transmitter for User i

and chips are assumed to be rectangular pulses. Since the output signal has a wide bandwidth of $1/T_c$, the signal appears only as weak background noise to the other users. The information can only be recovered if the transmitted signal is matched filtered by the same PN sequence at the receiver, which is explained in the following section.

2.2.2.2 DS Receiver

A simple DS-SS receiver is shown in Figure 2.2. The received signal $r_i(t)$ is given by

$$r_i(t) \quad = \quad s_i(t - \tau_i) + n(t) \tag{2.3}$$

where τ_i is the path delay and $n(t)$ is the white Gaussian noise with zero mean and a single-sided spectral density of N_o. In order for the receiver to optimally despread the incoming signal, it must multiply the received signal by the exact PN code used in the transmission. This may not be a simple task, since the receiver is unaware of the phase of the incoming PN sequence with respect to its own clock. Therefore, it must synchronize the locally generated PN sequence to that of the received signal. Numerous studies on the DS-SS synchronization problem have introduced a variety of synchronization techniques [39][42][17]. Most synchronization techniques are a variation of either the serial search or matched filter acquisition techniques. Assuming perfect synchronization and coherent demodulation, the signal-to-noise ratio (SNR) at the output of the matched filter is given by $2E_b/N_o$, where E_b is the energy per bit of the transmitted data signal. The complete derivation is provided in Appendix A. The SNR calculated here is the same as the SNR obtained from a standard BPSK

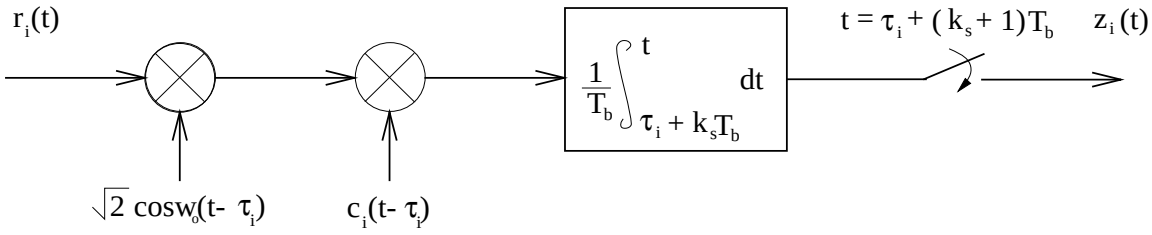

Figure 2.2: DS-SS Receiver

transmission. For commercial applications, it is costly to use a wide bandwidth for transmitting only one signal and yet perform with the same probability of error as a standard BPSK transmission. This can be overcome by allowing multiple users to share the same channel. This technique is referred to as Code Division Multiple Access (CDMA), wherein each user is given its own unique code used for spreading. This technique is further described in Section 2.2.3.

2.2.3 Code Division Multiple Access Technique

Multiple access schemes provide the means by which multiple users can establish communication. The two most common multiple access techniques in current use are Frequency Division Multiple Access (FDMA) and Time Division Multiple Access (TDMA). In FDMA, users can transmit simultaneously on separate designated frequencies. In TDMA, all users occupy the same frequency band, but transmit in sequential time slots. CDMA combines FDMA and TDMA in the sense that all users can transmit at the same time and occupy the same frequency band.

In CDMA, each user is given its own spreading code. The codes can either be orthogonal (e.g. Walsh codes) or instead have very small crosscorrelations (long PN codes). To demonstrate the operation of CDMA, assume we have a system with M active users, where each user uses a separate long code for spreading. Referring to Figures 2.1 and 2.2, $d_i(t)$, and $c_i(t)$ are the modulating signal and spreading code of the i^{th} user respectively, k_s is the sampling index, and τ_i is the delay introduced by the channel for the i^{th} user. All data symbols and PN chips are assumed to be rectangular

pulses. Data is BPSK modulated. The total signal detected by the receiver can be written as

$$r(t) \;=\; \sum_{i=1}^{M} s_i(t-\tau_i) + n(t) \tag{2.4}$$

where $s_i(t) = \sqrt{2P_i}c_i(t)d_i(t)\cos w_o t$. P_i is the power received from the i^{th} user. Assuming that the desired user is at $i = 1$, τ_1 can be set to zero with no loss of generality. With perfect self-synchronization and coherent demodulation, the output of the receiver for the user of interest can be written as

$$\begin{aligned} z_1(t=T_b) &= \frac{\sqrt{2}}{T_b}\int_0^{T_b}\sum_{i=1}^{M}\sqrt{2P_i}c_i(t-\tau_i)d_i(t-\tau_i)\cos w_o(t-\tau_i)c_1(t)\cos(w_o t) \\ &\quad + \frac{\sqrt{2}}{T_b}\int_0^{T_b} n(t)c_1(t)\cos w_o t\; dt \\ &= \int_0^{T_b}\frac{2\sqrt{P_1}}{T_b}d_1(t)\cos^2 w_o t + I + N \end{aligned} \tag{2.5}$$

This can be written as

$$z_1 \;=\; d_1(t)\sqrt{P_1} \;+\; I \;+ N \tag{2.6}$$

where I and N are given by the following equations

$$I \;=\; \frac{1}{T_b}\sum_{i=2}^{M}\int_0^{T_b}\sqrt{P_i}d_i(t-\tau_i)c_i(t-\tau_i)c_1(t)\cos w_o(\tau_i)\; dt \tag{2.7}$$

$$N \;=\; \frac{\sqrt{2}}{T_b}\int_0^{T_b} n(t)c_1(t)\cos w_o(t)\; dt \tag{2.8}$$

The first term in (2.6) is the desired signal, and I and N are the interference due to other users and thermal noise respectively. As can be seen, the signal transmitted by the user at $i = 1$ was despread, while signals from all other users were further spread with the $c_1(t)$ code, and are contained in the interference term, I.

CDMA networks can be operated in synchronous or asynchronous modes. In a synchronous system, the transition of the PN chips and data symbols of all users coincide. In an asynchronous system, however, the transition times are not adjusted to coincide. The ultimate goal in improving multiple access techniques is to increase system capacity. System capacity refers to the maximum allowable number of users

that can simultaneously communicate in the system. In Section 2.2.3.1, a simple approximation for calculating the capacity of a coherent asynchronous CDMA system is given. Section 2.2.3.2 gives a brief overview of IS-95, which is the cellular CDMA standard for North America [19].

2.2.3.1 CDMA Capacity Approximation

Numerous studies have been performed on CDMA to determine the system capacity for various conditions and system configurations [6][46][25]. The approximation described below is used by Gilhousen *et al.* in [13].

This approximation assumes that all users communicate via a common carrier frequency channel and are spread using long PN codes. The transmission is assumed to be asynchronous and the data is BPSK modulated. Perfect self-synchronization and coherent reception is assumed. As described earlier, in CDMA the power received from all users other than the desired user appears as background noise after despreading in the receiver. If the user of interest is at $i = 1$, the equivalent one-sided interference spectral density due to the i^{th} user is given by $I^{(i)} = P_i/W_s$, where W_s is the spread spectrum bandwidth. The total interference spectral density is therefore given by

$$I_t = \sum_{i=2}^{M} I^{(i)} \tag{2.9}$$

where M is the total number of users. Considering a single-sided thermal noise spectral density of N_o in the receiver, the total interference-noise spectral density IN is given by

$$IN = N_o + I_t \tag{2.10}$$

The signal-to-interference-noise ratio (SINR) can therefore be written as

$$SINR = \frac{2P_1T_b}{N_o + I_t} = \frac{2E_b}{N_o + I_t} \tag{2.11}$$

where E_b is the received bit energy. The derivation above assumes that all interferers are transmitting continuously. Studies have shown that in a two-way conversation,

each user on average speaks only 35% to 40% of the time [14]. Since the user who is not speaking does not contribute to the system self-noise, an improvement in capacity is achieved. In this way, the co-channel self-interference I_o in (2.11) would be reduced by the voice activity factor VA. Therefore, the SINR can now be written as

$$SINR = \frac{2E_b}{N_o + \frac{VA}{W_s}\sum_{i=2}^{M} P_i} \tag{2.12}$$

From (2.12) it is clear that CDMA's performance is limited by co-channel interference. Thus, an increase in the number of users results in a degradation of performance, or a prescribed level of performance limits the number of active users.

2.2.3.2 IS-95 Overview

In June 1989, the use of DS-CDMA technology was proposed by Qualcomm Inc. to replace the existing analog cellular systems. The DS-CDMA digital cellular system became a North American standard known as IS-95 in 1993. In IS-95, data is transmitted at a maximum rate of 9600 bps and signals are spread by PN codes of rate 1.2288 mega chips/s. Knowledge of IS-95 is important since the CDMA system introduced in this thesis is inspired by the IS-95 standard. The following gives a brief review of the downlink and uplink traffic channels implemented in IS-95 [19] [40].

On the downlink (base-to-mobile), the information bits are encoded by a rate 1/2, constraint length 9 convolutional code and are then BPSK modulated. Each signal is multiplied by one of 64 different orthogonal codes (Walsh codes) assigned to each user. Walsh codes are 64 chips long and ensure orthogonality for all users in a given cell. Signals are quadriphase spread using a quadrature pair of PN codes of rate 1.2288 M chips/s. Each base station transmits a pilot signal which is not data modulated and is assigned the zero Walsh function. This signal provides a coherent reference for the users. The downlink traffic channel is synchronous and is coherently demodulated by the receiver.

On the uplink (mobile-to-base), the information bits are convolutionally encoded using a rate 1/3 code of constraint length 9. The uplink channel uses 64-ary orthogonal modulation with noncoherent demodulation at the receiver. Here, the encoded

bits are grouped in sets of six to form symbol groups or codewords. These codewords are used to select one of the 64 different orthogonal Walsh functions for transmission. The result is then combined with a long code and is quadriphase spread. It should be noted that in the downlink channel, Walsh codes are used to provide isolation, whereas in the uplink they are determined by the information symbols and are employed for orthogonal, coded modulation.

2.3 Link Budget Analysis

In satellite communications, the performance of the RF link is determined through an analysis called the link budget. The RF link is divided into two parts, the uplink and the downlink. Uplink is the link from the user, or earth-station, to the satellite and downlink is the link from the satellite to the receiving user, or earth-station.

The objective of the link budget analysis is to determine the available carrier power to noise density ratio (C/N_o) at the input of the receivers. The ratio C/N_o is a very important parameter for satellite engineers, since it is closely related to the ratio of energy per received data bit to noise density (E_b/N_o). This quantity is found by dividing C/N_o by the the data rate. The ratio C/N_o strongly depends on the characteristics of the transmitters and receivers, the propagation medium, and possible interference. Therefore, the antenna characteristics such as gain, transmitted power and input noise temperature play an important role in the link analysis.

The parameters in the link budget are usually set out in tabular form in decibels. This allows the system engineers to adjust various parameters such as transmitted power, beamwidth, or antenna gain, and quickly recalculate C/N_o. The analysis can be divided into 3 parts.

1. The received carrier power, C

2. The noise spectral density, N_o

3. The overall C/N_o

These parts are described in the following sections.

2.3.1 Received Carrier Power

The calculation of power received by a user terminal from a satellite or vice versa is a fundamental part of the link analysis. Consider a transmitting antenna T_A and a receiving antenna R_A separated by a distance d_{TR}. The power radiated per unit solid angle by the transmitting antenna fed by a source of power P_T is given by [30]

$$\frac{G_T P_T}{4\pi} \quad \text{(W/Steradian)} \tag{2.13}$$

where G_T is the antenna gain in the direction of interest. The product $G_T P_T$ in the link budget is frequently referred to as *equivalent isotropic radiated power* or EIRP. The signal power intercepted by the receiver with an antenna of effective area A_{eff} can be written as [30]

$$\phi = \frac{G_T P_T}{4\pi} \times \frac{A_{eff}}{d_{TR}^2} \quad \text{(W)} \tag{2.14}$$

where A_{eff} is given by

$$A_{eff} = \frac{\lambda^2 G_R}{4\pi} \quad \text{(W)} \tag{2.15}$$

where λ is the wavelength of the signal, and G_R is the receiving antenna gain in the direction of the incident signal. Carrier power can hence be written as

$$C = \frac{P_T G_T G_R}{L_u} \quad \text{(W)} \tag{2.16}$$

where $L_u = (4\pi d_{TR}/\lambda)^2$ and is referred to as the free space loss. The loss strongly depends on the carrier frequency. The higher the carrier frequency, the greater the loss.

In practice, the signals are attenuated in the atmosphere due to the presence of gaseous components and water. The overall effect can be taken into consideration by replacing L_u in (2.16) by a general expression for losses L_g, where $L_g = L_u L_{at}$, and L_{at} is the atmospheric attenuation.

It should be noted that since most satellite systems use either frequency or phase modulation techniques, the received power P_R is commonly referred to as carrier power C.

2.3.2 Noise Spectral Density

To determine the performance of a receiver, it is essential to find the total thermal noise against which the signal must be demodulated. The noise spectral density is given by [31]

$$N_o = kT_i \quad (\mathrm{W/Hz}) \tag{2.17}$$

where k is the Boltzman's constant, and T_i is the noise temperature at the receiver input. The equivalent input noise temperature is the temperature of a 1 Ω resistance which, if placed at the input of the element assumed to be noise free, establishes the equivalent available noise power at the output.

In satellite communications, large distances are involved and the signals received by the terminals or satellite are very weak. Consequently, to ensure that the best carrier-to-noise ratio is achieved, the noise at the receivers has to be reduced as much as possible. In satellites and earth-stations, various techniques are used to decrease the equivalent noise bandwidth and to keep the input noise as low as possible. In commercial handsets, however, only so much can be done since the cost of implementation and maintenance may be too high. Typical values for the input noise temperature of satellites and handsets range from 450° to 600° K and 150° to 300° K respectively.

2.3.3 Overall (C/N_o)

From (2.16) and (2.17) C/N_o can be written as

$$\frac{C}{N_o} = \frac{P_T G_T}{L_g k}\left(\frac{G_R}{T_i}\right) \quad (Hz) \tag{2.18}$$

where, on the uplink P_T and G_T refer to the handset terminal, and G_R and T_i represent the antenna gain and the input noise temperature of the satellite respectively.

Similarly, on the downlink P_T and G_T are satellite parameters, and G_R and T_i are those of the handset.

2.4 Earth-Satellite Geometry

Knowledge of earth-satellite geometry is required for a variety of tasks in the link budget calculations. This includes determination of the satellite antenna beam coverage, calculation of free space loss, and calculation of multiple access interference. These calculations become very important for geostationary (GEO) satellites, where in many cases the satellite has to support users located at high latitudes.

The most important aspect of a GEO satellite is that it remains fixed relative to an observer on earth at all times. The GEO satellites have an orbital altitude of 35,786 km above the equator. Figure 2.3 shows basic earth-satellite geometry. The satellite is positioned at point P_s, and an arbitrary user on earth is located at E. The parameters of interest are:

ϕ_g = latitude of the user at E

$\Delta\lambda$ = difference in longitude between E and the subsatellite point S_E (a point on the equator directly below the satellite)

T = tilt angle at the satellite

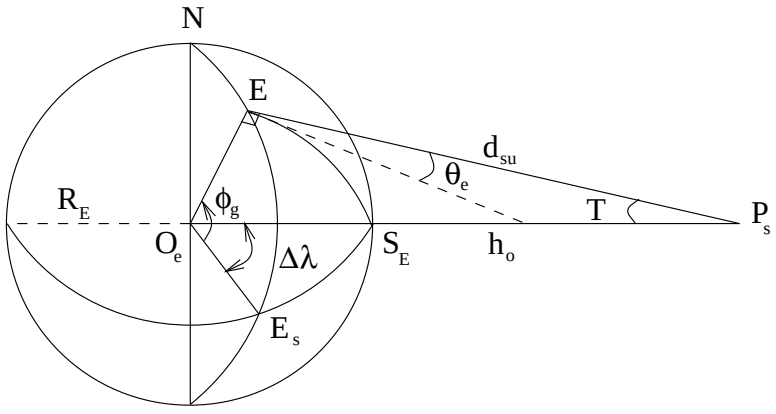

Figure 2.3: Basic Earth-Satellite Geometry

θ_e = elevation angle of the user

d_{su} = distance from the satellite to the user

R_E=radius of the earth (6,378 km)

h_o=orbital altitude from the satellite (35,786 km)

In Figure 2.3, $\Delta\lambda$ is taken to be positive if the user is to the west of the satellite. The parameters d_{su}, T, and θ_e can be determined if the positions of the satellite and user are known. These parameters are given by the following equations [37]:

$$d_{su} = \sqrt{h_o^2 + 2R_E(R_E + h_o)(1 - \cos\phi_g \cos\Delta\lambda)} \tag{2.19}$$

$$\theta_e = \arccos\left(R_E + h_o\sqrt{\frac{1 - \cos^2_{\phi_g}\cos^2_{\Delta\lambda}}{h_o^2 + 2R_E(R_E + h_o)(1 - \cos\phi_g \cos\Delta\lambda)}}\right) \tag{2.20}$$

$$T = \arcsin(\frac{R_E \cos\theta_e}{R_E + h_o}) \tag{2.21}$$

To determine the beam footprint corresponding to the 3 dB antenna gain contour of any circular spot beam (3 dB contour), three variables must be known.

(1) The position of the satellite in orbit,

(2) the direction of the beam boresight, and

(3) the 3 dB beamwidth of the projected beam.

Beam footprints can be determined by finding the intersection of the earth with the cone corresponding to the 3 dB antenna gain of the projected beam. To do this, the angle subtended by the satellite at any two given positions on earth must be known. Figure 2.4 shows two users at points A and B. Assume that users A and B are at latitudes ϕ_A and ϕ_B respectively, and are separated by longitude $\Delta\lambda_{AB}$ (not shown in the figure). The GEO satellite is at P_s and subtends an angle β at the two points. The angle β is related to A and B by the following equation [37]

$$\beta = \arccos\left(\frac{d_A^2 + d_B^2 - p^2}{2d_A d_B}\right) \tag{2.22}$$

where d_A and d_B are found using (2.19) and p is given by

$$p = 2R_E \sin(\chi/2) \tag{2.23}$$

where

$$\chi = \arccos(\sin\phi_A \sin\phi_B + \cos\phi_A \cos\phi_B \cos\Delta\lambda_{AB}) \tag{2.24}$$

To determine the 3 dB contour, B and β are assumed to be the location of the centre of the beam and the half-beamwidth respectively. The points on the beam border are therefore found by finding the solutions to ϕ_A and λ_{AB} in equation (2.22). Clearly, the 3 dB beam border is defined by an infinite number of points and solving equation (2.22) results in infinite number of solutions. However, in order to plot the 3 dB contour to determine the boundaries only a limited number of solutions are sufficient (e.g. 500 points end to end).

2.5 Satellite Antenna Theory and Design

In recent years, growing demands on satellite communications have led to stringent demands on satellite antennas. In the case of GEO satellites, where the distance between the satellite and terrestrial users is in the vicinity of 40,000 km, systems are noise limited and antennas with significantly large gains are required. In a multiple

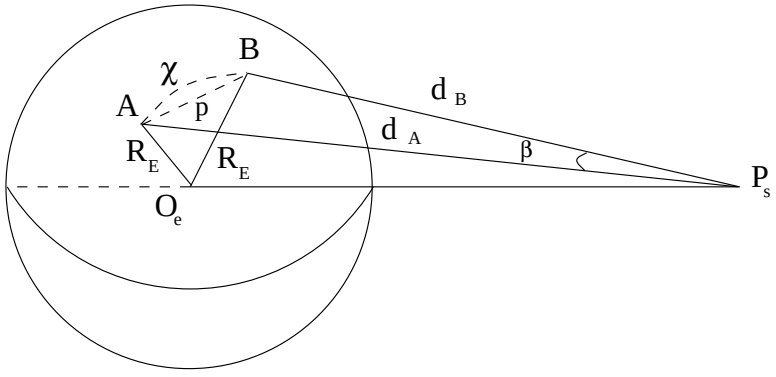

Figure 2.4: Geometry of Two Points with Respect to the Satellite

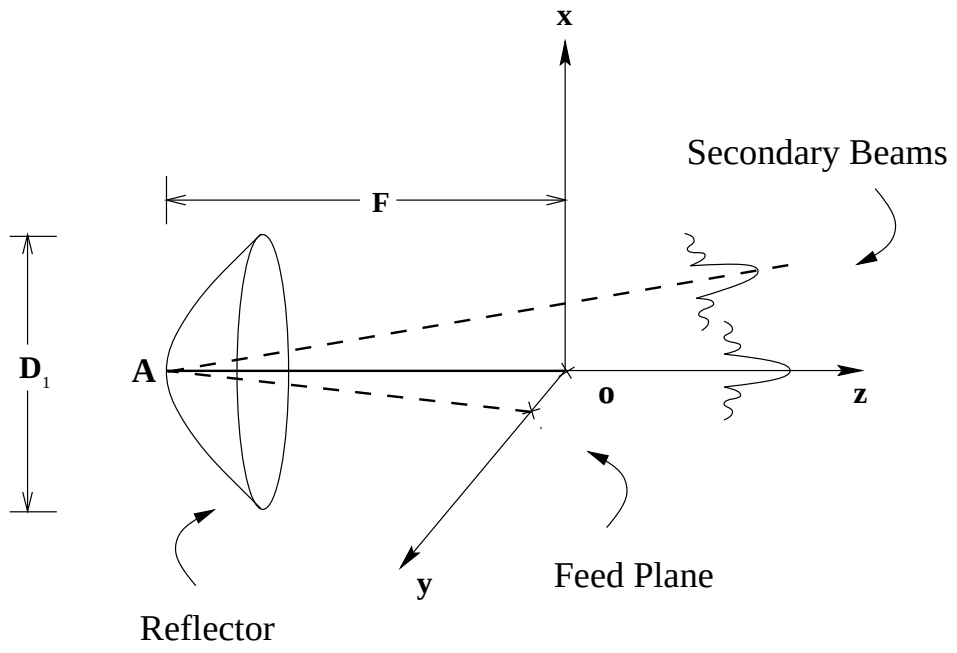

Figure 2.5: Zero-Offset Parabolic Reflector

access environment, the requirements on the gain and sidelobes become more stringent. These requirements have a direct impact on the size of the antenna. At the same time, the design constraints imposed by the available technology on the size, shape, weight, and power are important factors and must be taken into consideration.

Reflector antennas are the most popular satellite antennas and are widely used in multiple beam applications. Reflectors are suitable due to their structural simplicity, light weight, and design maturity. The reflector surface can take the form of a paraboloid, hyperboloid, ellipsoid, spheroid, or other general shapes. Parabolic reflectors are the most widely used antennas in today's multibeam antenna systems. The geometry of a parabolic reflector is shown in Figure 2.5, where D_1 is the reflector diameter, F is the focal length of the paraboloid, and xy is the plane of feed. The paraboloid equation is given by [27]

$$Z = \frac{x^2 + y^2}{4F} - F \tag{2.25}$$

The drawback in using such antennas is feed blockage, especially for the multibeam applications. To overcome blockage effects, offset parabolic reflectors are frequently

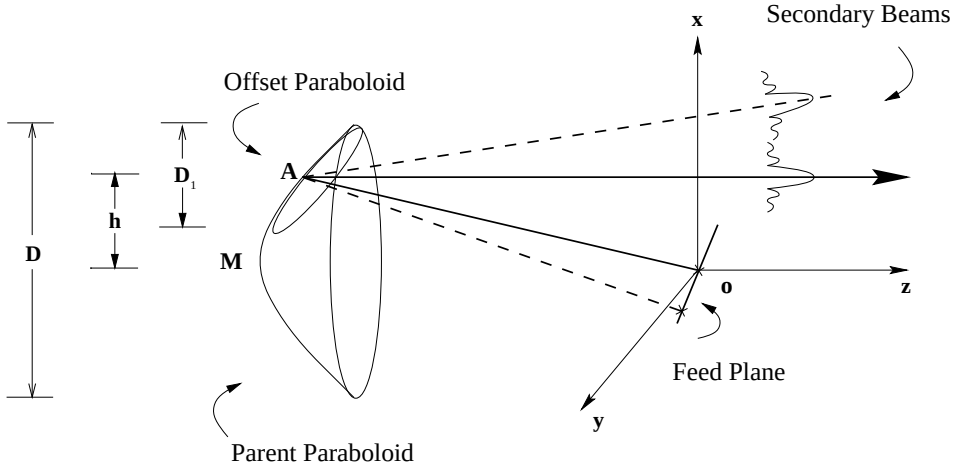

Figure 2.6: Offset Parabolic Reflector with Circular Aperture

used in satellite communication systems. The geometry of an offset parabolic reflector is shown in Figure 2.6. The offset reflector is the portion of the parent paraboloid carved out by a cylinder of diameter D_1. The same notation is used as for the reflector diameter of the zero-offset antenna (Figure 2.5), since antenna design formulas given later on apply to both types of reflectors. The optimum plane of feed is a plane passing through the focus (origin) and is normal to the line OA. This plane was found to be optimum since the feeds on this plane experience the least amount of phase distortion compared to feeds on any other plane [32]. Both offset and zero-offset designs have been investigated and are compared in this thesis.

The satellite antennas should be designed to meet a given set of desired performance parameters and specifications. These specifications can, for example, be the 3 dB gain beamwidth, the sidelobe level of the far-field pattern, and the total number of beams needed to provide coverage for the area of interest. Simple formulas and equations can be used to determine the reflector configuration for both offset and zero-offset reflectors [27]. Once the reflector geometry is determined, the far-field patterns can be found.

2.5.1 Antenna Design and Configuration

A systematic procedure based on simple formulas is presented here to determine the antenna configurations for both offset and zero-offset cases [27].

2.5.1.1 Feed Specifications

The placement of the feeds on the feed plane is determined by the desired direction of the maximum power in the beam projected by each given feed. When a feed is displaced from the reflector focus, O in Figures 2.5 and 2.6, the effective aperture electric field distribution experiences phase variation, which in turn gives rise to beam pattern distortion. The distortion is not, however, significant for small displacements. The feeds can be horn or microstrip antennas with a rotationally symmetric radiation pattern described by the following [27]

$$g(\gamma) = \cos(\gamma)^q \tag{2.26}$$

where γ is the polar angle measured from the line OA in Figure 2.6, and q is a constant that satisfies sidelobe requirements, and is given by

$$q = \frac{\log(1-\Delta)}{\log(\cos(\frac{\Omega_2-\Omega_1}{2}))} \tag{2.27}$$

with Ω_1 and Ω_2 being given by the following equations:

$$\Omega_1 = \arctan\left\{\left(\frac{h-D_1/2}{F}\right)\left[1-\frac{1}{4}(\frac{h-D_1/2}{F})^2\right]^{-1}\right\} \tag{2.28}$$

$$\Omega_2 = \arctan\left\{\left(\frac{D}{2F}\right)\left[1-\frac{1}{4}\left(\frac{D}{2F}\right)^2\right]^{-1}\right\} \tag{2.29}$$

In (2.27), Δ is given by [27]

$$\Delta = \sum_{n=0}^{3}\alpha_n\left(\frac{SL}{10}\right)^n \tag{2.30}$$

where $\alpha_0 = -8.87$, $\alpha_1 = 9.32$, $\alpha_2 = -3$, $\alpha_3 = .32$, and SL is the amount in dB (+ve) by which the first sidelobe is below the maximum gain.

2.5.1.2 Reflector Diameter

The reflector diameter D_1 in Figures 2.5 and 2.6 is given by [27]

$$D_1 = \frac{\lambda}{\pi \sin(\theta_{3dB}/2)} \sum_{n=0}^{3} \gamma_n(\Delta)^n \tag{2.31}$$

where $\gamma_0 = -8.87$, $\gamma_1 = 9.32$, $\gamma_2 = -3$, $\gamma_3 = .32$. In (2.31) λ is the wavelength, and θ_{3dB} is the 3 dB beamwidth.

Due to beam pattern distortion resulted from feed displacements, the maximum number of beams scanned is limited to a few beams. The aberrations represent themselves as losses in the peak gain and degradation in the general beam shape. Distortions are more significant in the offset paraboloid shown in Figure 2.6, where the degradation strongly depends on the F/D and θ_n/θ_{3dB} ratios where in the second ratio, θ_n is the angle that the furthest beam boresight makes with the on-focus beam boresight. The loss in gain in the furthest beam can be estimated by [27]

$$GL = 5\left\{ 1 - \cos\frac{2\pi(\theta_n/\theta_{3dB})}{190 k_e (F/D)} \right\} \quad \text{in dB} \tag{2.32}$$

where $k_e = 1 - \exp(-.12\sqrt{D_1/\lambda})$. The F/D ratio can be chosen such that GL is very small. It has been shown that for $F/D > 1$ and a small number of beams scanned (e.g. 5), the degradation in the furthest beam shape will be small [30].

2.5.1.3 Maximum Antenna Gain

The importance of the knowledge of the satellite antenna gain in link budget calculations is already described in Section 2.3.1. The gain of an antenna is the ratio of the power radiated (or received) per unit solid angle by the antenna in a given direction, to the power radiated (or received) per unit solid angle by an isotropic antenna fed with the same power. The gain in the direction of maximum radiation is given by [31]

$$G_{max} = \left(\frac{4\pi}{\lambda^2}\right) A\eta \tag{2.33}$$

where A is the physical area of the aperture, and η is the aperture efficiency. The efficiency of the antenna is given by $\eta = \eta_i \eta_s \eta_o$, where η_i is the illumination efficiency,

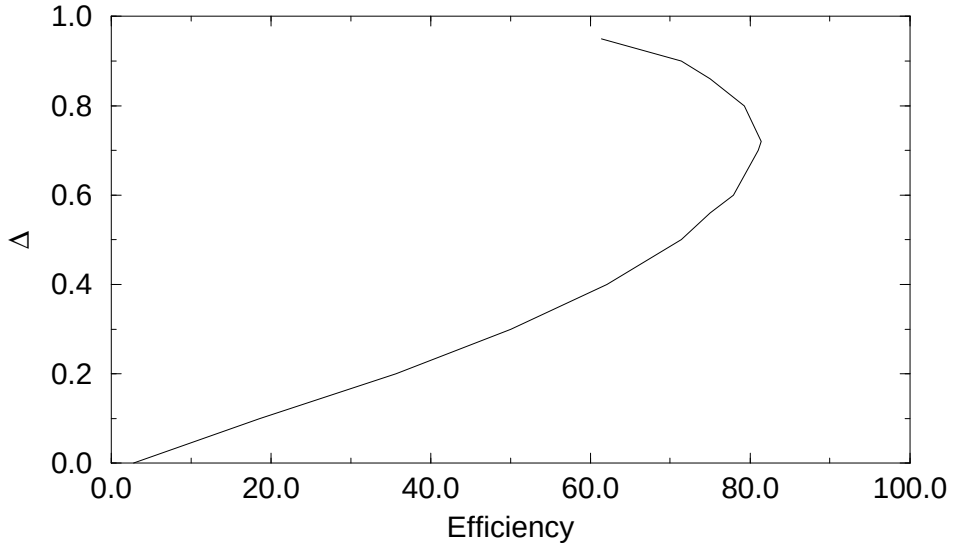

Figure 2.7: Efficiency ($\eta_i\eta_s$) vs Δ

η_s is the spillover efficiency, and η_o is attributed to the surface errors and other losses. The parameter η_i is a measure of how well the aperture is utilized for collimating the radiated energy, and η_s is the ratio of the power intercepted by the reflector to the total power transmitted from the feed element. Surface errors are due to the reflector thermal and manufacturing distortions, and η_o is usually about 80% [31]. If Δ given by (2.30) is known, $\eta_i\eta_s$ can be found using the curve shown in Figure 2.7 [27].

2.5.1.4 Antenna Radiation Pattern

A simple approximation of the normalized far-field gain pattern for the on-focus feed is given by [27]

$$g(\theta_b) = \frac{1}{1-.5\xi}\left\{\frac{2J_1(u)}{u} + \xi\left(\frac{4J_2(u)}{u^2} - \frac{2J_1(u)}{u}\right)\right\} \tag{2.34}$$

where θ_b is the angle that the user makes with the beam boresight, and J_1 and J_2 are the first and second order Bessel functions respectively. In (2.34) u is given by

$$u = \frac{\pi D_1 \sin\theta_b}{\lambda} \tag{2.35}$$

where ξ is given by an equation similar to (2.30), with $\alpha_0 = -26.55$, $\alpha_1 = 35.17$, $\alpha_2 = 15.59$, and $\alpha_3 = 2.37$. From (2.34) and (2.33), the overall gain pattern of the far-field can be written as

$$G(\theta_b) = G_{max}g(\theta_b) \tag{2.36}$$

where G_{max} and $g(\theta_b)$ are given by equations (2.33) and (2.34), respectively. The above equation gives the far beam pattern for feed placed on the focal point (on-focus). As mentioned earlier, if the number of spotbeams is not large and F/D is set such that $GL_{max} < .1$ dB, the degradation in other beams will not be significant [27]. Therefore, an identical beam pattern for all beams can be assumed.

2.5.1.5 Design Procedure

The design flowchart is shown in Figure 2.8. The design must meet the following requirements:

1. Provide beam coverage for the area of interest.
2. Provide a far-field pattern with the minimum required gain and the desired sidelobe level.

It should be noted that the formulas presented only apply if the following conditions are met [27].

1. $0 < \Delta < .85$
2. $0 \leq GL \leq 3$
3. $F/D \leq 1.5$
4. $\Omega < 30^o$
5. $\theta_n \approx \tan\theta_n$

Once the antenna configuration has been found, the far-field electric field for each feed can be found.

2.5.2 Received Complex Electric Field

In this section, a closed form expression is given for the far-field complex electric field of a zero-offset parabolic antenna [9]. Referring to Figure 2.5, the plane of feed for

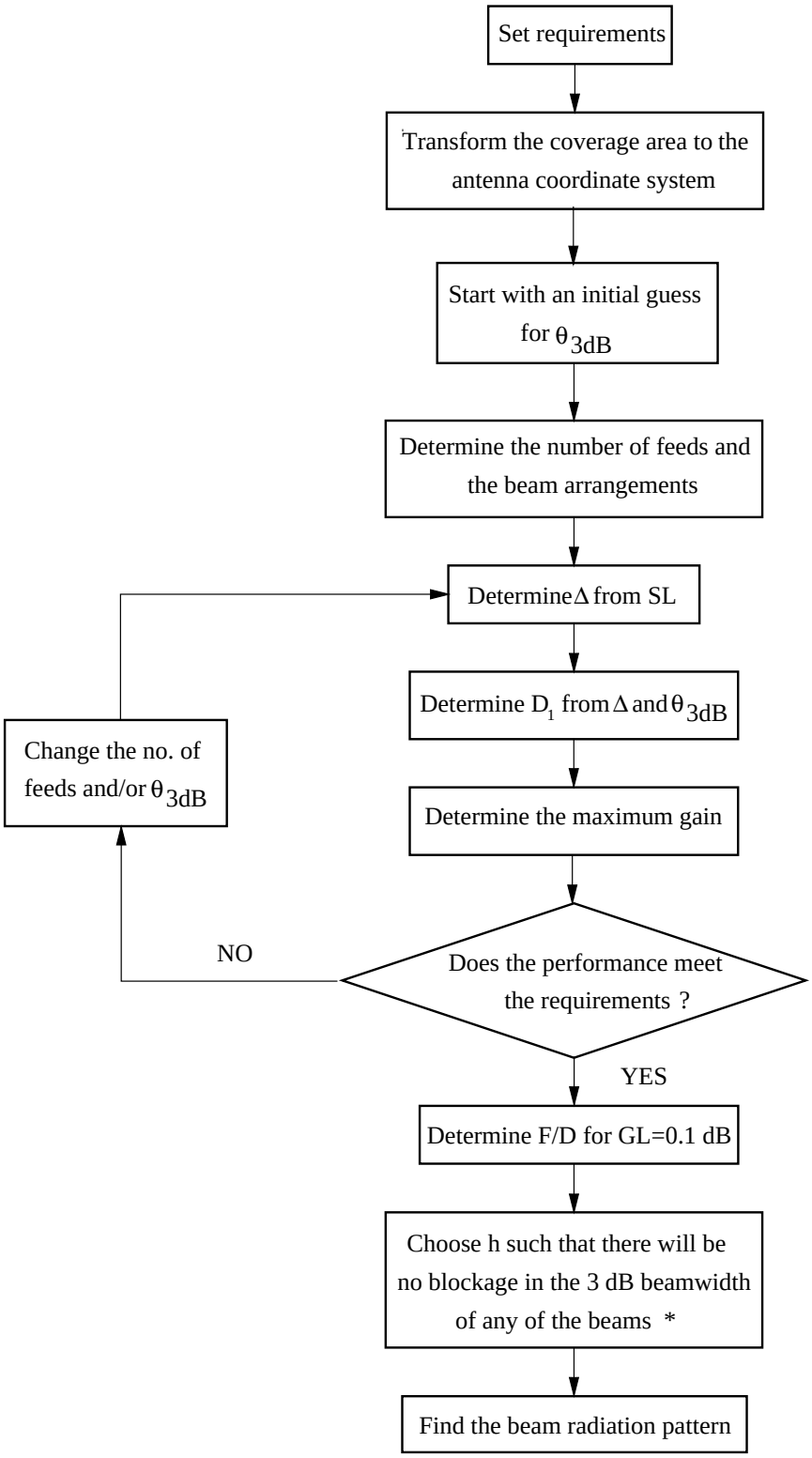

* For the zero-offset reflector, h=0 and D = D_1

Figure 2.8: Reflector Antenna Design Procedure

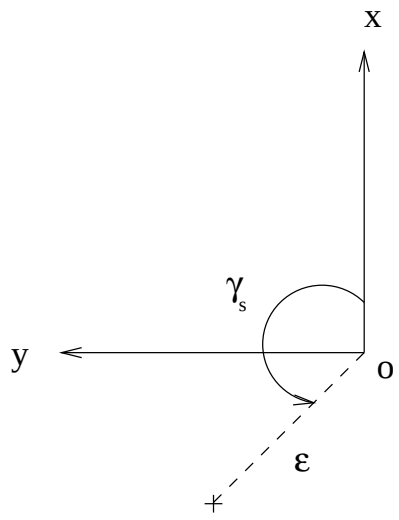

Figure 2.9: Feed Plane For the Zero-Offset Reflector

the zero-offset parabolic is the xy plane. For a given feed with the polar coordinates (ϵ, γ_s) on the xy plane (Figure 2.9), the received electric field as a function of the location of the user on earth is given by [9]

$$E(\theta_i, \phi_i) = \int_0^1 \int_0^{2\pi} s E_f(s,\zeta) \exp\left[-j\frac{\pi}{\lambda} D_1 s\mu \cos(\zeta - \varrho)\right] ds d\zeta \qquad (2.37)$$

where θ_i, ϕ_i are the angles that the signal incident upon the satellite antenna makes with the z-axis and x-axis respectively. In (2.37), E_f is the effective aperture distribution and is given by [9]

$$E_f(s,\zeta) = P(s)Q(s,\zeta)F_r(s) \qquad (2.38)$$

where $Q(s,\zeta) = \exp j[-\beta\epsilon\cos(\zeta - \gamma_s)]$, and $P(s)$ is given by

$$P(s) = \exp j\left\{\frac{\pi}{\lambda F}\epsilon^2\frac{1+N^2}{1+N^3} - \frac{2\pi F}{\lambda}(1-N)\left[1 - \sqrt{1 - \left(\frac{B_u\epsilon}{F}\right)^2}\right]\right\} \qquad (2.39)$$

where $N = (sD_1/4F)^2$ and F is the focal length of the parabola. In (2.38), $F_r(s)$ is the radiation pattern of a rotationally symmetric feed given by (2.26) and can be written as [9]

$$F_r(s) = \left(\frac{1-N}{1+N}\right)^q \qquad (2.40)$$

where q is given by equation (2.27) and B_u is the beam deviation factor and is defined as [10]

$$B_u = -\frac{\int_0^1 F_r(s)s^3/(1+N)^3\ ds}{\int_0^1 F_r(s)s^3/(1+N)^2\ ds} \tag{2.41}$$

The normalized coordinates of the intersection of the incident signal on the xy plane can be written as [9]

$$u = \sin\theta_i \cos\phi_i \qquad (x-\text{coordinate}) \tag{2.42}$$

$$v = \sin\theta_i \sin\phi_i \qquad (y-\text{coordinate}) \tag{2.43}$$

Using the beam deviation factor given by (2.41), beam boresight created by the given feed can be found by [9]

$$u_m = B_u(\epsilon/F)\cos\gamma_s \qquad (x-\text{coordinate}) \tag{2.44}$$

$$v_m = B_u(\epsilon/F)\sin\gamma_s \qquad (y-\text{coordinate}) \tag{2.45}$$

Finally, ϱ and μ in (2.37) are given by [9]

$$\varrho = \arctan\frac{v-v_m}{u-u_m} \tag{2.46}$$

$$\mu = \sqrt{(u-u_m)^2+(v-v_m)^2} \tag{2.47}$$

Once the electric field for a given feed has been determined, its gain pattern can easily be found by the following equation.

$$G(\theta_i,\phi_i) = G_{max}E_n^2(\theta_i,\phi_i) \tag{2.48}$$

where $E_n(\theta_i,\phi_i)$ is the normalized $E(\theta_i,\phi_i)$ given by (2.37) and G_{max} is given by (2.33).

Chapter 3

Land-Mobile Geostationary Satellite System

3.1 Introduction

A mobile satellite system essentially consists of two main elements: a ground segment and a space segment. The space segment relates to the satellite's characteristics and the type of orbits used by the satellite. The ground segment consists of user terminals and gateway stations. Gateway stations provide the interface between the satellite, the public switched telephone network (PSTN), and the public land mobile network (PLMN). Therefore, to communicate with individuals using the terrestrial networks, access is obtained via gateway stations. For the mobile-satellite system presented here, one earth station is sufficient to provide the connection between fixed and mobile networks to the satellite. Since limitations such as power, size and weight are no longer of concern in the design of earth stations, they can employ reflector antennas as large as thirty meters in diameter and transmit at high power. Therefore, the link between earth stations and the satellite can be easily established as compared to hand-held terminals. For this reason, in this thesis only the links between user terminals and the satellite is discussed, and no attempt has been made to investigate the link between the earth station and the satellite.

In this chapter, the land-mobile geostationary satellite system is presented and

its performance is discussed. The system employs an isolated feed satellite antenna configuration and provides personal hand-held communications for users located in sparsely populated areas in the southern half of Canada. The uplink and downlink operate at separate L-band frequencies and, hence employ separate antennas. In this chapter and Chapter 4, the signal-to-interference-noise ratio (SINR) is calculated with an approximation used by Gilhousen *et al.* [14]. In Chapter 5, however, a Gaussian approximation is used to the determine the received SINR. This chapter is organized as follows: In Section 3.2, the uplink and downlink reflector configurations are discussed and the system beam coverage is described. Section 3.3 describes the system communication model and the coherent uplink and downlink receivers. Finally, in Section 3.4, link budget analysis is performed and system performance is discussed.

3.2 Satellite Reflectors and Beam Pattern

Due to the large distances between GEO satellites and terrestrial users, satellite antennas with large gains are required. In the case where the terrestrial user is only equipped with a portable handset, demands on the satellite antenna capability increase. Reflector antennas have proven to be reliable and technologically realizable. As mentioned in Section 2.5 of Chapter 2, there are two popular types of parabolic antennas: *offset* and *zero-offset* reflectors. In this section, reflector configurations for both antennas are determined and their performance is compared. The required uplink and downlink antennas have to meet the following requirements:

1. Provide beam coverage for the lower half of Canada.

2. Provide a far-field pattern with a peak gain of at the least 40 dB and first sidelobe at 24 dB below the peak.

The gain requirement was determined after a preliminary link analysis was performed. The uplink and downlink carrier frequencies were chosen to be 1.6 GHz and 2.0 GHz, respectively. The uplink frequency is lower than that of the downlink, since path loss

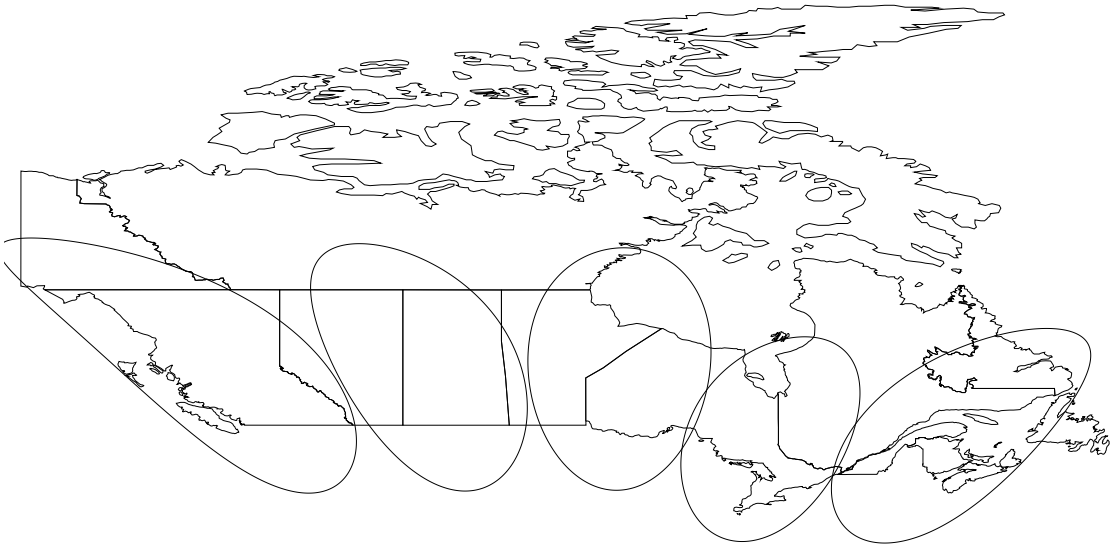

Figure 3.1: Beam Footprints on the Coverage Area
Beams are numbered (1) to (5) from left to right.

is greater at higher frequencies. On the downlink, path loss can be combatted by an increase in the transmitted satellite power. On the uplink, however, due to handset limitations the user is unable to increase transmitted power. Therefore, the lower end of the L-band is designated for the uplink, and the higher end is given to the downlink transmission.

The antenna design procedure described in Section 2.5.1.5 of Chapter 2 was followed to determine the antenna parameters for both offset and zero-offset reflectors. The design equations revealed that coverage can be provided using 5 spot beams each with a 3 dB beamwidth of 1.5°. The 3 dB below maximum gain contours for these beams are shown in Figure 3.1. The beams are numbered (1) to (5) from west to east, respectively. The satellite's position in orbit was chosen to be at 93.5° longitude, *i.e.*, half-way between the east and west coasts. The beams geographical centres are given in Table 3.1. Sections 3.2.1 and 3.2.2 discuss the zero-offset and offset reflector designs. In Section 3.2.3, the antennas are compared and conclusions are made.

Beam no.	Longitude	Latitude
(1)	123.7	52
(2)	107.4	52
(3)	92.5	52
(4)	80.7	47
(5)	67.0	47

Table 3.1: Geographical Centres of the Beams

3.2.1 Offset Parabolic Antenna

Referring to Figure 2.6 of Chapter 2, parameters for the uplink and downlink offset reflectors are given in Table 3.2. Each reflector antenna employs five feeds with each feed being responsible for projecting one beam. The feed allocated to the central beam is located on the focal point of the antennas. The far-field radiation pattern for the feed on focus can be found using the approximation given by equation (2.34). The normalized radiation pattern for the uplink antenna is shown in Figure 3.2, where θ_i is the angle that the incident signal makes with the z-axis.

Equation (2.34) assumes that the far beam radiation is circularly uniform. The downlink antenna also produces a similar gain pattern, where the first sidelobe is at -24 dB and the beamwidth is 1.5°. The other four feeds are located on both sides of the focal point. As the feeds move further away from the focal point, the effective aperture distribution experiences more phase variation, which results in beam pattern distortion. The distortion in the offset reflectors is more severe than in the zero-offset reflectors due to the loss of reflector symmetry. To reduce the distortion, the ratio F/D in Figure 2.6 is chosen such that the maximum loss in the peak gain given by (2.32) in beams (1) and (5) is less than 0.1 dB. Since the number of beams scanned on both sides of the focal point is no more than two, the degradations in the furthermost beams are small [30]. Therefore, the gain pattern produced by the other feeds can be

Parameters	Uplink reflector	Downlink reflector
Carrier Frequency (GHz)	1.60	2.00
Diameter of the reflector D_1 (m)	8.34	6.70
Focal length F (m)	9.99	7.99
h (m)	4.17	3.34
Antenna beamwidth $\theta_{3\text{dB}}$ (deg.)	1.50	1.50
Efficiency	0.65	0.65
Maximum antenna gain $G_{\max}$ (dBi)	41.00	41.00

Table 3.2: Parameters for the Offset Reflectors

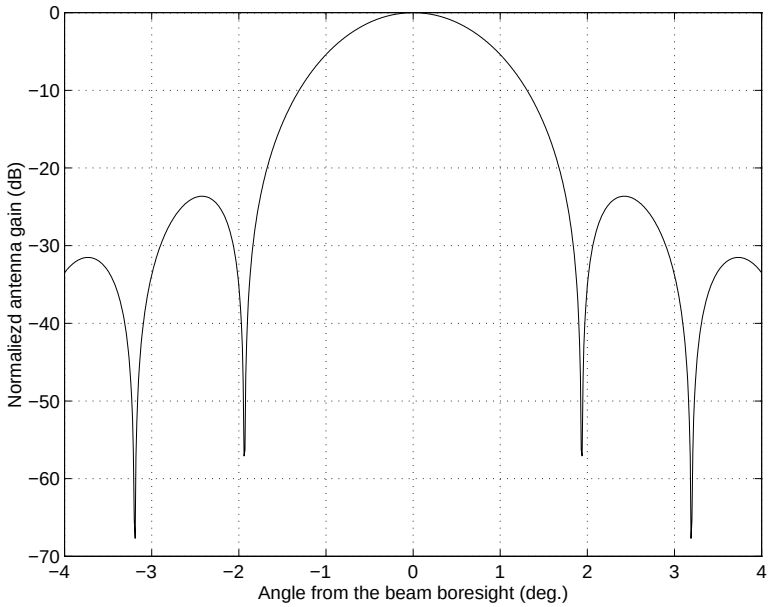

Figure 3.2: Normalized Gain vs. θ_i for the Offset Reflector

Parameters	Uplink reflector	Downlink reflector
Carrier Frequency (GHz)	1.60	2.00
Diameter of the reflector D_1 (m)	8.34	6.70
Focal length F (m)	5.00	4.00
Antenna beamwidth $\theta_{3\text{dB}}$ (deg.)	1.50	1.50
Efficiency	0.65	0.65
Maximum antenna gain $G_{\max}$ (dBi)	41.00	41.00

Table 3.3: Parameters for the Zero-Offset Reflectors

assumed to be similar to that of the central feed.

3.2.2 Zero-Offset Parabolic Antenna

The zero-offset reflectors are also designed using the equations and procedure given in Section 2.5.1. The feed coordinates and beam pattern for the zero-offset reflectors can be more accurately determined than for the offset reflectors [9]. Referring to Figure 2.5 of Chapter 2, the uplink and downlink reflector parameters are given in Table 3.3.

Allocating the feed on the focal point to the central beam (2), the placement for any other feed can be found using the following procedure:

1. Determine the intersection of the line connecting the desired beam centre on Earth to the reflector focus on the xy-plane (Figure 2.5).

2. Set the normalized x and y intersection coordinates equal to u_m and v_m, respectively, and find the polar coordinates of the feed ϵ and γ_s using the equations given in Section 2.5.2.

The feed coordinates for the uplink and downlink reflectors are listed in Table 3.4. For a given feed with polar coordinates (ϵ, γ_s) in the xy plane as shown in Figure 2.9,

Antenna	Coordinates	Feed no.				
		(1)	(2)	(3)	(4)	(5)
Uplink	ϵ (in λ)	1.53	0.76	0.00	0.72	1.45
	γ_s (deg.)	86.4	87.54	0.0	288.0	279.3
Downlink	ϵ (in λ)	1.23	0.61	0.00	0.58	1.16
	γ_s (deg.)	86.4	87.54	0.0	288.0	279.3

Table 3.4: Feed Coordinates

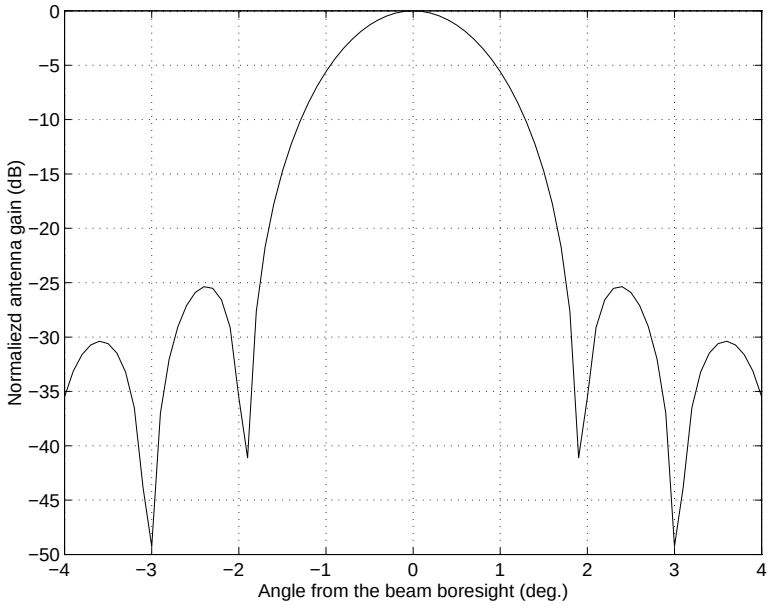

Figure 3.3: Normalized Gain vs. θ_i for the Zero-Offset Reflector

the received electric field as a function of the user's location on Earth is given by equation (2.37) of Chapter 2. As shown in Table 3.4, feed (3) is on the focal point of the parabola. The radiation pattern in the $\phi_i = 0$ plane for the feed on the focal point is shown in Figure 3.3, where θ_i and ϕ_i are the angles that the signal incident upon the satellite antenna makes with the z-axis and x-axis respectively. Parameters for this reflector are given in Table 3.3. In equation (2.37), the pattern is not necessarily assumed to be circularly uniform, and hence a more accurate gain estimation is obtained according to user's location on earth. In the above, feed blockage was not taken into consideration.

3.2.3 Discussion

Comparing Figures 3.2 and 3.3, we observe that the zero-offset and offset reflectors produce almost identical patterns and provide the same peak gain. The electric field for each feed of the zero-offset reflector can be found separately, whereas in the approximations used for the offset reflector, other feeds were assumed to produce a pattern similar to that of the feed on focus. Between the two antenna models, the offset reflector is the antenna of practical choice since there is no feed blockage involved. However, since a more comprehensive and accurate expression for the zero-offset electric field is available, the zero-offset design is used throughout this thesis for analysis purposes. Since both designs produce the same results for the feed on focus and their parameters are found such that the maximum gain loss in the furthermost beams is no more than 0.1 dB, the radiation patterns for the zero-offset feeds can also be assumed to represent those of the offset reflector.

3.3 System Communication Model

In cellular systems, the coverage area is divided into multiple cells, where each cell is serviced by its designated base station. As described in the previous section, satellite beam coverage here is accomplished by five spot beams stretching from the east to

the west coast. Analogous to the cellular case, each spot beam can be regarded as one cell. However, the satellite acts as the only base station in the system. In the 5-beam arrangement discussed, each feed on board the reflectors is responsible for projecting one spotbeam and supporting users within its own 3 dB beamwidth. The communication model adopted here is based on the cellular CDMA IS-95 standard [19]. In IS-95 due to the inclusion of a pilot signal, the downlink is demodulated coherently. On the uplink, however, no pilot signal is used, and instead a non-coherent 64-ary orthogonal modulation is implemented. Ikegami *et al.* have shown that a coherent uplink can be realized by implementing coherent matched filters in the satellite receivers [18]. Both coherent and non-coherent systems are investigated in this thesis. The downlink and coherent uplink system structures are described in Sections 3.3.1 and 3.3.2, respectively. The non-coherent uplink system is described in Chapter 4. The CDMA bandwidth used is 4.9 MHz and can be reduced or increased by simple modifications to the system.

3.3.1 Downlink Channel

Similar to the IS-95 standard, data is encoded using a rate 1/2, constraint length 9 convolutional code. Code symbols are then interleaved and each symbol is spread using a binary orthogonal code based on Walsh functions. For this system 256 Walsh codes are used, with each being 256 chips long. The Walsh code symbol duration is equal to the data symbol period T_s, and hence $T_s = 256T_c$, where T_c is the Walsh chip period. Each user in the beam will be assigned one of the Walsh codes for the duration of transmission. The resulting signal is binary phase-shift-keying (BPSK) modulated and further spread using a long period PN code with a chip duration equal to that of the Walsh. The same long PN code is used for all users in the system. All signals are transmitted synchronously. On the downlink, Walsh codes provide perfect isolation between the signals transmitted for users in a single beam. Since Walsh codes are repeated in the neighbouring beams, an overlap may occur if two users in adjacent beams are assigned the same Walsh code. To provide isolation, each beam uses the

same PN code, but with a different time offset. Due to the time shift, signals intended for users in the neighbouring beams appear as background noise. This will allow up to 255 traffic channels per beam. To provide a coherent reference for the users, a pilot signal is transmitted on each beam at all times. As mentioned earlier in Chapter 2, pilot signals consist only of the PN code transmitted by each beam and enable users to establish initial synchronization. The receiver diagram for the downlink is shown in Figure 3.4, where $r_i^{(h)}(t)$ is the total received signal by the desired user i in beam (h) and can be written as

$$r_i^{(h)}(t) \quad = \quad s_i^{(h)}(t - \tau_i^{(h)}) + n(t) \tag{3.1}$$

where $n(t)$ is white Gaussian noise with zero mean and spectral density of $N_\circ$, $\tau_i^{(h)}$ is the path delay, and $s_i^{(h)}(t)$ is given by

$$s_i^{(h)}(t) \quad = \quad \sum_{k=1}^{N} \sum_{j=1}^{M_k} \sqrt{2P_{ij}^{(k)}} b_j^{(k)}(t) L_j(t) c^{(k)}(t) \cos w_\circ t \tag{3.2}$$

where N is the number of spotbeams, M_k is the number of users in spotbeam (k), $w_\circ$ is the carrier frequency, $b_j^{(k)}(t)$ and $P_{ij}^{(k)}$ are, respectively, the data symbol and power intercepted by the desired user i, which were intended for user j in beam (k). The Walsh code for user j is represented by $L_j(t)$ and $c^{(k)}(t)$ is the PN code for users in beam (k). Data bits are transmitted at 9600 bps, and hence Walsh and PN code chip frequencies are 4.9154 MHz. In Figure 3.4, k_s is the sampling index, and $L_i(t)$ is the Walsh code designated to the desired user. Since all signals arrive at the user with the same delay, $\tau_i^{(h)}$ can be assumed to be zero with no loss of generality.

Assuming there is no multipath, since signals are transmitted synchronously and Walsh codes are orthogonal, *i.e*, $E(L_i(t)L_j(t)) = 0$ for $i \neq j$, the multiple access interference within a single beam will be zero. However, in satellite communications systems multipath exists, since signals will be reflected by buildings, trees, mountains, and other objects. Therefore, orthogonality is not maintained between multipath components, thereby resulting in mutual interference between code channels. To determine the signal-to-interference-noise ratio (SINR), the approximation given by equation (2.12) of Chapter 2 is used here. This approximation, however, applies to

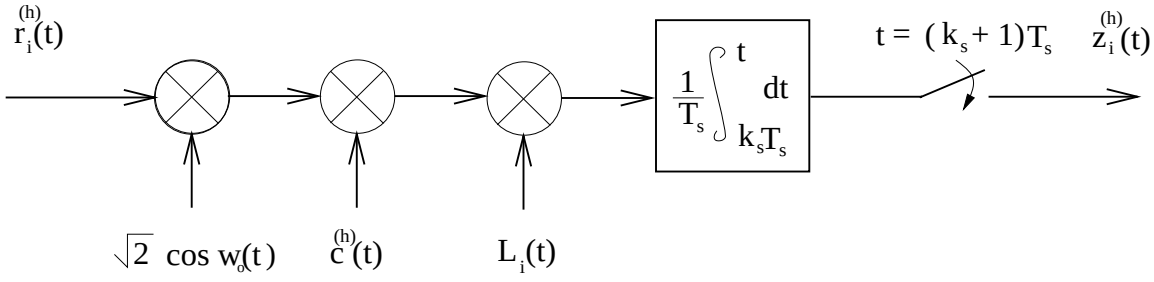

Figure 3.4: Downlink Receiver

asynchronous transmission where long codes provide signal isolation, and hence gives a pessimistic estimation of the SINR. For satellite link analysis, this approximation is sufficient and will provide a conservative estimate of downlink system performance.

Assuming that the satellite transmits at equal power for all users, and that the desired user i is in beam (1), from (2.12) the SINR is given by

$$\text{SINR}_{\text{down}} = \frac{2P_i^{(1)}T_s}{N_\circ + I_{down}} \tag{3.3}$$

where $P_i^{(1)}$ is the signal power received by the desired user, T_s is the data symbol duration, and I_{down} is given by

$$I_{down} = (\text{VA})\frac{(M_1 - 1)P_i^{(1)} + \sum_{k=2}^{N} M_k P_i^{(k)}}{W_s} \tag{3.4}$$

where VA is the voice activity factor, assumed to be 40%, and $W_s \equiv 1/T_c$ is defined as the CDMA system bandwidth. In (3.4), M_k represents the active number of users in beam (k), and $P_i^{(1)}$ and $P_i^{(k)}$ are the power received by the desired user from beams (1) and (k), respectively. The user receives all signals transmitted in a given beam at the same power. Since there are five spot beams, the user will receive signals at five different power levels.

For acceptable voice quality, a maximum bit error rate of 10^{-3} must be ensured. The receiver implements soft-decision Viterbi decoding [29] to recover the data bits (not shown in the figure). In the following sections, the minimum required received SINR for the white Gaussian noise and fading channel scenarios are discussed.

3.3.1.1 AWGN Channel

Simulation [22] was used to determine the minimum SINR requirement. Data bits are randomly generated and encoded by a rate 1/2 convolutional code of constraint length 9, and are then BPSK modulated. The data symbols then enter a white Gaussian noise channel, where the noise power is set such that the desired SINR is obtained. Channel output symbols are then quantized using an eight-level quantization method described in [8]. The quantized symbols then enter the Viterbi decoder, where soft decision decoding is implemented to recover the data bits. Simulations show that a maximum bit error rate of 10^{-3} is achieved for a SINR of 2.6 dB. Therefore, the minimum required received SINR for the downlink is 2.6 dB.

3.3.1.2 Rician Fading Channel

On the downlink, all signals received by the desired user fade to the same degree, and since the desired signal power is attenuated, the interference power also is attenuated. Since CDMA is an interference limited system, it should be more resistant to the effects of fading compared with other multiple access techniques. To determine the fading margin, assume that the signal power is attenuated by an average amount Γ. Using (3.3) the received SINR can then be written as

$$\text{SINR}_{\text{fad}} = \frac{2\Gamma P_i^{(1)} T_s}{N_\circ + \Gamma I_{down}} \tag{3.5}$$

Therefore, the fading margin fad_{down} is given by

$$\text{fad}_{\text{down}} = 10\log \text{SINR}_{\text{down}} - 10\log \text{SINR}_{\text{fad}} = \frac{1}{\Gamma}\frac{N_\circ + \Gamma I_{down}}{N_\circ + I_{down}} \tag{3.6}$$

where $\text{SINR}_{\text{down}}$ is given by (3.3). The fading margin can be determined by estimating the average attenuation factor Γ through simulations. To determine Γ, initially assume that the only signal attenuated is the desired signal. In that case, from (3.5) the received SINR can be written as

$$\text{SINR} = \frac{2\Gamma P_i^{(1)} T_s}{N_\circ + I_{down}} = \Gamma \text{SINR}_{\text{down}} \tag{3.7}$$

The above SINR can be determined through simulations [23], and since $\text{SINR}_{\text{down}} =$ 2.6 dB for a BER of 10^{-3}, Γ can subsequently be found. The fading margin can hence be calculated using (3.6) if the ratio $N_\circ/I_{down}$ is known.

The simulation used to determine the SINR given by (3.7) is similar to the one described in the previous section, except that the white Gaussian noise channel is replaced by a Rician fading channel with K=10 dB, where K is the ratio of specular energy to diffuse energy (K-factor). In suburban and rural areas, the signals are usually not blocked by tall buildings and structures, and therefore a line of sight to the satellite is present. Rician fading with K=10 dB has proven to be a suitable choice to simulate this scenario [1]. In the simulations, the Doppler effect for the mobile is taken into consideration, and a third-order Butterworth low pass filter is used to emulate fading dynamics [26]. The filter cutoff frequency is set equal to the normalized Doppler frequency and is given by [28]

$$f_D \quad = \quad \frac{\text{Doppler shift}}{\text{baud rate}} \quad = \quad \frac{f_c v_b}{v_c f_s} \cos(\alpha_n) \tag{3.8}$$

where f_c is the carrier frequency, f_s is the data symbol rate, and v_c and v_b are the speed of light and the mobile, respectively. In 3.8, α_n is the angle between the direction of mobile movement and the incident wave. The fading simulator diagram is shown in Figure 3.5, where at time k the received symbols R_k are related to the transmitted symbols T_k by

$$R_k \quad = \quad C_k T_k + n_k \tag{3.9}$$

where C_k is the channel gain, n_k is the additive white Gaussian noise, and K is the K-factor of Rician fading [20]. In the simulations the maximum possible Doppler shift was assumed and, hence, $\cos(\alpha_n)$ was set equal to one. This assumption is rather optimistic since it results in shorter periods of deep fade. However, it is a tradeoff since, as mentioned earlier, only the desired signal is assumed to be fading, where in reality the interfering signals are also faded. The fading simulator is designed such that the variance of the channel gain is equal to one.

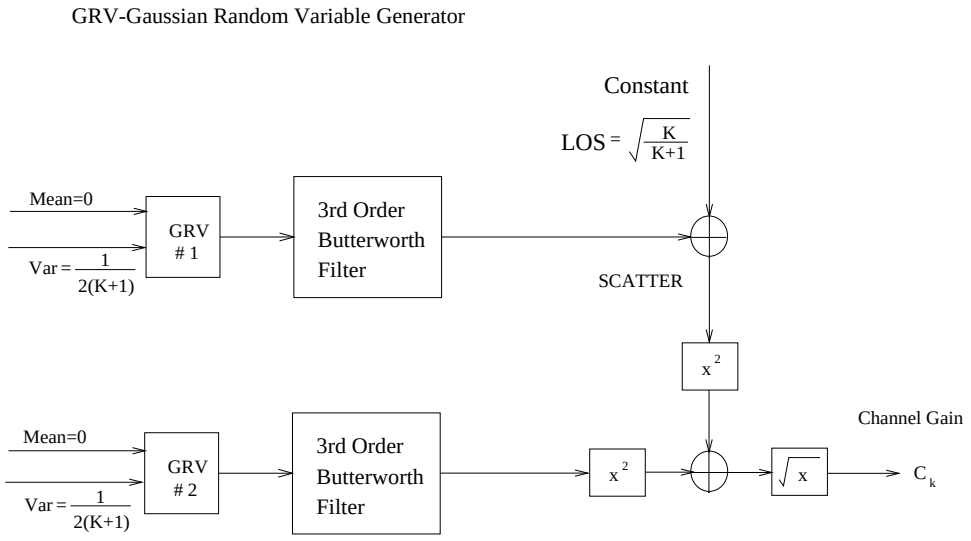

Figure 3.5: Rician Fading Simulator

Since fading channels exhibit burst-error characteristics, symbol interleaving is implemented with an interleaving depth of $\lambda_{int} = 20$ [20]. Symbol interleaving and deinterleaving are implemented prior to the symbols entering the channel and after the symbols are quantized, respectively.

Simulations show that for a mobile moving at a speed of 100 km/h and receiving signals at a carrier frequency of 2 GHz (downlink), the minimum required SINR becomes 3.7 dB for a maximum bit error rate of 10^{-3}. As mentioned in the previous section, $\text{SINR}_{\text{down}} = 2.6$ dB; therefore, using (3.7) Γ is found to be -1.1 dB. The downlink fading margin can then be found using (3.6) if $N_\circ/I_{down}$ is known. This ratio is determined through link budget analysis as will be shown in Section 3.4.

3.3.2 Coherent Uplink Channel

A simple uplink structure with a bit stream based on IS-95 is adopted here. The information bits are transmitted at 9600 bps and are convolutionally encoded using a rate 1/3 code of constraint length 9. The code symbols are then interleaved and BPSK modulated, and the resulting signal is then spread using a long code of 4.9152 MHz chip frequency designated to the user. One long code can be used for all

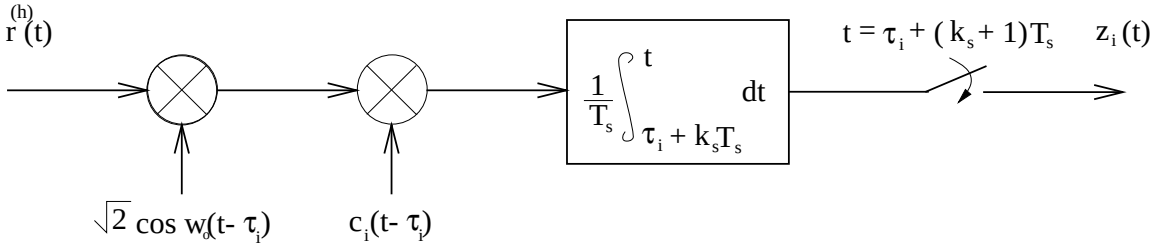

Figure 3.6: Coherent Uplink Receiver

users. However, each user must transmit with a different time offset so that signals from other users appear as background noise. Users are assumed to be transmitting asynchronously. The uplink receiver is shown in Figure 3.6, where $r^{(h)}(t)$ is the signal received by the feed (h) allocated to the desired user and can be written as

$$r^{(h)}(t) = \sum_{i=1}^{M} s_i^{(h)}(t - \tau_i) + n(t) \tag{3.10}$$

where $s_i^{(h)}(t) = \sqrt{2P_i^{(h)}}c_i(t)b_i(t)\cos w_\circ t$. In (3.10), $P_i^{(h)}$ is the power received from the i^{th} user by feed (h), M is the number of active users in the system, τ_i is the channel delay for the i^{th} user, and $b_i(t)$ and $c_i(t)$ are the modulating signal and the spreading code of the i^{th} user, respectively. Other parameters in Figure 3.6 are as defined in the previous section.

The uplink SINR can be estimated using the approximation given in Chapter 2. Assuming that the desired user is at $i = 1$, the SINR is given by

$$\text{SINR}_{\text{up}} = \frac{2P_1^{(h)}T_s}{N_\circ + I_{up}} \tag{3.11}$$

where I_{up} is given by

$$I_{up} = \frac{(\text{VA})}{W_s}\sum_{i=2}^{M} P_i^{(h)} \tag{3.12}$$

Similar to the downlink, the uplink receiver implements Viterbi decoding for data bit recovery (not shown in the figure).

In the following sections, the minimum required received SINR for white Gaussian noise and fading channel scenarios are discussed.

3.3.2.1 AWGN Channel

The method used for the downlink AWGN channel described in the previous section was modified to determine the required SINR for the rate 1/3, constraint length 9 code. Simulations showed that the received SINR must be at least 0.34 dB to ensure that the bit error rate does not exceed 10^{-3}. From equation 3.11, this SINR requirement can be expressed by the more familiar $E_b/(N_\circ + I_{up})$ of 2.1 dB, where E_b is the energy per received data bit.

3.3.2.2 Rician Fading Channel

Unlike the downlink, signals arriving at the satellite are faded differently. Assuming a worst-case scenario where only the desired signal is faded, from (3.11) the received SINR can be written as

$$\text{SINR}_{\text{fad}} = \frac{2\Psi P_1^{(h)} T_s}{N_\circ + I_{up}} \tag{3.13}$$

where Ψ is the average amount by which the signal power is attenuated. In that case, the uplink fading margin is given by

$$\text{fad}_{\text{up}} = 10\log \text{SINR}_{\text{up}} - 10\log \text{SINR}_{\text{fad}} = -10\log \Psi \tag{3.14}$$

where SINR_{up} is given by (3.11). Since the required SINR_{up} and SINR_{fad} for the desired bit error rate can be determined through simulation, the average attenuation factor Ψ be can found. Once again, the simulation technique used for the downlink fading channel was modified to determine the required SINR for the rate 1/3, constraint length 9 code. Results show that for a mobile moving at a speed of 100 km/h and receiving signals at a carrier frequency of 1.6 GHz (uplink), the minimum required SINR_{fad} becomes 1.94 dB for a maximum bit error rate of 10^{-3}. As mentioned in the previous section, $\text{SINR}_{\text{up}} = 0.34$ dB, using (3.14), the uplink fading margin is found to be 1.60 dB. Hence, the overall minimum SINR requirement for the uplink becomes 1.94 dB.

3.4 Satellite Link Performance Analysis

In this section, uplink and downlink system performances are evaluated through link budget analysis. System capacity is defined as the maximum allowable number of active users in the system such that the minimum recommended SINR is maintained for the most geographically disadvantaged user inside or on the 3 dB beam borders. In Section 3.4.1, link performance is calculated for the 4.9 MHz bandwidth CDMA system, and system capacity is determined. In Section 3.4.2, capacity improvement is investigated for a system bandwidth of 9.8 MHz. For capacity analysis, only users on or inside the 3 dB beam borders are considered to be supported by the system. System performance for users located between the spot beams will be discussed in Section 3.4.1.

3.4.1 System Performance and Capacity

Downlink and uplink analyses are described in Sections 3.4.1.1 and 3.4.1.2, respectively, and results are given for the most geographically disadvantaged user located on a 3 dB beam border in each case. The overall coverage performance is discussed Section 3.4.1.3.

3.4.1.1 Downlink Budget Analysis

The goal here is to determine the received signal-to-interference-noise ratio by a given terrestrial user. According to the beam coverage scheme, a worst-case location scenario for the downlink would be where beams (3) and (4) intersect (Figure 3.1). A user located in that area would be at the 3 dB edge of its allocated beam as well as one of the interfering beams. Figure 3.7 shows the 3 dB gain contours for all five beams and the coverage area bounded by straight lines. User 32 in Figure 3.7, with 48° latitude and 86.5° longitude, was selected and was assumed to be supported by feed (3). The downlink budget for this user is shown in Table 3.5.

Table 3.5 is divided into seven parts. The system parameters are given in parts

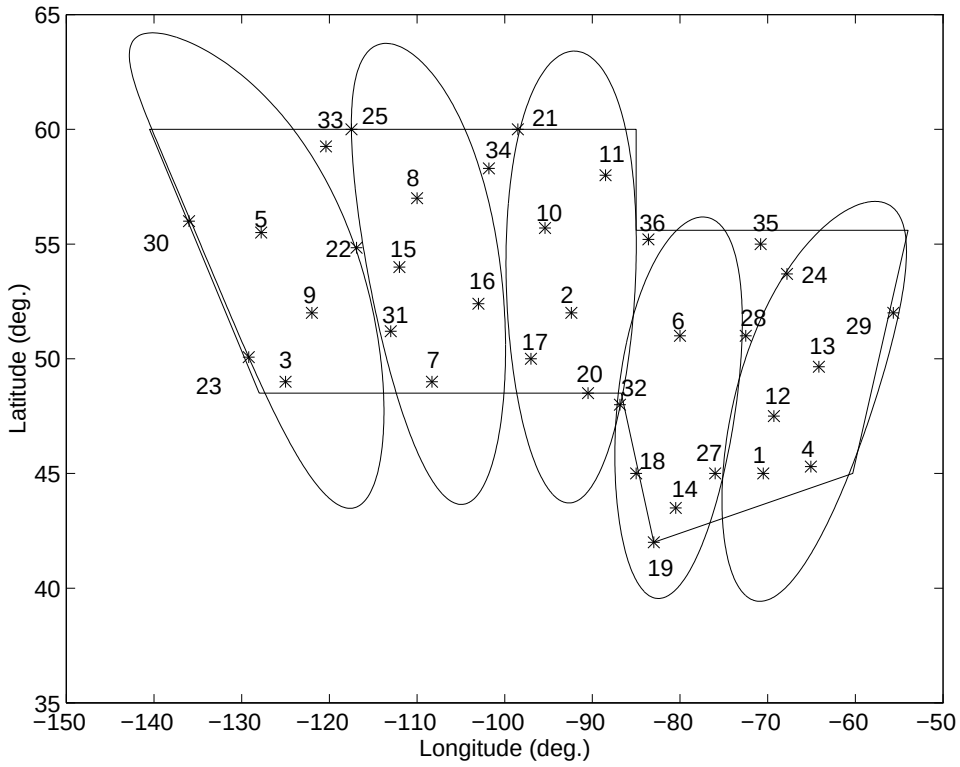

Figure 3.7: Locations for the Desired User in the Coverage Area
Beams are numbered (1) to (5) from left to right.

I to IV and calculation results in parts V to VII. In part I, the maximum number of active users in the system, the voice activity factor, and the carrier frequency are given. The number of active users is assumed to be 125 per beam, and the voice activity factor is assumed to be 40% throughout this thesis. The data rate is set at 9600 bps, and the CDMA bandwidth is 4.1952 MHz. In part II, relevant satellite antenna parameters taken from Table 3.3 are given. The satellite high power amplifier (HPA) output for all users is equal and set at 0.7 W per user. Antenna gain produced by feed (3) in the direction of the desired user is found using (2.48). Handset receiver parameters are given in part III. Handsets are assumed to employ omnidirectional stub antennas of gain 3 dBi and circular polarization to eliminate antenna pointing requirements [7] [3]. The handset receiver noise temperature is assumed to be 250° K. This is higher than the 80° temperature suggested in [7], to be more in-line with

todays handset technology. In part IV, the path loss and atmospheric loss for the user are given. The free space loss L_u is given by [31]

$$L_u = (4\pi d_u/\lambda_d) \tag{3.15}$$

where λ_d is the downlink wavelength and d_u is the distance between the user and the satellite. The atmospheric loss for rainy conditions is about 0.1 dB. For low carrier frequencies such as L-band, rain does not have much impact on the communication link, whereas for higher carrier frequencies such as Ka-band, the loss may be as much as 1.0 to 1.5 dB.

Received signal power, noise spectral density, and multiple access interference are found in part V. The multiple access interference term $\mathrm{I_{down}}$ in the SINR expression (3.3) can be numerically determined if the total power received from all 5 feeds is known. From equation (2.16) in Chapter 2, the received carrier power transmitted by feed (n) on-board the transmitting satellite antenna can be written as

$$P_1^{(n)} = \frac{P_{nu}G_{nu}G_u}{L_uL_{at}} \tag{3.16}$$

where P_{nu} and G_{nu} are the satellite HPA output power and the antenna gain in the direction of the desired user by feed (n), respectively. The user's antenna gain is given by G_u, and L_{at} is the atmospheric loss. In (3.16), G_{nu} is calculated using equation (2.48) with the knowledge of the user location, and $P_{nu} = 0.7$ W for all users. Hence, $\mathrm{I_{down}}$ for the desired user is calculated for the case where there are 125 interfering users per beam. The received signal power $P_1^{(3)}$ is also found using (3.16). As described earlier in Chapter 2, the receiver noise spectral density is given by

$$N_o = kT_i \quad (\mathrm{W/Hz}) \tag{3.17}$$

where k is the Boltzman's constant, and $T_i = 250°$ K is the noise temperature at the receiver input.

In part VI, the received SINR and fading margin are calculated. The signal-to-interference-noise ratio is calculated using (3.3), and the fading margin is calculated using (3.6) with $\Gamma = -1.1$ dB as found in Section 3.3.1.2. Finally, the excess link

	Downlink		
I	Total number of simultaneous users	625	
	Voice activity factor	0.4	
	Carrier frequency	2.0	GHz
	Data rate	9600	bps
	Convolutional code rate	1/2	
	CDMA bandwidth	4.9152	MHz
II	Satellite antenna diameter	6.675	m
	Satellite 3 dB beamwidth	1.5	deg.
	Satellite peak antenna gain, G_{max}	41.025	dBi
	Satellite antenna gain for the user, G_{3u}	38.125	dBi
	HPA output/user, P_{nu}	0.7	W
	Satellite EIRP for the user	36.6	dBW
III	Handset antenna	stub	
	Handset antenna gain, G_u	3	dBi
	Handset antenna temperature, T_i	24	dBK
	Handset antenna G_u/T_i	-21	dB/K
IV	Path loss for the user, L_u	190.11	dB
	Atmospheric loss, L_{at}	0.1	
	Boltzman's constant, k	-228.6	dBW/Hz-K
V	$P_1^{(3)}$ (Received power)	-150.63	dBW
	$N_\circ$ (Noise spectral density)	-204.61	dBW/Hz
	I_{down} (Multiple access interference)	-197.11	dBW/Hz
VI	SINR	6.17	dB
	Fading margin	-0.22	dB
	SINR minimum	2.6	dB
VII	Excess margin	3.36	dB

Table 3.5: Satellite-Mobile Link Analysis (Downlink)

margin in part VII is found by subtracting the fading margin and the minimum required SINR from the received SINR. As can be seen, an excess margin of 3.3 dB is available. This excess margin decreases as the number of users increase. Since this is a worst-case scenario, it is expected that other users in the system benefit from higher excess margin. In satellite communications, systems are designed with high excess margins to ensure acceptable performance in the event of any unexpected losses. By setting 3.3 dB to be the minimum required excess margin on the downlink, the system capacity on the downlink becomes 125 active users per beam or 625 users in total.

The user location selected for this analysis is a worst-case scenario since, due to the beam overlap, the gain observed by the user from its allocated feed (3) is lower than that of the gain received from the feed projecting the neighbouring beam (feed (4)). The user observes an antenna gain of 2.9 dB below the peak value from feed (3), and gains of 25.5 dB, 32 dB, 2.7 dB, and 26.5 dB below the peak from feeds (1), (2), (4) and (5) respectively. This indicates that interference is mainly due to signals intended for users in the same beam (intra-beam interference) and users in the neighbouring beam (4). From the total received multiple access interference I_{down}, it is found that 47.7% is due to intra-beam interference and 52.3% is due to the interference received from all other beams (inter-beam interference). As expected, of this 52.3%, 51% is due to the interference from the neighbouring beam (4). This interference power distribution significantly changes as the user moves towards the centre of the beam. For example, if the user is located at the centre of beam (3), 92.6% of the total interference will be due to the intra-beam interference. The reduction in the inter-beam interference is due to the sharp antenna beam roll-off. For users on the beam border crossings, however, inter-beam interference is a major concern.

Unlike the uplink, the transmitted power can be increased on the downlink. In the above analysis, satellite HPA output per user was chosen to be 0.7 W. Figure 3.8 shows various transmitted power levels plotted versus the excess link margin. As can be seen, the rate of increase in the excess margin is decreased beyond 1.5 W per user. Transmitted power, however, cannot be significantly increased since the amount of

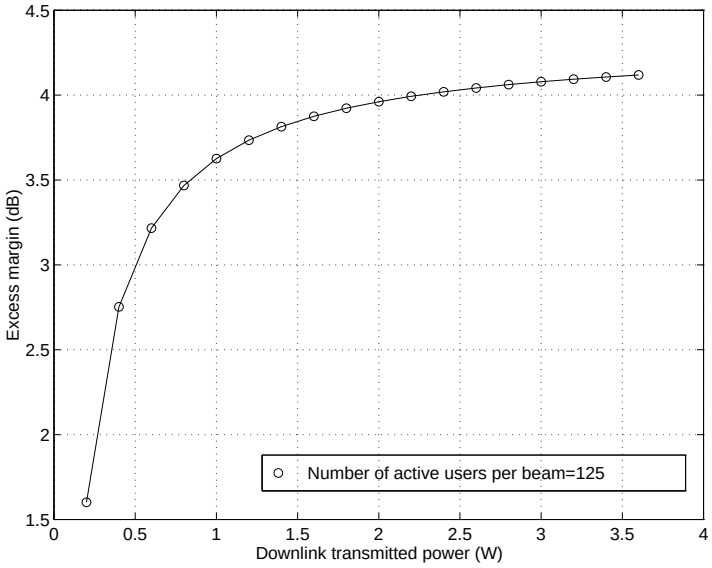

Figure 3.8: Excess Margin vs Downlink Transmitted Power Per User

satellite power generated by the solar panels is limited. In the budget analysis, total transmitted power for 625 users in the system is 26.4 dBW. This amount is safely below the maximum available power of 28 dBW in the MSAT [2]. Therefore, more RF power can be delivered by the satellite, should the need arise.

3.4.1.2 Uplink Budget Analysis

Uplink analysis is performed for a user located on the border of beams (1) and (2) (Figure 3.7). This is expected to be a worst-case-location scenario for the uplink, since the desired user is on the 3 dB edge of the beam projected by feed (2), which receives more interference compared with any other feed. The user is at 54.8° latitude and 117° longitude, and is marked as user 22 in Figure 3.7. The uplink budget for this user is shown in Table 3.6.

Similar to the downlink, Table 3.6 is divided into seven parts. The system parameters are given in parts I to IV and calculation results in parts V to VII. In part I, the uplink carrier frequency is given and the number of active users is set at 85 per beam, *i.e.* 425 users in total. Hand-held terminal parameters are listed in part II. Similar to the cellular phones, the handsets are assumed to perform at no more than

600 mW average transmitted power to ensure that the transmitted power is within the radiation safety limits for human use and to minimize the handset's weight and cost. All handsets have an antenna gain of 3 dBi. In part III, the satellite receiving antenna parameters are given. The receiver noise temperature on-board the satellite T_r is assumed to be 500° K, and the receiving gain G_{u2} for the incident signal is found using (2.48). Path and atmospheric losses for the desired user are given in part IV.

From equation (2.16) in Chapter 2, the received power, noise spectral density, and multiple access interference are found in part V. Received power from the user by feed (n) is given by

$$P_1^{(n)} = \frac{P_u G_u G_{un}}{L_u L_{at}} \tag{3.18}$$

where P_u and G_u are the transmitted power and the handset antenna gain of the terrestrial user, respectively. In (3.18), G_{un} is the satellite antenna gain for the incident signal, and L_u and L_{at} are as described in the previous section. Here, feed (2) is allocated to the user, and hence, the signal power is determined by finding $P_1^{(2)}$. In order to determine the received SINR numerically, the power received from all users by the feed (2) needs to be known. The multiple access interference term I_{up} in (3.12) can be approximated by its average value according to the following Monte-Carlo procedure: At each iteration, M users are randomly distributed across the coverage area. Utilizing the coordinates of all users, I_{up} is calculated as the sample average. Iterations are continued until the sample average converges to a stable value. The number of runs N_r was chosen to be 40, since beyond 40 runs no significant change in I_{up} was observed in all cases. The receiver noise spectral density $N_\circ$ is determined as explained in the previous section.

In part VI, the SINR is calculated using equation (3.11). To estimate the fading margin, it was assumed that only the desired signal is faded. As shown in Section 3.3.2.2, this margin is 1.6 dB for the K=10 dB Rician channel considered. Excess margin in part VII is found by subtracting the fading margin and the minimum required SINR from the received SINR. The excess margin available is about 3.3 dB, which is the minimum recommended. Once again, since this is a worst-case scenario,

	Uplink		
I	Maximum number of simultaneous users	425	
	Voice activity factor	0.4	
	Carrier frequency	1.6	GHz
	Data rate	9600	bps
	Convolutional code rate	1/3	
	CDMA bandwidth	4.9152	MHz
II	Handset antenna	stub	
	Handset antenna gain, G_u	3	dBi
	Handset transmitted power, P_u	0.6	W
	Handset EIRP	0.782	dBW
III	Satellite antenna diameter	8.34	m
	Satellite 3 dB beamwidth	1.5	deg.
	Satellite peak antenna gain, G_{max}	41.025	dBi
	Satellite peak antenna gain, G_{u2}	39.73	dBi
	Satellite G_{u2}/T_r	12.73	dBi/K
IV	Path loss for the user, L_u	188.38	dB
	Atmospheric loss, L_{at}	0.1	dB
	Boltzman's constant, k	-228.6	dBW/Hz-K
V	$P_1^{(2)}$ (Received power)	-149.89	dBW
	$N_\circ$ (Noise spectral density)	-201.61	dBW/Hz
	I_{up} (Multiple access interference)	-198.34	dBW/Hz
VI	SINR	5.20	dB
	Fading margin	-1.6	dB
	SINR minimum	0.34	dB
VII	Excess margin	3.26	dB

Table 3.6: Mobile-Satellite Link Analysis (Uplink)

other users in the system are expected to operate at higher excess margins. Therefore, with 85 users per beam, no more than 425 active users may be allowed to operate on the uplink.

For feed (2), of the total received multiple access interference I_{up}, 78% is due to intra-beam interference and only 22% is due to the inter-beam interference. From this 22%, only 0.3% of the interference comes from beams (4) and (5). Therefore, almost all of the inter-beam interference comes from users in beams (1) and (3). On the uplink, intra-beam interference is much more dominant than the inter-beam interference due to the antenna beam isolation. This is since the sharp roll-off antenna gain pattern results in each feed receiving signals from users in the other beams at much lower gains compared with users in its own beam. As can be seen from this analysis, uplink performance is poorer than downlink performance and is more difficult to improve due to handset power and gain limitations.

3.4.1.3 Overall System Performance

As defined earlier, system capacity is the maximum number of active users allowed such that the minimum required SINR is maintained for the worst-case user. Establishing 3.3 dB as the minimum required excess margin, it was shown in the previous section that maximums of 85 and 125 active users per beam are allowed for the uplink and downlink, respectively. Therefore, system capacity here is uplink limited and the overall system capacity becomes 425 simultaneous users since there are 5 spot beams in the system. In general, uplink performance is more difficult to improve, since the terrestrial handset terminals operate at a limited power of 600 mW and employ small gain stub antennas. However, whether or not system capacity is always uplink limited in satellite communications is an open question. Downlink budget analysis shows that reducing the active number of users from 625 to 425 results in a link margin of 4.3 dB for the worst-case user on the downlink. This amount is 1.0 dB higher than the set requirement.

System capacity, however, can be increased at the expense of the extra link margin.

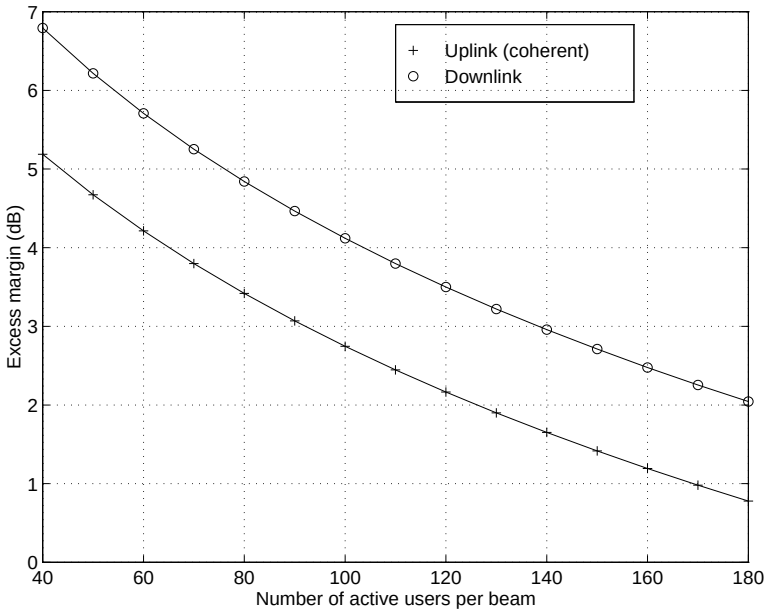

Figure 3.9: Excess Margin vs Uplink and Downlink Capacity

Figure 3.9 shows the maximum number of users per beam on the uplink and downlink versus their respective excess margins. Once again, these results are for the worst-case users 22 and 32 (Figure 3.7) for uplink and downlink, respectively. As expected, the downlink has a better performance and provides an extra margin of at least 1.0 dB above that of the uplink. Using Figure 3.9, the system capacity for various minimum link margin requirements can be determined by just finding the number of active users on the uplink for the given margin.

The uplink capacity can be improved if the received SINR for users on the beam borders can be increased. In Section 3.4.1.2, it was shown that about 78% of the total interference is due to intra-beam interference. This interference can be reduced by implementing a power control scheme on the uplink. So far, in the cases discussed, all handsets were transmitting at an equal power of 600 mW. Hence, the signal powers received from users in the central areas are almost twice as strong compared with those from users on the 3 dB edge. If users inside the beams reduce their transmitted powers such that the satellite receives all transmissions from a given beam at the same power, the intra-beam interference is reduced, and hence capacity is improved.

Assuming perfect power control, uplink budget analysis shows that I_{up} in equation (3.12) reduces by 38 % for the link example given in Section 3.4.1.2. This results in an excess margin of 4.4 dB for 85 users per beam, which is a 1.1 dB increase as compared to the no power control scheme. Uplink capacity with perfect power control is also shown in Figure 3.9. Results show that with perfect power control, the uplink performance curve approaches that of the worst-case downlink performance for the cases where there are more than 100 users per beam. Downlink performance, however, can be improved by increasing satellite transmitted power, if necessary. Using Figure 3.9, it is found that by employing perfect power control, the system capacity increases to 120 users per beam for the minimum required margin of 3.3 dB. This is a 41% increase in capacity compared with the no power control scheme. The disadvantage of the power control scheme is that it is difficult to implement and that all users will operate at the same SINR on the uplink, and hence, just meet the minimum margin requirement. Therefore, users located inside the beams will no longer benefit from high SINRs. Maintaining a high excess margin is important since in satellite communications other losses due to implementation and shadowing may occur.

All results discussed so far were for users 22 and 32 (Figure 3.7) for uplink and downlink, respectively. These are worst-case locations amongst users on or inside the beam borders. In order to investigate the system performance for users in different parts of the coverage area, thirty-six southern Canada locations for the desired user have been chosen and shown in Figure 3.7. The number of active users is assumed to be 85 per beam and no power control is implemented on the uplink. For each designated location, a separate link budget analysis is performed. To analyze the results, the users in the locations shown in Figure 3.7 can be divided into 3 main groups.

A) Users inside the 3 dB beamwidth of at least one beam.

B) Users on or just inside the beam borders.

C) Users inside the coverage area, but not within any of the beams.

Table 3.7 shows Excess link margins for groups A, B, and C. Users in locations 1 to 20 belong to group A, 21 to 32 belong to group B, and 33 to 36 belong to group C. Results show that downlink performance for all user locations is above the minimum required SINR. As can be seen, users in group A have the best performance, since they benefit from higher satellite antenna gain. Users in group B perform at or just above the minimum required margin on the uplink and are therefore supported by the system. Users in group C, however, have excess margins well below the recommended amount on the uplink and cannot be supported by the system. It will be shown in Chapter 5 that with beamforming, users in group C can also be supported by the system and an overall improvement for all users can be obtained.

3.4.2 Capacity Improvement for a System Bandwidth of 9.8 MHz

As discussed in the previous section, although most users in the system operate at above the recommended SINRs, the number of active users cannot be increased due to the poor performance of the geographically disadvantaged users. For uplink and downlink, the worst-case locations are the beam borders, where the uplink and downlink satellite antenna gains are 3 dB below the peak value. On the downlink, users located at the beam crossings suffer from severe interference produced by signals intended for users in the neighbouring beam. This interference could be as much as 51% of the total interference as in the case of user 32 (discussed in Section 3.4.1.1). For the uplink, assuming that users are uniformly distributed, the interference caused by users in the neighbouring beams remains constant, regardless of the desired user's location. On both uplink and downlink, inter-beam interference is mainly due to the users in the immediate neighbouring beams of the desired user. In the case discussed in Section 3.4.1.1 where feed (3) was allocated to the desired users (Figure 3.7), about 98% of the total downlink inter-beam interference came from the users in beams (2) and (4). One way to reduce the inter-beam interference is to implement a beam frequency reuse scheme, where two sets of carrier frequencies are used on each link,

(A) User no.	Excess margin (dB)	
	Uplink	Downlink
1	6.75	7.15
2	6.76	7.52
3	5.73	7.40
4	6.56	7.53
5	6.20	7.46
6	6.24	7.15
7	6.03	7.32
8	5.69	7.35
9	6.56	7.41
10	5.84	7.10
11	5.00	6.90
12	6.83	7.13
13	6.68	7.56
14	6.33	7.31
15	5.72	6.99
16	5.54	6.60
17	5.45	6.45
18	5.95	6.75
19	5.65	7.22
20	6.05	6.90

Table 3.7: (a) Excess Margin for the Desired User - Number of users per beam=85 Users inside 3 dB beamwidth of at least one beam.

(B) User no.	Excess margin (dB)	
	Uplink	Downlink
21	3.42	5.73
22	3.30	4.72
23	4.53	6.95
24	3.78	5.51
25	3.55	6.07
26	3.71	5.12
27	4.90	5.63
28	3.75	4.98
29	4.22	6.65
30	4.53	6.95
31	4.74	5.94
32	3.94	4.65

Table 3.7: (b) Excess Margin for the Desired User - Number of users per beam=85 Users on or just inside the beam borders.

(C) User no.	Excess margin (dB)	
	Uplink	Downlink
33	2.16	4.54
34	2.55	4.61
35	2.29	4.83
36	2.70	4.45

Table 3.7: (c) Excess Margin for the Desired User - Number of users per beam=85 Users outside of the beams.

such that no two neighbouring beams have the same carrier frequencies. Therefore, beams (1), (3), and (4) will operate at the same carrier frequency and beams (2) and (4) will operate at a carrier frequency different from the other three beams. In this CDMA/FDMA system, interference from the immediate neighbouring beams of the desired user is eliminated, and hence system capacity is improved. Since two sets of carrier frequencies are used on each link, the overall system bandwidth increases to 9.8 MHz per link. This is twice the bandwidth used by the CDMA system described in the previous sections. Therefore, in order to compare this CDMA/FDMA system to a CDMA system with no frequency reuse, a 9.8 MHZ CDMA system is considered. The 9.8 MHz CDMA system model is similar to that of the 4.9 Mhz, except that on the downlink there are 512 Walsh codes as opposed to 256, and on the uplink the long code frequency is 9.8 MHz. Each Walsh code consists of 512 chips, and hence a Walsh chip is 512 times smaller than the data symbol duration on the downlink.

Link analysis was performed for the CDMA/FDMA and the 9.8 MHz CDMA systems. Figure 3.10 shows the excess link margin plotted versus the number of active users for both systems. Similar to the results given in Section 3.4.1, users 32 and 22 were used as worst-case scenarios amongst the users on or inside the beam borders for downlink and uplink, respectively. As can be seen, both systems produce the same received SINR on the downlink for user 32. Compared with the 4.9 Mhz CDMA system capacity shown in Figure 3.9, the maximum allowable number of active users on the downlink is almost doubled on average. For example, for a minimum of 3.3 dB extra margin, capacity will increase from 125 to 240 users per beam on the downlink. On the uplink, however, the 9.8 MHz CDMA system is superior to the CDMA/FDMA system, where, for a minimum requirement of 3.3 dB margin, the capacity becomes 165 compared with 115 users per beam in the CDMA/FDMA system. Referring to Figure 3.9, the CDMA/FDMA system still provides an improvement of about 30 users per beam for the same link margin compared with the 4.9 MHz CDMA system. Therefore, the uplink capacity is improved by 35% and 100% employing the CDMA/FDMA and the 9.8 MHz CDMA systems, respectively. For the

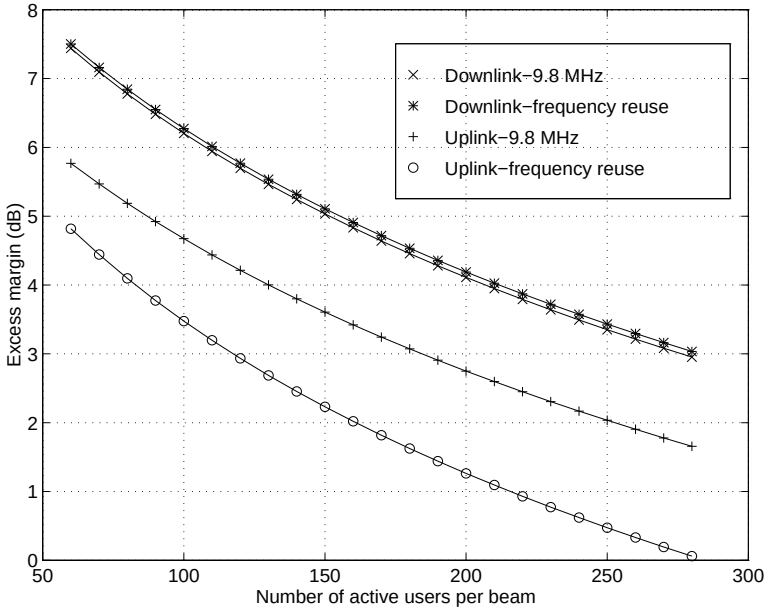

Figure 3.10: Excess Margin vs Uplink and Downlink Capacity (9.8 MHz)

CDMA/FDMA system, the uplink improvement is 75% lower than that of the downlink. This can be explained by the fact that the neighbouring beams only account for 22% of the total interference compared with 51% on the downlink. Consequently, just eliminating the 22% will not result in a substantial improvement. Therefore, to improve capacity, increasing CDMA bandwidth has proven to be more effective than employing the CDMA/FDMA scheme introduced. A disadvantage with the 9.8 MHz CDMA is implementation complexity since at high chip rates, tasks such as synchronization and despreading will be more difficult to accomplish.

As discussed earlier, system capacity is dictated by the performance of the worst-case user in the system, which in this case is user 32 on the downlink as shown in Figure 3.7. Figure 3.10 shows that the downlink performance for both systems is almost identical for this user. This will not be true, however, for users in locations other than the beam borders. For example, for user 2 located at the centre of beam (3) (Figure 3.7), only 7% of the total downlink interference is from the two neighbouring beams. Therefore, the CDMA/FDMA system is not expected to provide a significant improvement. In Table 3.8, excess margins for all three systems are compared for this

System	Excess Margin (dB)	
	Downlink	Uplink
4.9 MHz CDMA	7.5	6.8
9.8 MHz CDMA/FDMA	7.7	7.4
9.8 MHz CDMA	9.5	8.5

Table 3.8: Excess Margins for User 2 in the Coverage Area

user. The number of active users per beam is assumed to be 85.

The gap between the excess margins in the 9.8 MHz CDMA system and the CDMA/FDMA system on the uplink for user 2 is similar to that obtained for user 22 as shown in Figure 3.10 (85 users). This is since the inter-beam interference contribution to the total received interference is almost identical for feeds (2) and (3). All three excess margins for user 2 are higher than their counterparts for users 22 and 32, since the received signal power is increased due to the user being at the centre of the beam. As expected, the frequency reuse scheme is unable to improve the downlink performance for user 2 since, in this case, the intra-beam interference is the dominant source of interference. Therefore, the CDMA/FDMA system cannot duplicate the improvement obtained by the CDMA-only system for users located in areas other than at the beam borders, and hence is inferior to the CDMA system of equal bandwidth on both the uplink and downlink.

Chapter 4

Non-Coherent Uplink Receiver

4.1 Introduction

In the IS-95 scheme, it is not feasible to establish a pilot signal from each user to the base station. Therefore, base stations perform non-coherent demodulation of the received signals [19]. As mentioned in Chapter 2, IS-95 employs a 64-ary orthogonal modulation technique using Walsh symbols on the uplink. Since maximum likelihood detection is used for m-ary orthogonal demodulation, the soft-decision decoding scheme used for systems employing BPSK modulation described in Chapter 3 cannot be implemented here [25] [4]. The coherent uplink receiver has already been discussed in Chapter 3. In this chapter, non-coherent receiver performance on board the satellite is investigated, and a soft-decision decoding technique is introduced. The hard-decision decoding performance is also discussed and compared with that of the soft-decision decoding.

This chapter is organized as follows. Section 4.2 describes the uplink transmitter. The uplink non-coherent receiver employing hard-decision decoding is described in Section 4.3, and Section 4.4 discusses the structure and performance of the non-coherent receiver employing soft-decision decoding.

4.2 Uplink Transmitter

Similar to the coherent system discussed in Chapter 3, signals are transmitted asynchronously on the uplink. Therefore the masking technique employing orthogonal Walsh codes on the downlink is not able to provide user isolation if used on the uplink: mutual code orthogonality is not maintained due to phase offsets between Walsh symbols. The uplink transmission scheme adopted here is based on the IS-95 standard [19]. On the uplink, data is convolutionally encoded using a rate 1/3 code of constraint length 9. The encoded information is grouped in six bits at a time to form symbol groups or code-words. Each of these code-words is mapped onto one of the 64 different orthogonal Walsh symbols. Therefore, Walsh symbols are determined by the information being transmitted, where each Walsh symbol represents two data bits (six data symbols). The resulting Walsh symbols are then combined with a long ($2^{41} - 1$ chips) PN code designated to the user. The long codes provide mutual code orthogonality between uplink users. Since data is transmitted at 9600 bps, the Walsh chip frequency becomes 307.2 kHz. Finally, the long code chip frequency is set equal to 16 times that of Walsh symbols, in order to obtain a system bandwidth of 4.9152 MHz.

4.3 Uplink Receiver with Hard Decision Decoding

The uplink receiver implements maximum likelihood detection to demodulate the desired signal. Assuming that the desired user is at $i = 1$, the receiver block diagram is shown in Figure 4.1, where $R(t)$ is the total received signal, with complex representation given by

$$R(t) = \sum_{i=1}^{M} s_i(t - \tau_i) + N(t) \tag{4.1}$$

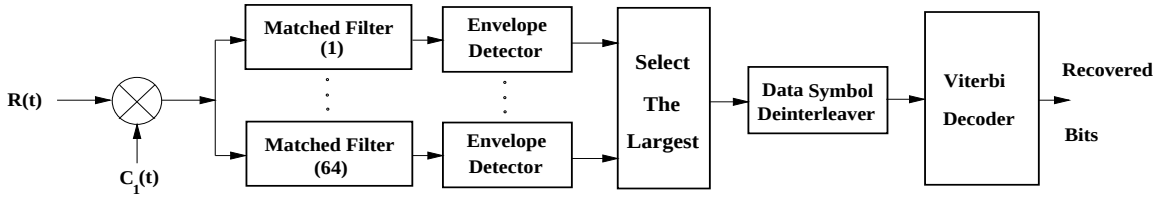

Figure 4.1: Hard-Decision Decoding Non-Coherent Receiver

where M is the total number of active users, $N(t)$ is the additive white Gaussian noise with zero mean and autocorrelation function given by

$$E\{N(t)N^*(p)\} = 2N_o\delta(t-p) \tag{4.2}$$

where $N_\circ$ is the noise spectral density. In (4.1), τ_i is the path delay for the i^{th} user, and $s_i(t)$ is given by

$$s_i(t) = \alpha\sqrt{2P_i}W_m(t)c_i(t) \tag{4.3}$$

where α is the attenuation factor due to Rician fading, W_m is the m^{th} Walsh symbol (m=1,...,64), and $c_i(t)$ and P_i are the long PN code and signal power for the i^{th} user. For analysis, the general non-coherent signaling model from [38] is used which can be applied to the Walsh codes introduced in the IS-95 standard [19]. Long code chips for the i^{th} user can be represented by $c_i(t)$ where

$$c_i(t) = u_c(t)e^{(j\phi i)} \tag{4.4}$$

where $\phi_i = 0$ or π and $u_c(t)$ is a square pulse with unit magnitude and duration T_c. Since ϕ_i can either be 0 or π, $c_i^*(t) = c_i(t)$.

As shown in Figure 4.1, the signal is first despread with the desired user's long code and next the outputs of the 64 matched filters (correlators) are compared. Each filter is matched to one of the Walsh symbols. According to the maximum likelihood detection technique [38], the symbol corresponding to the matched filter with the highest output is chosen as the detected symbol. The detected Walsh symbol is then mapped back to its designated code-word. Each code-word consists of six data symbols. These data symbols are then sent to the Viterbi decoder [29]. It should be

noted that data symbol quantization cannot take place at this point, since the data symbols are binary digits, *i.e.*, are either 1's or 0's. Therefore, the decoder implements hard-decision decoding to recover the data.

From Figure 4.1, assuming perfect synchronization, the output of the envelope detector for the correlator matched to the Walsh symbol W_m can be written as [38]

$$U_m = \left| \int_0^{T_w} R(t) c_1(t) W_m^*(t) dt \right|^2 \tag{4.5}$$

where $R(t)$ is given by (4.1), and $T_w = 2T_b$ is the Walsh symbol duration, with T_b being the data bit duration. In the above, path delay for the desired user is assumed to be zero with no loss of generality. At this point, there are two possibilities:

I) The transmitted symbol is W_m, or

II) The transmitted symbol is not W_m.

Assuming that an arbitrary Walsh symbol W_j is transmitted, from (4.1), (4.3) and (4.5) the output of the envelope detector for the j^{th} matched filter can be written as

$$U_j = \left| \int_0^{T_w} \alpha\sqrt{2P_1} W_j(t) W_j^*(t) dt + \int_0^{T_w} \left(\sum_{i=2}^{M} s_i(t-\tau_i) + N(t) \right) c_1(t) W_j^*(t) \right|^2 \tag{4.6}$$

$$\tag{4.7}$$

Equation (4.7) can be written as

$$U_j = \left| \alpha\sqrt{2P_1} T_w + I_j + N_j \right|^2 \tag{4.8}$$

where

$$Ij = \sum_{i=2}^{M} \int_0^{T_w} s_i(t-\tau_i) c_1(t) W_j^*(t) dt \tag{4.9}$$

$$N_j = \int_0^{T_w} N(t) c_1(t) W_j^*(t) dt \tag{4.10}$$

In (4.8), the first term represents the desired signal, I_j represents the multiple access interference and N_j represents the thermal noise. N_j is zero mean with variance σ_N^2 given by

$$\sigma_N^2 = E\{N_j N_j^*\} = \int_0^{T_w} \int_0^{T_w} N(t) N^*(p) W_j^*(t) W_j(p) c_1(t) c_1(p) dt dp \tag{4.11}$$

Using (4.2), equation (4.11) reduces to

$$\sigma_N^2 \;=\; 2N_\circ \int_0^{T_w} W_j^*(t)W_j(t)c_1(t)c_1(t)dt \;=\; 2N_\circ T_w \tag{4.12}$$

Since the number of users is large, we can use the Central Limit Theorem to approximate I_j in (4.9) by a Gaussian distribution. From (4.9), I_j is zero-mean since Walsh symbols and the spreading codes are independent of one another and $E(c_i(t)) = 0$. Similar to (4.12), the variance of I_j can be written as

$$\sigma_I^2 \;=\; E\{I_j I_j^*\} \;=\; 2I_\circ T_w \tag{4.13}$$

where $I_\circ$ is the interference spectral density and is found using the approximation given by (3.12) in Chapter 3. Since the thermal noise is independent of interference, from (4.12) and (4.13), $I_j + N_j$ in (4.8) has a mean of zero and a variance of $2(I_\circ + N_\circ)T_w$.

As mentioned earlier, it was assumed that the transmitted Walsh symbol is W_j. Therefore, using (4.5) the output of the envelope detector for k^{th} matched filter can be written as

$$U_k \;=\; \left| \int_0^{T_w} \alpha\sqrt{2P_1} W_j(t)W_k^*(t)dt + I_k + N_k \right|^2 \tag{4.14}$$

$$\;=\; |I_k + N_k|^2 \tag{4.15}$$

where $k = 1, ..., 64$ and $k \neq j$, and I_k and N_k are given by similar equations as (4.9) and (4.10), respectively, and hence, have the same means and variances. As can be seen, the first term in (4.14) is reduced to zero due to Walsh code orthogonality, and hence, a single expression is obtained for the outputs of envelope detectors of all other matched filters not corresponding to the correct Walsh symbol in the receiver. Clearly, if no fading or noise is present in the system, U_j will always be greater than U_k, and therefore the correct decision will be made at all times. This, however, is not realistic. In [38] it is shown that the probability of Walsh symbol error as a function of data symbol energy is given by

$$P_M(e) \;=\; \sum_{n=1}^{M_s-1} (-1)^{n+1} \frac{1}{n+1} \begin{pmatrix} M-1 \\ n \end{pmatrix} e^{-nk_m\alpha^2 E_s/(n+1)N_\circ} \tag{4.16}$$

where E_s is energy per data symbol, M_s is the number of Walsh symbols, and $k_m = \log_2 M_s$. The error probability equation given above is true for any orthogonal signal set. Since each Walsh symbol contains 2 data bits or 6 data symbols (encoded), the probability of data symbol error becomes $2^{6-1}P_M(e)/2^6 - 1 = 32P_M(e)/63$ [38].

In order to obtain an expression for U_j in terms of $E_b/(N_\circ + I_\circ)$ (eqn. (4.8)), $2(N_\circ + I_\circ)T_w$ can be factored out from equations (4.8) and (4.15), and the equations can be rewritten as follows:

$$U_j = 2(N_\circ + I_\circ)T_w \left| \alpha \frac{\sqrt{P_1}T_w}{\sqrt{(N_\circ + I_\circ)T_w}} + \frac{I_j + N_j}{\sqrt{2(N_\circ + I_\circ)T_w}} \right|^2 \quad (4.17)$$

$$U_k = 2(N_\circ + I_\circ)T_w \left| \frac{I_k + N_k}{\sqrt{2(N_\circ + I_\circ)T_w}} \right|^2 \quad (4.18)$$

The above equations can be written as

$$U_j = 2(N_\circ + I_\circ)T_w \left| \alpha\sqrt{E_w/N_\circ} + x_j \right|^2 \quad (4.19)$$

$$U_k = 2(N_\circ + I_\circ)T_w \left| x_k \right|^2 \quad (4.20)$$

where $E_w = P_1 T_w = 2E_b$ is the energy per Walsh symbol, and $x_j = (I_j + N_j)/\sqrt{2(N_\circ + I_\circ)T_w}$ and $x_k = (I_k + N_k)/\sqrt{2(N_\circ + I_\circ)T_w}$. As mentioned earlier, $I_j + N_j$ and $I_k + N_k$ are Gaussian variables with means and variances of zero and $2(N_\circ + I_\circ)T_w$, respectively, therefore x_j and x_k are also Gaussian random variables with means and variances of zero and one.

Since only the relative magnitudes of the envelope detector outputs are of importance, the $2(N_\circ + I_\circ)T_w$ factor in equations (4.19) and (4.20) can be dropped. In order to evaluate U_j and U_k numerically using random number generators, from (4.19) and (4.20) it follows that

$$U_j = \left(\alpha\sqrt{E_w/(N_\circ + I_\circ)} + x_{ji} \right)^2 + x_{jq}^2 \quad (4.21)$$

$$U_k = x_{ki}^2 + x_{kq}^2 \quad (4.22)$$

where x_{ji} and x_{jq} are Gaussian variables representing the real and imaginary parts of x_j and have means and variances of zero and $1/2$, respectively [38]. Similarly, x_{ki} and x_{kq} have means and variances of zero and $1/2$, respectively.

In order to determine the non-coherent receiver performance for both AWGN and fading channel scenarios, the computer simulations written for the coherent receiver in Section 3.3.2 of Chapter 2 have been modified to implement the receiver shown in Figure 4.1. In simulations, every six data symbols are grouped as one code-word, and for each transmitted code-word, the envelope detector output U_j (eqn. (4.21)) for the matched filer corresponding to the code-word is compared to that of the other 63 filters (eqn. (4.22)). If the output of the matched filter corresponding to the transmitted symbol is higher than all the other filters, the correct data symbols are sent to the Viterbi decoder. However, if the output of any other matched filter is higher, then the code-word corresponding to that matched filter is selected and the corresponding data symbols are sent to the Viterbi decoder.

This can be illustrated by the following example. Assuming that a code-word is obtained by translating the code's binary representation to a decimal number, code-words can be numbered from 0 to 63. Assume that the six symbols arriving at the channel are 110101, this translates to code-word 53. Equation (4.21) is used to determine U_{53}, and (4.22) is used to evaluate the outputs of the other 63 envelope detectors. If U_{53} is found to be greater than all the other outputs, then the correct decision is made and 110101 is sent to the decoder. However, if an arbitrary matched filter such as $k = 23$ has the highest output, code word 23 is selected and the symbols 010111 are sent to the decoder.

In the event of an error, for each incorrect Walsh symbol potentially six incorrect data symbols in a row may be sent to the decoder. In order to combat burst-error characteristics, data symbol interleaving with an interleaving depth of $\lambda_{int} = 20$ is implemented [20]. Data symbol interleaving is implemented prior to the 64-ary orthogonal modulation in the transmitter, and deinterleaving is implemented after the maximum likelihood detector in the receiver, as shown in Figure 4.1.

Simulations were performed for AWGN and Rician fading (K=10 dB) channel scenarios for a mobile moving at a speed of 100 km/h and transmitting at a carrier frequency of 1.6 GHz. As mentioned earlier, the Rician fading simulator is described

$P(e) = 10^{-3}$	AWGN Channel	Rician Fading Channel, K=10 dB
NON-COHERENT		
Minimum Required SINR (dB)	4.24	5.14
Number of active users per beam	30	20
COHERENT		
Minimum Required SINR (dB)	0.34	1.94
Number of active users per beam	135	85

Table 4.1: Non-coherent Receiver with Hard-Decision Decoding vs. Coherent Receiver

in Section 3.3.1.2 of Chapter 3. Results show that in order to ensure a maximum probability of error of 10^{-3}, the minimum required $E_b/N_\circ + I_\circ$ for AWGN and Rician fading scenarios are 6.0 dB and 6.9 dB, respectively. In order to compare these results with those of the coherent receiver in the previous chapter, equation (3.11) of Chapter 3 is used to present results in the form of SINR requirement. Using (3.11), the minimum required SINR for AWGN and fading scenarios are found to be 4.24 dB and 5.14 dB respectively. To determine the system capacity for this non-coherent receiver, the link budget analysis described in Section 3.4.1.2 of Chapter 3 is performed. The maximum allowable number of active users per beam is found such that an excess SINR margin of 3.3 dB is maintained for all cases. Therefore the minimum recommended SINR for the non-coherent receiver becomes 7.54 dB and 8.44 dB for AWGN and fading scenarios, respectively. Link analysis shows that to meet these SINR requirements the maximum allowable number of users per beam becomes 30 and 20 for AWGN and fading scenarios, respectively. Results for the coherent and non-coherent receivers are compared in Table 4.1. Results for the coherent receiver are taken from Sections 3.3.2.2 and 3.4.1.3. As can be seen in, system capacity is significantly reduced if this non-coherent receiver system is employed on the uplink. This is due to a significant increase in the minimum SINR requirement. Therefore, if a

non-coherent scheme is to be used on the uplink, the receiver needs to be significantly improved.

4.4 Uplink Receiver with Soft Decision Decoding

Results for the non-coherent receiver in the previous section showed that the performance of the hard-decision decoder is far from satisfactory. To improve the non-coherent receiver performance, soft-decision Viterbi decoding can be implemented. As mentioned in Section 4.3, the output of the maximum likelihood detector is in digital form, so data symbols arriving at the decoder can no longer be quantized. Viterbi *et al.* in [48] have introduced a soft-decision decoding scheme in which the receiver quantizes the magnitude of the maximum matched filter output, and attaches this quantized value to the data symbols arriving at the decoder. The choice of binary metrics at the decoder is based only on the data symbols and this quantized value. The drawback in using the technique presented in [48] is that in order to perform quantization, knowledge of the received $E_b/N_\circ$ is required. This information is not usually known and is difficult to estimate. In this section, a soft-decision decoding technique is presented where knowledge of the received $E_b/N_\circ$ is not required for quantization. In this technique, instead of choosing the code-word corresponding to the matched filter with the highest output, all filter outputs are quantized and these quantized outputs are used to make decisions in the Viterbi decoder.

The probability distribution function (pdf) of a random variable y given by

$$y = (s + x_i)^2 + x_q^2 \tag{4.23}$$

where s is a constant, and x_i and x_q are Gaussian random variables with means and variances of zero and σ_x^2, respectively, is given by [38]

$$f(y) = \frac{1}{2\sigma_x^2} e^{-(s^2+y)/2\sigma_x^2} I_{zb}\left(2\alpha\sqrt{y}\frac{s}{\sigma_x^2}\right) \tag{4.24}$$

where I_{zb} is the 0th-order modified Bessel function. Using (4.24) and (4.21), the pdf of the envelope detector for the matched filter corresponding to the correct Walsh

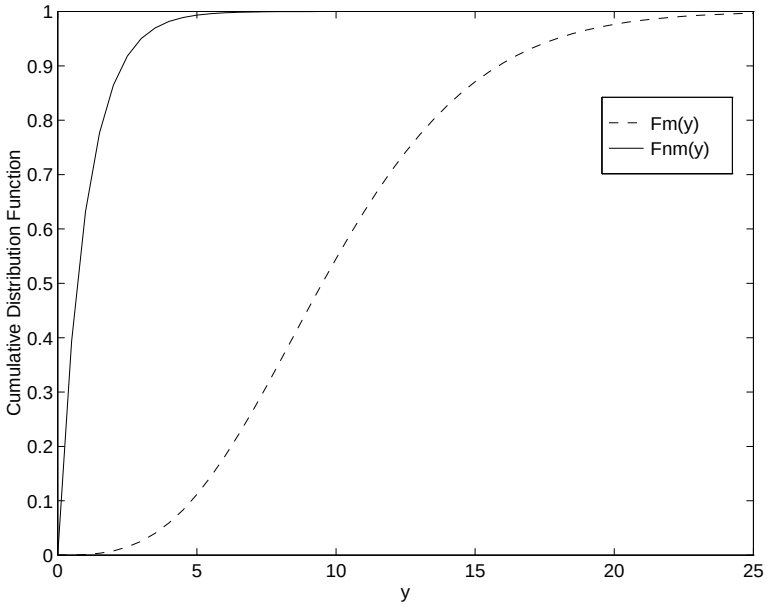

Figure 4.2: $F_m(y)$ and $F_{nm}(y)$ vs. y for $E_b/N_\circ$=6 dB

symbol can be written as

$$f_m(U_j) = e^{-(\alpha^2 E_w/N_\circ + U_j)} I_{zb}\left(2\alpha\sqrt{U_j \frac{E_w}{N_\circ}}\right) \tag{4.25}$$

Similarly, from equations (4.24) and (4.22), the probability distribution functions for the remaining 63 envelope detectors for matched filters not corresponding to the correct Walsh symbol can be written as

$$f_{nm}(U_k) = \frac{1}{2\sigma_x^2} e^{-U_k/2\sigma_x^2} = e^{-U_k} \tag{4.26}$$

since $\sigma_x^2 = 1$. As can be seen, the pdf for the matched filter corresponding to the correct Walsh symbol depends on the received $E_w/N_\circ$. However, the pdfs of other 63 matched filters in the receiver which correspond to the incorrect Walsh symbols are independent of E_w. To analyze the correlators output range, the cumulative distribution functions (cdf) for both cases are plotted in Figure 4.2 for an $E_b/N_\circ$ of 6 dB, where $F_m(y)$ and $F_{nm}(y)$ are the cdfs for the matched filter corresponding to the correct symbol and the other 63 matched filters corresponding to incorrect symbols, respectively. The plot of $F_m(y)$ approaches that of $F_{nm}(y)$ as $E_b/N_\circ$ is decreased, and

becomes identical to $F_m(y)$ if the signal energy is zero. As can be seen from Figure 4.2, the outputs of the envelope detectors for the 63 matched filters not corresponding to the correct symbol are almost entirely contained between 0 and 5. Therefore, matched filter outputs can be quantized according to the distribution given by (4.26), where the higher the output, the greater the chance that the matched filter corresponds to the correct symbol.

To perform quantization, the Lloyd-Max quantizer is used. This quantizer was chosen since it minimizes the mean-squared error between the input signal x and the quantized signal y. In [50], it is shown that the representation levels are obtained by

$$x_{k,opt} = \frac{\int_{y_{k,opt}}^{y_{k+1,opt}} y f_{nm}(y) dy}{\int_{y_{k,opt}}^{y_{k+1,opt}} f_{nm}(y) dy}, \qquad k = 1, 2, ...L \tag{4.27}$$

where $y_{k,opt}$, $k = 1, ..., L+1$ are the decision levels, $x_{k,opt}$, $k = 1, ..., L$ are the representation levels, and L is the number of levels. Since the outputs of the envelope detectors are non-negative, $y_{1,opt} = 0$. The optimum decision levels are given by [50]

$$y_{1,opt} = 0 \tag{4.28}$$

$$y_{k,opt} = \frac{1}{2}(x_{k,opt} + x_{k-1,opt}), \qquad k = 2, 3, ...L \tag{4.29}$$

$$y_{L+1,opt} = \infty \tag{4.30}$$

To perform quantization, we start with an initial guess of all representation levels. Next, using (4.29) the corresponding decision levels are calculated, and with these a new set of representation levels is computed using (4.27). The iteration is repeated until the mean-squared error is negligible. Using this method, quantization was performed for $L = 8$ and $L = 16$. The eight-level quantization scheme is shown in Table 4.2.

To aid the decoder in making soft-decisions, only the knowledge of the decision levels is of interest, since for each given interval an integer metric will be assigned. This metric assignment is on the basis of the probability of the event that the matched filter corresponds to the correct signal. Integer metrics are used instead of log likelihoods, since according to [16] the use of integers as symbol metrics instead of log

Level (k)	Decision level y_k	Output level x_k
1	0.0000	0.1753
2	0.3740	0.5725
3	0.8015	1.0305
4	1.3008	1.5712
5	1.9012	2.2313
6	2.6553	3.0792
7	3.6729	4.2665
8	5.2665	6.2556

Table 4.2: 8-Level Lloyd-Max Quantization

likelihoods will only result in a negligible performance degradation. The Log likelihood for a given interval is the log of the probability that the matched filter output lies in that interval. The quantization intervals and the assigned metrics for the eight-level quantization scheme are illustrated in Table 4.3, where y_1 to y_8 are given in Table 4.2. If the envelope detector output of a given matched filter lies in the first interval, clearly, there is not much chance that this matched filter corresponds to the correct signal, and hence the lowest metric is assigned to this interval. On the other hand, if the output lies in the last interval, there is a greater chance that the matched filter corresponds to the correct signal. This can be said since if a matched filter does not correspond to the correct signal, the probability that its output falls in the last interval is only about 0.5 %. This is shown as follows:

$$P(y > y_8) \;=\; \int_{y_8}^{\infty} e^{-y} dy \;=\; e^{-y_8} - e^{-\infty} \;=\; 0.51\ \% \tag{4.31}$$

Therefore, the higher the metric, the greater chance that the matched filter corresponds to the correct signal.

As described in [29] and [42], a Viterbi decoder works by maintaining paths of survivors and the metrics associated with them at each step in the trellis. Since

Output Interval	$y_1 \leq y < y_2$	$y_2 \leq y < y_3$	. . .	$y_7 \leq y < y_8$	$y \geq y_8$
Metric	0	1	. . .	6	7

Table 4.3: Metric Look-up Table for Eight-Level Quantization

the encoder is rate 1/3, *i.e.*, for every data bit it outputs 3 data symbols, there are two branches leaving and entering each state in the decoder trellis diagram, and each state transition results in 3 output bits. Therefore, each branch is labeled with 3 data symbols. In a conventional Viterbi decoder, as explained in [23], a metric awarded to a branch or state transition is calculated by adding the pertaining bit metrics. Each bit metric is found using the quantization look-up table by comparing the data symbol of interest (expected output) with the received data symbol (channel output). In this case there are three bit metrics, since each branch represents three data symbols. In [48], using maximum likelihood detection one Walsh symbol from the 64 possible choices is selected as the symbol most likely being transmitted. Since each Walsh symbol represents 6 data symbols, metrics can be assigned to single data symbols, and hence no change in the Viterbi decoder algorithm is necessary. Unlike the receivers discussed in [23] and [48], for the receiver introduced here the input to the decoder is not just the output of one matched filter, but all 64. Therefore, metrics are assigned to the Walsh symbols as opposed to the data symbols. Since each state transition produces 3 data symbols, 2 state transitions are required to obtain a 6 symbol code-word. Hence, for a given state four paths will be competing as opposed to two. Therefore, the Viterbi decoder needs to be adapted to proceed two steps in the trellis for each received Walsh symbol. This can be illustrated by a simple trellis diagram as shown in Figure 4.3. Here, the competing paths for state c at time t_3 are, $a-b-c$, $b-d-c$, $c-b-c$, and $d-d-c$ in the adapted Viterbi decoder. In the standard Viterbi algorithm, paths $b-c$ and $d-c$ would instead be competing. As mentioned earlier, each branch represents 3 data symbols; therefore combining the outputs of two branches will result in a six symbol code-word. For example, in

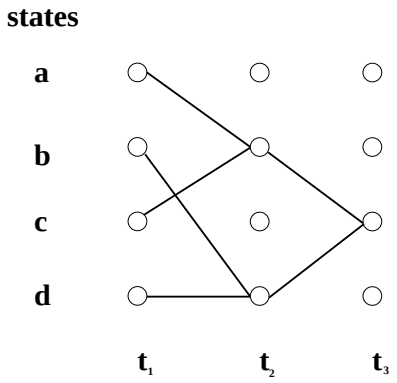

Figure 4.3: Trellis Example

Figure 4.3, assuming that the state transitions $d-d$ and $d-c$ result in outputs 100 and 101, respectively, the transition $d-d-c$ will result in 100101 which corresponds to the Walsh symbol W_{37}. Since each two-state transition (path) will correspond to one of 64 Walsh symbols, a metric can be assigned to a given path by looking at the envelope detector output of the matched filter corresponding to the Walsh symbol produced by the path, and using the quantization table given above. In this way, a low/high metric is awarded if it is less/more likely that the path under investigation has produced the transmitted Walsh symbol.

The hard-decision decoder simulation algorithm described in the previous section was modified according to the above algorithm to make soft-decisions based on the eight-level quantization scheme. Assuming that the desired user is at $i = 1$, the receiver block diagram is shown in Figure 4.4. Since the input to the decoder is the output of all 64 envelope detectors (as opposed to data symbols), Walsh symbol interleaving (as opposed to data symbol interleaving) is implemented to combat burst-error events in this system. In the transmitter, Walsh symbol interleaving takes place after the 64-ary orthogonal modulation, and in the receiver deinterleaving is implemented for each matched filter output in the receiver, as shown in Figure 4.4.

Simulations were performed for AWGN and Rician fading (K=10 dB) channel scenarios for a mobile moving at a speed of 100 km/h and transmitting at a carrier frequency of 1.6 GHz. Walsh symbol interleaving with an interleaving depth of

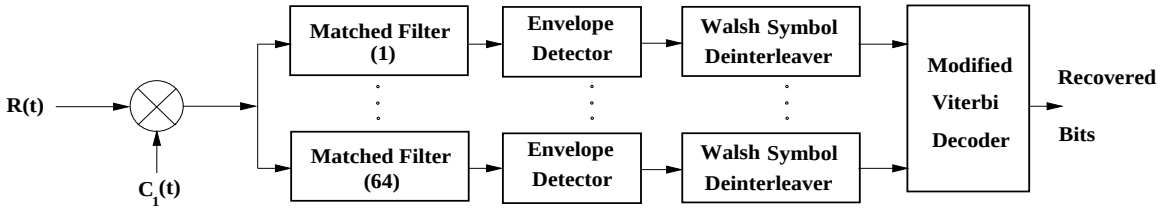

Figure 4.4: Soft-Decision Decoding Non-Coherent Receiver

$\lambda_{int} = 20$ was used. Results show that in order to ensure a maximum probability of error of 10^{-3}, the minimum required $E_b/N_\circ + I_\circ$ for AWGN and Rician fading scenarios are 4.0 dB and 4.6 dB, respectively. Simulations were also performed for a receiver employing 16-level quantization, and no significant improvement was observed. To compare the above results with those of the coherent receiver in the previous Chapter, equation (3.11) of Chapter 3 is used to present results in the form of SINR requirement. In order to determine the system capacity for this non-coherent receiver, the link budget analysis described in Section 3.4.1.2 of Chapter 3 is performed. The maximum allowable number of active users per beam is found such that an excess SINR margin of 3.3 dB is maintained for all cases. Therefore the minimum recommended SINR for the non-coherent receiver becomes 5.54 dB and 6.14 dB for AWGN and fading scenarios, respectively. Link analysis shows that to meet these SINR requirements the maximum allowable number of users per beam becomes 70 and 60 for AWGN and fading scenarios, respectively. Results are shown in Table 4.4.

By comparing Tables 4.4 and 4.1, it is clear that for the non-coherent system soft-decision decoding has provided a significant improvement as compared with hard-decision decoding. Soft-decision decoding decoding is expected to be superior to hard-decision decoding by about 2.0 dB [16]. Here, hard-decision decoding in AWGN and fading scenarios is inferior to soft-decision decoding by 2.0 dB and 2.3 dB respectively. Employing non-coherent demodulation with soft-decision decoding on the uplink will allow up to 60 simultaneous users per beam in a fading environment. This is 40 users more than the allowable number of users per beam for a non-coherent system that employs hard-decision decoding and only 25 users less than the maximum

$P(e) = 10^{-3}$	AWGN Channel	Rician Fading Channel, K=10 dB
Minimum Required SINR (dB)	2.24	2.84
Number of active users per beam	70	60

Table 4.4: Non-coherent Receiver with Soft-Decision Decoding

allowable number of simultaneous users per beam for a coherent system, as shown in Table 4.1. Therefore, if this soft-decision decoding technique is used, it will be feasible to implement non-coherent demodulation on the uplink for the satellite system. In a recent issue of *IEEE Transactions on Communications* a similar soft-decision decoding scheme was proposed [5]. The only difference in the scheme presented in [5] is that the envelope detector outputs are not quantized and are instead directly used as metrics in the Viterbi decoder. In the scheme presented here, however, the envelope detector outputs are quantized and are assigned integer metrics in the decoder. Results documented in [5] confirm our finding for the minimum $E_b/N_\circ$ requirement to ensure a maximum bit probability of error of 10^{-3} over an AWGN channel .

Chapter 5

Satellite Beamforming Receiver

5.1 Introduction

In this chapter, an on-board satellite beamforming technique is presented to improve the system performance and capacity of the mobile to satellite link of the system described in Chapter 3. Spatial processing with antenna arrays is used to implement optimum beamforming. This Chapter is organized as follows. Section 5.2 describes the satellite antenna array arrangement. In Section 5.3, the beamforming receiver structure is described and an expression for its SINR is found. In Section 5.4, the SINR expression for the non-beamforming receiver is found using the method demonstrated in Section 5.3. Finally, in Section 5.5, simulation results for various scenarios are presented, and non-beamforming and beamforming receivers are compared. In all receivers, coherent reception is assumed. In this chapter, the notation T specifies the transpose, $*$ indicates the conjugate, and $\dagger$ refers to the conjugate transpose of the matrices and vectors.

5.2 Satellite Antenna Array

The use of antenna arrays to improve cellular CDMA system capacity has been suggested in the literature [49] [45]. In the cellular case, as found in terrestrial radio, the arrays usually consist of simple omni-directional antennas arranged in circular or

linear configurations at the base station. All techniques take advantage of the element spacings and phase differences induced by the incident signals on the elements. In satellite antennas with reflectors on board, feed placements determine the direction of the projection of the spotbeams and thus the coverage area. As discussed in Chapter 3, usually the feed placements are determined such that their beam footprints on earth intersect at their 3 dB below maximum gain borders. In addition, a very small feed displacement will affect the spot beam arrangement. Therefore, rearranging feed placements will have significant impact on the system.

In contrast to simple antennas, the phase of the voltage induced by an incident signal on the feed of a reflector antenna, does not readily correspond to the signal's direction of arrival. Relative phase differences between feeds on the antenna become irrelevant since the incident plane waves (from a user) reflected by different portions of the reflector arrive with different phases at a given feed. This degrades the reflector antenna's ability to coherently focus the desired wavefront, as it is only when the feed is at the focal point that the desired signal can be coherently focused. Therefore, if the feed is placed at the focal point of the parabolic reflector, the complex electric field will only consist of a real part. However, if the feed is placed at any other position, the induced field at the feed will have both real and imaginary parts. Depending on the user's location, the received electric field magnitude and the phase will vary, and this information can be used to distinguish between distantly located users. Due to the focussing arrangement, the imaginary part of the signal is much smaller than the real part, however, the imaginary part increases as the feed moves further away from the focus. Although, as explained in Chapters 2 and 3, the cost in phase discrimination is borne by a loss in the general beam shape and a peak gain loss.

In the five beam arrangement introduced in Chapter 3, each feed was responsible for projecting one spot beam and supporting users within its own 3 dB beamwidth. In order to take advantage of the complex electric field, all five feed readings can be taken into consideration and stored in an array. Without changing the feed placements given in Table 3.4 of Chapter 3, the overall received signal can be written using complex

bandpass representation, as follows:

$$\begin{aligned} x(t) &= (x_1(t), x_2(t), ..., x_L(t)))^T && (5.1) \\ &= \sum_{i=1}^{M} \sqrt{2} c_i(t-\tau_i) b_i(t-\tau_i) e^{j\theta_i} (\sqrt{P_i^{(1)}} A_i^{(1)}, \sqrt{P_i^{(2)}} A_i^{(2)}, ..., \sqrt{P_i^{(L)}} A_i^{(L)})^T \\ &\quad + n_v(t) && (5.2) \end{aligned}$$

where L is the number of feeds on board the satellite antenna (equal to five in this system). The five beams are numbered as (1) to (5) from west to east as show in Figure 3.1 of Chapter 3, and $x_1(t)$ to $x_L(t)$ represent the total received signal at feeds (1) to (L) respectively, M is the total number of active users, and $b_i(t)$ and $c_i(t)$ are, respectively, the data symbol and the PN code used by the i^{th} user. The time and phase delays for the i_{th} user are given by τ_i and θ_i, respectively. The complex electric field reading of feed (n) for the i^{th} user is represented by $\sqrt{P_i^{(n)}} A_i^{(n)}$, where $P_i^{(n)}$ is the power received from the i^{th} user, and $A_i^{(n)}$ represents the phase component of the received electric field. The thermal noise vector is given by $n_v(t)$, and can be written as

$$n_v(t) = (n^{(1)}(t), n^{(2)}(t), ..., n^{(L)}(t))^T \quad (5.3)$$

where $n^{(1)}(t)$ to $n^{(L)}(t)$ represent independent white Gaussian noise terms with zero means for feeds (1) to (L) respectively. Since $E(n_v(t)) = 0$, the covariance matrix of $n_v(t)$ is given by

$$E(n_v(t) n_v^{\dagger}(t)) = 2N_o I_L \quad (5.4)$$

where N_o is the noise spectral density and I_L is the $L \times L$ identity matrix. Equation (5.2) can also be written as

$$x(t) = \sum_{i=1}^{M} \sqrt{2P_i} c_i(t-\tau_i) b_i(t-\tau_i) e^{j\theta_i} A_i + n_v(t) \quad (5.5)$$

where

$$\sqrt{P_i} = \sqrt{P_i^{(1)} + P_i^{(2)} + ... + P_i^{(L)}} \quad (5.6)$$

$$A_i = (\frac{\sqrt{P_i^{(1)}}A_i^{(1)}}{\sqrt{P_i}}, \frac{\sqrt{P_i^{(2)}}A_i^{(2)}}{\sqrt{P_i}}, ..., \frac{\sqrt{P_i^{(L)}}A_i^{(L)}}{\sqrt{P_i}})^T \quad (5.7)$$

where A_i is a $L \times 1$ complex unit vector called the *array response vector*. The received signal is now in a format that is usually associated with the more familiar cellular systems.

5.3 Narrow-Band Beamforming Receiver

Naguib and Paulraj in [34][35][43] have presented a beamforming technique to reduce co-channel interference by forming optimal beams for the desired users in a cellular CDMA system. Optimal beamforming was implemented by using the array response vector estimates of the desired signals. In the suggested method, the knowledge of the direction of arrival is not required. This method appeals to the satellite communications with reflector antennas, since the determination of the direction of arrival is difficult. In this thesis, we have adopted the general approach of [34] to improve the uplink satellite system performance. Our work differs from [34][35][43] in three fundamental ways:

1. In [34] and [35], perfect power control is assumed in the uplink for all users, and all elements at the base station receive the signal from a given user, at equal power. In our satellite model, however, the received power depends on the user's geographical location, and due to the different type of beam coverage model, power received from a given user is different for each feed on board the satellite antenna.

2. In [43], beamformer weighting is performed before despreading, whereas in our model, beamforming is performed after despreading.

3. A more accurate method, using long code properties, is presented here to approximate the signal-to-interference-noise ratio and optimum weights.

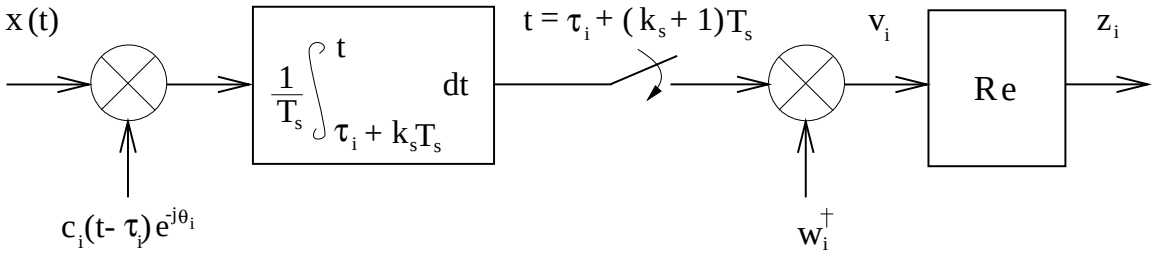

Figure 5.1: Narrow-Band Beamforming Receiver

Figure 5.1 shows the beamforming receiver block diagram for the i^{th} user. The received signal $x(t)$ is given by (5.5). In Figure 5.1, T_s is the data symbol period, k_s is the sampling index, and w_i is the $L \times 1$ complex weight vector for the i^{th} user, where

$$w_i = (w_{i1}, w_{i2}, ..., w_{iL})^T \tag{5.8}$$

The remaining parameters are as defined in Section 5.2. In the following section, the signal-to-interference-noise ratio (SINR) expression for the above receiver is found, in Section 5.3.2, the optimum weights are determined, and in Section 5.3.2.2 a sub-optimum receiver is introduced and its SINR expression is given.

5.3.1 SINR Calculation for the Beamforming Receiver

As mentioned earlier in this chapter, the uplink is assumed coherent, and the users are assumed to transmit asynchronously. Similar to IS-95, data is convolutionally encoded with a rate 1/3, $k = 9$ code and is then BPSK modulated. Data symbols for the i^{th} user can be represented by $b_i(t)$ where

$$b_i(t) = u_b(t)e^{(j\phi i)} \tag{5.9}$$

where $\phi_i = 0$ or π and $u_b(t)$ is a square pulse with unit magnitude and duration T_s. The PN code for the i^{th} user, $c_i(t)$, is also given by a similar equation, where the pulse duration is equal to T_c. The PN codes are assumed to have very long periods (e.g. 2^{41} chips). Their crosscorrelation is given by

$$E(c_i(t - \tau_i)c_j(t)) = 0 \qquad \text{where } i \neq j \tag{5.10}$$

and their autocorrelation function is given in Appendix B by (B.6).

Assuming that the desired user is at $i = 1$, we proceed to determine the received SINR. All users are assumed to be mutually uncorrelated and uncorrelated with the thermal noise. Noise samples between different feeds are also assumed to be independent. Perfect self-synchronization is assumed, and without loss of generality τ_1 and θ_1 are assumed to be zero. Therefore, from (5.5) $x(t)$ can be written as

$$x(t) = \sqrt{2P_1}c_1(t)b_1(t)A_1 + \sum_{i=2}^{M}\sqrt{2P_i}c_i(t-\tau_i)b_i(t-\tau_i)e^{j\theta_i}A_i + n_v(t) \quad (5.11)$$

In Figure (5.1), $z_1(t = T_s)$ is given by

$$z_1(T_s) = Re\left\{\frac{w_1^\dagger}{T_s}\int_0^{T_s} x(t)c_1(t)dt\right\} \quad (5.12)$$

$$= Re\left\{\frac{w_1^\dagger}{T_s}\int_0^{T_s}\sqrt{2P_1}b_1(t)\ dt + MAI + N(T_s)\right\} \quad (5.13)$$

In (5.13), the first term is the desired signal, the second term represents the multiple access interference (MAI) and the third term represents the thermal noise in the received signal. It can be shown that the first term reduces to $\sqrt{2P_1}b_1(T_s)w_1^\dagger$ and MAI and $N(T_S)$ are given by the following equations.

$$MAI = \frac{1}{T_s}\sum_{i=2}^{M}\sqrt{2P_i}\int_0^{T_s} b_i(t-\tau_i)c_i(t-\tau_i)c_1(t)w_1^\dagger w_1 e^{j\theta_i}\ dt \quad (5.14)$$

$$N(T_s) = \frac{w_1^\dagger}{T_s}\int_0^{T_s} n_v(t)c_1(t)\ dt \quad (5.15)$$

The desired signal power P_s in (5.13) is given by

$$P_s = \frac{1}{T_s}\int_0^{T_s} 2P_1|w_1^\dagger|^2 = 2P_1|w_1^\dagger|^2 \quad (5.16)$$

Since the number of users is large, we can use the Central Limit Theorem to approximate MAI in (5.13) by a Gaussian distribution. The real part of MAI, $Re\{MAI\}$, is zero-mean, since data symbols and the spreading codes are independent of one another and $E(b_i(t)) = 0$. The variance of $Re\{MAI\}$ is thus equal to $E(R_e\{MAI^2\})$ and is given by

$$\frac{1}{2}E(MAI(MAI)^\dagger) \quad (5.17)$$

$$= \frac{1}{T_s^2} E\left(\left\{\sum_{i=2}^{M}\sqrt{2P_i}\int_0^{T_s} b_i(t-\tau_i)c_i(t-\tau_i)c_1(t)(w_1^\dagger A_i)e^{j\theta_i}\ dt\right\}\right.$$
$$\left.\left\{\sum_{j=2}^{M}\sqrt{2P_j}\int_0^{T_s} b_j(p-\tau_j)c_j(p-\tau_j)c_1(p)(w_1^\dagger A_j)^\dagger e^{-j\theta_j}\ dp\right\}\right) \quad (5.18)$$

Since BPSK modulation is used, $b_i^*(t) = b_i(t)$ and $c_i^*(t) = c_i(t)$. Also, since users are independent of one another, $E(b_i(t-\tau_i)b_j(p-\tau_j)) = E(b_i(t-\tau_i))E(b_j(p-\tau_j)) = 0$ at all times, unless $i = j$. Therefore (5.18) reduces to

$$\frac{1}{T_s^2} E\left(\sum_{i=2}^{M} P_i \int_0^{T_s}\int_0^{T_s} b_i(t-\tau_i)b_i(p-\tau_i)c_i(t-\tau_i)c_i(p-\tau_i)c_1(t)c_1(p)|w_1^\dagger A_i|^2 dtdp\right) \quad (5.19)$$

Expression (5.19) can be simplified to

$$\frac{1}{T_s^2}\sum_{i=2}^{M} P_i|W_1^\dagger A_i|^2 E\{Y^2(\tau_i)\} \quad (5.20)$$

where $Y(\tau_i)$ is given by

$$Y(\tau_i) = \int_0^{T_s} b_i(t-\tau_i)c_i(t-\tau_i)c_1(t)\ dt \quad (5.21)$$

In Appendix B it is shown that as long as $T_s \gg T_c$,

$$E(Y^2(\tau_i)) \approx \frac{2}{3}T_sT_c \quad (5.22)$$

Therefore the variance of MAI in (5.19) can be written as

$$E(R_e\{MAI\}^2) = \frac{2T_c}{3T_s}\sum_{i=2}^{M} P_i|w_1^\dagger A_i|^2 \quad (5.23)$$

The thermal noise in (5.13) is given by

$$N(T_s) = \frac{(w_1)^\dagger}{T_s}\int_0^{T_s} n_v(t)c_1(t)\ dt \quad (5.24)$$

where $n_v(t)$ is given by (5.3). As mentioned earlier, the noise samples at each feed are assumed to be independent. Thus

$$E(n^{(i)}(t)(n^{(j)}(p))^\dagger) = \begin{cases} 2N_oI_L\delta(t-p) & if \quad i=j \\ 0 & \text{elsewhere} \end{cases} \quad (5.25)$$

where $\delta(t-p)$ is the Dirac delta function. The mean of $R_e\{N(T_s)\}$ is zero, since $E\{n_v(t)\} = 0$, and its variance is given by

$$E(R_e\{N(T_s)\}^2) = \frac{1}{2}E(N(T_s)N^\dagger(T_s)) \quad (5.26)$$

$$= \frac{1}{2T_s^2}\left\{\int_0^{T_s}\int_0^{T_s} w_1^\dagger n_v(t)\left(w_1^\dagger n_v(p)\right)^\dagger c_1(t)c_1(p)\ dtdp\right\} \quad (5.27)$$

Using (5.3) and (5.8) $E\left\{(w_1^\dagger n_v(t)(w_1^\dagger n_v(p))^\dagger\right\}$ can be written as

$$= E\{(w_{11}^* n^{(1)}(t) + ... + w_{1L}^* n^{(L)}(t))(w_{11}(n^{(1)}(p))^* + ... + w_{1L}(n^{(L)}(p))^*\} \quad (5.28)$$

$$= w_{11}^* w_{11} E(n^{(1)}(t)(n^{(1)}(p))^*) + ... + w_{1L}^* w_{1L} E(n^{(L)}(t)(n^{(L)}(p))^*) \quad (5.29)$$

$$= (w_{11}^* w_{11} + ... + w_{1L}^* w_{1L})E(n^{(1)}(t)(n^{(1)}(p))^*) = 2N_o\delta(t-p)(w_1^\dagger w_1) \quad (5.30)$$

since $E(n^{(i)}(t)(n^{(i)}(p))^*) = 2N_o\delta(t-p)$, for $i = 1$ to L. Hence, the equation (5.27) reduces to

$$E(R_e\{N(T_s)\}^2) = \frac{1}{2T_s^2}\int_0^{T_s} 2N_o c_1^2(t)(w_1^\dagger w_1)\ dt = \frac{N_o}{T_s}(w_1^\dagger w_1) \quad (5.31)$$

The signal-to-interference-noise ratio for the beamforming receiver is therefore given by

$$\text{SINR} = \frac{2P_1|w_1^\dagger A_1|^2}{(w_1^\dagger w_1)\frac{N_o}{T_s} + \frac{2T_c}{3T_s}\sum_{i=2}^{M} P_i|w_1^\dagger A_i|^2} \quad (5.32)$$

$$= \frac{2P_1T_s|w_1^\dagger A_1|^2}{(w_1^\dagger w_1)N_o + \frac{2}{3W_s}\sum_{i=2}^{M} P_i|w_1^\dagger A_i|^2} \quad (5.33)$$

where $W_s \equiv 1/T_c$ is defined as the CDMA system bandwidth. Taking voice activity into consideration and assuming that the desired user is transmitting, SINR can be written as

$$\text{SINR} = \frac{2P_1T_s|w_1^\dagger A_1|^2}{(w_1^\dagger w_1)N_o + \frac{2VA}{3W_s}\sum_{i=2}^{M} P_i|w_1^\dagger A_i|^2} \quad (5.34)$$

where VA is the voice activity factor and is assumed to be 40% as described in Chapter 3. To improve the system performance, it is clear that w_1 should be chosen such that SINR is maximized.

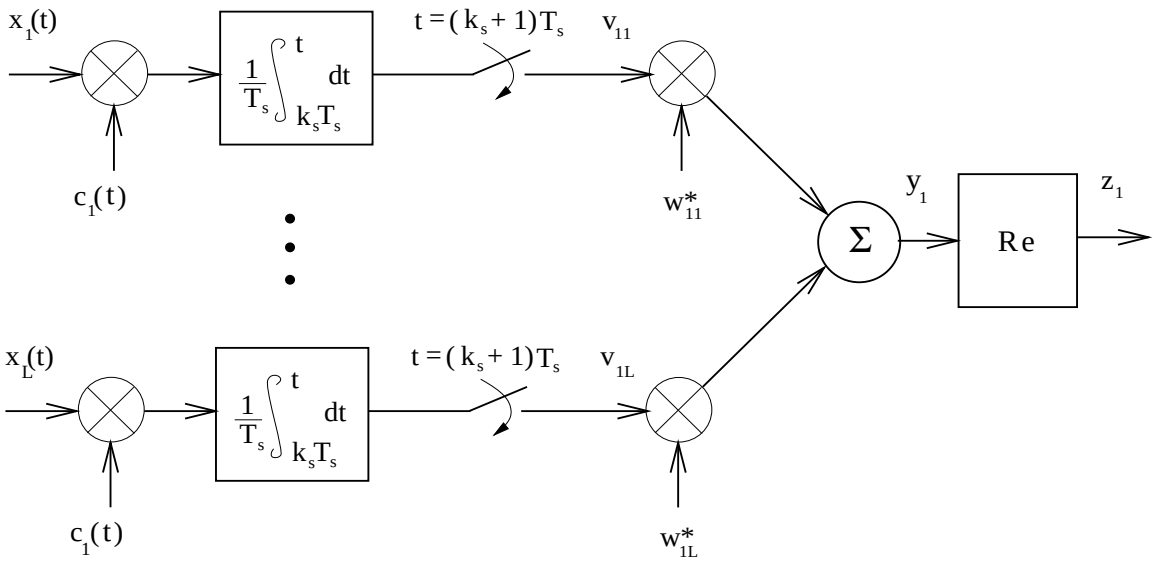

Figure 5.2: Optimum Beamforming Receiver for the Desired User

5.3.2 Determination of Optimum Weights

The weights for the desired user are obtained by maximizing the received SINR. A more detailed diagram of the receiver for the desired user at $i = 1$ is shown in Figure 5.2, where $x(t) = (x_1(t), x_2(t), ..., x_L(t))^T$ is given by (5.5). The input vector to user 1's beamforming network $v_1 = (v_{11}, v_{12}, ..., v_{1L})^T$ is given by

$$v_1 = \frac{1}{T_s}\int_0^{T_s} x(t)c_1(t)\,dt \tag{5.35}$$

Using (5.11), it can be shown that v_1 can be written as

$$\begin{aligned} v_1 &= \sqrt{2P_1}b_1(T_s)A_1 + \sum_{i=2}^{M}\frac{1}{T_s}\int_0^{T_s}\sqrt{2P_i}b_i(t-\tau_i)c_i(t-\tau_i)c_1(t)e^{-j\theta_i}A_1 dt \\ &\quad + \frac{1}{T_s}\int_0^{T_s} n_v(t)c_1(t)dt \qquad (5.36) \\ &= m_1 A_1 + Q \qquad (5.37) \end{aligned}$$

For simplicity, v_1 can be written as

$$v_1 = m_1 A_1 + Q \tag{5.38}$$

where $m_1 = \sqrt{2P_1}b_1(T_s)$, A_1 is the array response vector of the desired signal given by (5.7), and Q represents the multiple access interference and the thermal noise terms

and is given by

$$\begin{aligned} Q &= \sum_{i=2}^{M} \frac{1}{T_s} \int_0^{T_s} \sqrt{2P_i} b_i(t-\tau_i) c_i(t-\tau_i) c_1(t) e^{-j\theta_i} A_1 dt \\ &\quad + \frac{1}{T_s} \int_0^{T_s} n_v(t) c_1(t) dt \end{aligned} \tag{5.39}$$

Once again, the multiple access interference term in v_1 can be approximated by a Gaussian distribution. Thus, the combined noise-interference term Q can be approximated by a Gaussian distribution with zero mean and a covariance matrix R_{NI} given by

$$R_{NI} = E(QQ^{\dagger}) \tag{5.40}$$

As can be seen from Figure 5.2, unlike [43], beamformer weighting is performed after the signal is despread. The array output in Figure (5.2) can be written as

$$y_1 = \sum_{i=1}^{L} w_{1i}^{*} v_{1i} = w_1^{\dagger} v_1 \tag{5.41}$$

$$= w_1^{\dagger} m_1 A_1 + w_1^{\dagger} Q \tag{5.42}$$

The SINR is therefore given by

$$\text{SINR} = \frac{E|w_1^{\dagger} m_1 A_1|^2}{E|w_1^{\dagger} Q|^2} = \frac{E(m_1^2)|w_1^{\dagger} A_1|^2}{w_1^{\dagger} R_{NI} w_1} \tag{5.43}$$

The goal here is to maximize the SINR. It is shown in Pillai [47] that (5.43) is maximized if $w_1 = k_c R_{NI}^{-1} A_1$, where k_c is a constant. Since k_c does not affect the SINR, it can be set to 1. Therefore the optimum weight vector w_1 is given by

$$w_1 = (R_{NI})^{-1} A_1 \tag{5.44}$$

Hence, in order to implement optimum beamforming, the receiver should be able to estimate the array response vector of the desired signal A_1, and the noise-interference covariance matrix, R_{NI}. In Section 5.3.2.1, a new algorithm is introduced to determine these variables. Our approach is motivated by [34].

5.3.2.1 Estimating Optimum Weights

Pre-despreading and post-despreading array covariances in the optimum receiver are used to estimate the array response vectors and the required noise-interference covariance matrices. Using (5.5) since $E[x] = 0$, the pre-despreading covariance matrix R_{xx} is given by

$$R_{xx} = E[xx^{\dagger}] = E\left[\left(\sum_{i=1}^{M}\sqrt{2P_i}b_i(t-\tau_i)c_i(t-\tau_i)e^{-j\theta_i}A_i + n_v(t)\right)\right.$$
$$\left.\left(\sum_{j=1}^{M}\sqrt{2P_j}b_j(t-\tau_j)c_j(t-\tau_j)e^{j\theta_j}A_j^{\dagger} + n_v^{\dagger}(t)\right)\right] \quad (5.45)$$

Since data symbols, PN chips and noise samples are independent, and $E[b_i(t-\tau_i)b_j(t-\tau_j)] = 0$ for $i \neq j$, it can be shown that the above expression reduces to

$$R_{xx} = 2(P_1A_1A_1^{\dagger} + \sum_{i=2}^{M} 2P_iA_iA_i^{\dagger} + 2N_oI_L) \quad (5.46)$$

since $[n_v(t)n_v^{\dagger}(t)] = 2N_oI_L$.

From (5.36) since $E[v_1] = 0$, the post-despreading covariance matrix $R_{v_1v_1}$, for the desired user at $i = 1$ is given by $E[v_1v_1^{\dagger}]$. The covariance matrix is therefore given by

$$\frac{1}{2}E\left[\left(\sqrt{2P_1}b_1(T_s)A_1 + \sum_{i=2}^{M}\frac{1}{T_s}\int_0^{T_s}\sqrt{2P_i}b_i(t-\tau_i)c_i(t-\tau_i)c_1(t)e^{-j\theta_i}A_1\,dt\right.\right.$$
$$\left. + n_T(T_s)\right)\left(\sqrt{2P_1}b_1(T_s)A_1^{\dagger} + \sum_{j=2}^{M}\frac{1}{T_s}\int_0^{T_s}\sqrt{2P_j}b_j(p-\tau_j)c_j(p-\tau_j)c_1(p)\right.$$
$$\left.\left. e^{j\theta_j}A_1^{\dagger}\,dp + n_T^{\dagger}(T_s)\right)\right] \quad (5.47)$$

where $n_T(T_s) = N(T_s)/w_1^{\dagger}$ and $N(T_s)$ is given by (5.24). Following the same analysis as presented in Section 5.3.1, it can be shown that $R_{v_1v_1}$ given by (5.47) will reduce to

$$R_{v_1v_1} = 2(P_1A_1A_1^{\dagger} + \frac{2T_c}{3T_s}\sum_{i=2}^{M}P_iA_iA_i^{\dagger} + \frac{1}{T_s}I_LN_o) \quad (5.48)$$

Assuming that adequate data is available to obtain estimates for the covariance matrices R_{xx} and $R_{v_1v_1}$, (5.46) and (5.48) can be combined to form

$$T_s \hat{R}_{v_1 v_1} - \frac{2}{3} T_c \hat{R}_{xx} = 2P_1 A_1 A_1^{\dagger} (T_s - \frac{2}{3} T_c) + 2N_o (1 - \frac{2}{3} T_c) I_L \quad (5.49)$$

where $\hat{R}_{v_1 v_1}$ and $\hat{R}_{xx}$ are the estimated covariance matrices. As can be seen, the above expression eliminates the multiple access interference. For simplicity, equation (5.49) can be written as

$$T_s \hat{R}_{v_1 v_1} - \frac{2}{3} T_c \hat{R}_{xx} = B + dI_L \quad (5.50)$$

where $B = 2P_1 A_1 A_1^{\dagger}(T_s - (2/3)T_c)$ and $d = 2N_o(1 - (2/3)T_c)$. Where B is a rank 1 matrix with the eigenvector $e_1 = A_1$ and eigenvalue $d_1 = 2P_1(T_s - \frac{2}{3}T_c)$, i.e.,

$$Be_1 = \lambda_1 e_1 \quad (5.51)$$

Assuming $B + dI_L$ has eigenvectors $u_1, u_2, ..., u_L$ with eigenvalues $\xi_1, \xi_2, ..., \xi_L$, then

$$(B + dI_L)u_i = \xi_i u_i \quad (5.52)$$

where $i = 1$ to 5. Thus $Bu_i = (\xi_i - d)u_i$. From (5.51) it can be concluded that $e_1 = u_i$ and $\lambda_1 = \xi_i - d$. Therefore since B is a rank 1 matrix, $B + dI_L$ is also a rank 1 matrix. Hence, by estimating the eigenvector and eigenvalue of $T_s \hat{R}_{v_1 v_1} - \frac{2}{3} T_c \hat{R}_{xx}$, the eigenvector and eigenvalue of $2P_1 A_1 A_1^{\dagger}(T_s - (2/3)T_c)$ can be estimated. Since A_1 is equal to e_1, the desired array response vector is equal to the eigenvector of $T_s \hat{R}_{v_1 v_1} - \frac{2}{3} T_c \hat{R}_{xx}$, as long as $\hat{R}_{v_1 v_1}$ and $\hat{R}_{xx}$ are close to $R_{v_1 v_1}$ and R_{xx}, respectively. Equation (5.49) can be estimated by its closest rank 1 matrix, and hence an approximation for its eigenvalue and eigenvector can be found. Therefore,

$$T_s \hat{R}_{v_1 v_1} - \frac{2}{3} T_c \hat{R}_{xx} = \sum_{i=1}^{M} \lambda_i e_i e_i^{\dagger} \approx \lambda_1 e_1 e_1^{\dagger} \quad (5.53)$$

where λ_1 is the largest eigenvalue and e_1 is the corresponding eigenvector.

According to (5.44), in order to determine the optimum weights for the desired user, the post-despreading interference-noise covariance matrix R_{NI} must also be known. From (5.48), R_{NI} is given by

$$R_{NI} = R_{v_1 v_1} - 2P_1 A_1 A_1^{\dagger} \quad (5.54)$$

Since $R_{v_1 v_1}$ and A_1 can be estimated, the only unknown term in (5.54) remains P_1. If an accurate estimate for the noise spectral density N_o is available, P_1 can found using equation (5.49). Therefore, optimum weights for all desired users can be estimated. However, their accuracy depends on a good estimation of N_o. To summarize, the procedure for determining the optimum weight vector for the desired user is given below:

1. Post-spreading and pre-spreading covariance matrices are estimated.
2. The interference-free matrix given by (5.50) is found.
3. The array response vector A_1 for the desired user is found by estimating the eigenvector corresponding to the largest eigenvalue of (5.50).
4. P_1 is found using the equation (5.49).
5. Post-despreading interference-noise covariance R_{NI} is found using equation (5.54).
6. The optimum weight vector w_1 for the desired user, is calculated using (5.44).

A less computationally expensive method to determine the optimum weight vector is introduced in [33], where w_1 is directly found without an intermediate step to estimate A_1. In [33], the goal is to find w_1 such that the SINR given by (5.43) is maximized. It is shown that w_1 can be determined by solving for the generalized eigenvalue problem

$$R_{v_1 v_1} w = (\nu + 1) R_{NI} w \tag{5.55}$$

where $R_{v_1 v_1}$ and R_{NI} are given by (5.48) and (5.40) respectively, and ν is $SINR(w)$ given by (5.43).

5.3.2.2 Sub-optimum Receiver

As an alternative to the maximum SINR solution, w_1 can be instead set equal to A_1. In this case, from (5.34) the signal-to-interference-noise ratio becomes

$$\text{SINR} = \frac{2P_1 T_s}{N_o + \frac{2}{3W_s} \sum_{i=2}^{M} (VA) P_i |A_1^{\dagger} A_i|^2} \tag{5.56}$$

since $|A_1^{\dagger} A_1| = 1$. The weight vector was set equal to A_1, since A_1 can be estimated without the knowledge of N_o and will result in minimization of the thermal noise term in (5.34). Although A_1 will not maximize the SINR, it will nonetheless, reduce the multiple access interference term and increase the received desired signal power. From this point forward, this receiver will be referred to as the *sub-optimum* beamforming receiver. The sub-optimum beamformer corresponds to the optimum one in a cellular system, where perfect power control is assumed and users are uniformly distributed around the base station [35].

5.4 SINR Calculation for the Non-Beamforming Receiver

In order to compare SINR results for the beamforming receiver with that of the non-beamforming, derivations similar to that of Section 5.3.1 were followed to find an expression for the SINR of the coherent uplink receiver described in Chapter 3. As mentioned earlier, since the long code properties are taken into consideration, the method used in the previous section provides a more accurate approximation of SINR compared with expression (3.11) given in Chapter 3.

The receiver for the desired user at $i = 1$ is shown in Figure 5.3, where $r(t)$ is given by

$$r(t) = \sqrt{2P_1} b_1(t) c_1(t) + \sum_{i=2}^{M} \sqrt{2P_i} b_i c_i(t - \tau_i) e^{j\theta_i} + n(t) \tag{5.57}$$

where $n(t)$ is white Gaussian noise with zero mean and spectral density of $N_\circ$. The total received signal $r(t)$, in the above equation is scalar, since the user is being supported by only one of the feeds as explained in Chapter 3. All other variables are as defined in Section 5.3. Following the analysis provided in (5.3.1), it can be shown that the SINR expression for this receiver is given by

$$\text{SINR} = \frac{2P_1^{(n)} T_s}{N_o + \frac{2(VA)}{3W_s} \sum_{i=2}^{M} P_i^{(n)}} \tag{5.58}$$

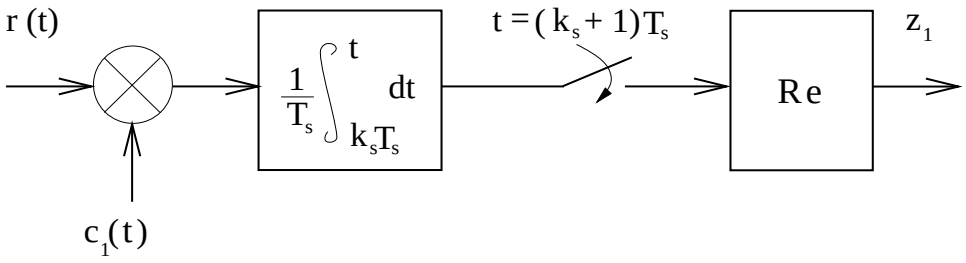

Figure 5.3: Non-Beamforming Receiver for the Desired User

where $P_1^{(n)}$ is the power received from the desired signal by the feed allocated to the signal's coverage area. Comparing (5.58) with the SINR expression by (2.12) given in Chapter 2, it is clear that the latter gives a more pessimistic approximation of the SINR, as the multiple access interference term in (5.58) is smaller by a factor of 2/3. From this point forward in this chapter, equations (5.34) and (5.58) are used for the SINR of the beamforming and non-beamforming receivers, respectively.

5.5 Simulation Results

In this section, the impact of beamforming on the performance of our mobile satellite system is investigated through simulations. The received signal-to-interference-noise ratios for various locations of the desired user in the coverage area are stated. Simulations were performed for three different user distributions in the coverage area.

I Uniform distribution. M users were assumed to be uniformly distributed in the coverage area.

II Nonuniform distribution. One-third of the M users were assumed to be uniformly distributed in selected major suburban areas. The rest of the users were uniformly distributed everywhere else in the coverage area.

III Nonuniform distribution. Similar to II, except that two-thirds of the users are concentrated in suburban areas as opposed to one-third.

For each of the above user distributions, three receiver models were compared. These models are listed below.

1. Non-beamforming receiver

2. Optimum beamforming receiver

3. Sub-optimum beamforming receiver

Section 5.5.1 describes the simulation method used to estimate the multiple access interference. Section 5.5.2 describes the results for a receiver employing the same up-link reflector antenna as described in Section 3.2.2 of Chapter 3. Finally, Section 5.5.3 provides results for a receiver with a different feed arrangement on board the reflector antenna.

5.5.1 Simulation Method

A dominant factor in the determination of SINR in CDMA systems is the multiple access interference. Multiple access interference strongly depends on the number of active users, their distribution and the location of the desired user. In order to numerically determine the SINR for the beamforming receiver, the received complex electric field from all users by all five feeds needs to be known. In the non-beamforming case, as described in Chapter 3, only the power received from all users by the feed allocated to the desired user needs to be known. For the optimum receiver, denote the multiple access interference term in the SINR in (5.34) by

$$I_b = \frac{2(\mathrm{VA})}{3W_s} \sum_{i=2}^{M} P_i |w_1^\dagger A_i|^2 \tag{5.59}$$

The received power P_i and the array response vector A_i for the i^{th} user are found using equations (5.6) and (5.7) respectively. The optimum weight vector w_1 depends on the multiple access interference and is given by (5.44). Since w_1 also appears in the desired signal and thermal noise terms in the SINR given by (5.34), these two

terms along with I_b given by (5.59) were individually approximated by their average values according to the same Monte-Carlo procedure described in Section 3.4.1.2 of Chapter 3. For the non-beamforming and sub-optimum receivers, a similar procedure was conducted. However, only their respective multiple access interference terms were approximated since the signal and the noise terms in (5.56) and (5.58) are constant.

5.5.2 Beamforming Receiver Analysis

Feed placements in this Section are similar to the original antenna system given in Table 3.4 of Chapter 3, where the feed projecting the central beam is on focus and the other four feeds are fixed on its sides. This Section is divided into two major parts. Section 5.5.2.1 describes the results for the case where all users are assumed to be uniformly distributed across the coverage area. In Section 5.5.2.2, system capacity for the three aforementioned receivers for uniform distribution case is discussed, and in Section 5.5.2.3, results are presented for both non-uniform cases described earlier.

5.5.2.1 Uniform Distribution

Referring to Figure 3.7 of Chapter 3, thirty-six locations for the desired user have been chosen to give an overview of the uplink performance across the coverage area. For each of these designated locations, a separate link budget analysis has been performed. In these results, the total number of users was chosen to be 625, i.e., approximately 125 users per beam. This number was chosen to ensure that the minimum required link margin in the non-beamforming receiver is maintained for all users within any of the 5 beams. A Rician fading channel with K=10 dB has been assumed for these simulations. According to the findings in Chapter 3, the recommended SINR to ensure a maximum probability of error of 10^{-3} is 5.25 dB, which allows a 3.3 dB safety margin. If the total number of users in this system exceed 625, some users on the beam borders will have to operate at a SINR below the recommended 5.25 dB. Similar to Chapter 3, desired user are divided into 3 main groups.

A) Users inside the 3 dB beamwidth of at least one beam.

B) Users on or just inside the beam borders.

C) Users inside the coverage area, but not within any of the beams.

Table 5.1, shows SINR results for groups A, B, and C. Users in locations 1 to 20 belong to group A, 21 to 32 belong to group B, and 33 to 36 belong to group C.

Results indicate that the optimum beamforming has produced an overall improvement in the received SINR of all selected desired users. Of particular interest are users in groups B and C. Users in group C are located outside of the main beams and do not meet the required link margin using the non-beamforming receiver. For this group, significant improvement was obtained using optimum or sub-optimum beamforming receivers. The improvement varies from 1 dB in the sub-optimum receiver for user no. 35, to 2.7 dB in the optimum receiver for user no. 36. All users in group C area can now be supported by the system, since their received SINRs are above the minimum requirement.

Users in group B are located on or just inside the beam borders, and therefore do not have comfortable link margins using the non-beamforming receiver. Once again, significant improvement is observed for the users on the borders between the neighbouring beams, using either optimum or sub-optimum beamforming receivers. The main reason for such improvement for users in groups B and C, other than the interference reduction, is the increase in the received signal power. The signal power is improved due to the power combining of all five feeds. Users between and on the borders of the neighbouring beams, further benefit from this combining compared with the users inside the beams. In the latter case, only one feed has a strong reading, due to the antenna beam isolation, whereas in the border situations, two feeds have relatively strong readings. Clearly, after combining, an increase in the received power for the users between neighbouring beams will be observed.

Performance improvement for group A users is not of great importance, since they already benefit from comfortable link margins using the non-beamforming receiver. Table 5.1 shows that the optimum receiver has nonetheless provided a general increase in the received SINR for this group. With the sub-optimum receiver, however, some

(A)	SINR (dB)		
User no.	No beamforming	Optimum beamforming	Sub-optimum beamforming
1	8.75	8.81	8.60
2	8.76	8.80	8.46
3	7.69	7.97	7.59
4	8.56	8.80	8.38
5	8.16	8.22	7.90
6	8.27	8.43	8.02
7	8.01	8.15	7.73
8	7.67	7.79	7.31
9	8.52	8.53	8.28
10	7.85	8.14	7.76
11	7.00	7.42	7.02
12	8.83	8.91	8.71
13	8.68	8.91	8.49
14	8.35	8.46	7.99
15	7.70	8.05	7.68
16	7.53	8.45	8.13
17	7.46	8.26	7.98
18	7.97	8.72	8.30
19	7.67	7.89	7.33
20	8.06	8.61	8.33

Table 5.1: SINR for the Desired User - Uniform Distribution

Users inside 3 dB beamwidth of at least one beam.

(B)	SINR (dB)		
User no.	No beamforming	Optimum beamforming	Sub-optimum beamforming
21	5.43	6.49	6.13
22	5.25	7.44	7.29
23	6.49	6.95	6.54
24	5.78	6.48	6.36
25	5.53	6.18	5.80
26	5.70	7.88	7.61
27	6.92	8.30	8.13
28	5.77	7.54	7.40
29	6.22	6.75	6.28
30	6.49	6.92	6.51
31	6.72	7.90	7.67
32	5.95	8.87	8.58

Table 5.1: SINR for the Desired User - Uniform Distribution (Cont.)

Users on or just inside the beam borders.

(C)	SINR (dB)		
User no.	No beamforming	Optimum beamforming	Sub-optimum beamforming
33	4.15	6.10	5.91
34	4.54	6.97	6.68
35	4.31	5.51	5.32
36	4.71	7.41	7.12

Table 5.1: SINR for the Desired User - Uniform Distribution (Cont.)

Users outside of the beams.

of the margins have been slightly reduced. All of the link margins in that group are still well above the minimum requirement.

Therefore using either optimum or sub-optimum CDMA beamforming receivers, significant improvement was obtained for the users on or between the borders of the adjacent beams. As described in Section 5.3.2.1, the suboptimum receiver can be more easily implemented than the optimum receiver. Using this receiver would, however, result in a loss of 0.1 to 0.5 dB in the received SINR compared with the optimum receiver. The sub-optimum receiver, however, is a satisfactory compromise , since it provides significant improvement for group B and C users, and maintains satisfactory performance for group A users. Hence, the sub-optimum receiver provides an overall satisfactory improvement and can be implemented in cases where the optimum receiver weights can not be accurately estimated.

5.5.2.2 System Capacity with a Beamforming Receiver

The system capacity was defined in Chapter 3 as the maximum number of users per beam such that an above threshold link margin is maintained by all users within the beams. Following this definition, the non-beamforming receiver, the sub-optimum receiver, and the optimum receiver have capacities of 125, 145, and 160 users per beam respectively. This however, does not accurately reflect the actual improvement of beamforming on the system performance, since many users operate well above the minimum required link margin using beamforming receivers compared with the non-beamforming receiver. It should be noted that the uplink system capacity found in Chapter 3 for the non-beamforming receiver was 85, which is lower than the 125 estimated in this chapter. As mentioned earlier, the approach used in Chapter 3 gives a more pessimistic approximation of the SINR compared with that of used in this chapter and will hence result in a lower estimate for the system capacity.

5.5.2.3 Non-Uniform Distribution

In practice, due to higher population density in the major suburban areas, more users in those areas are expected to use the system. Eight major suburban areas were selected for simulation purposes. Figure 5.4 shows these areas and the 36 locations for the desired user. Two different user distributions were investigated. Tables 5.2 and 5.3 show the SINR results for the cases where 1/3 and 2/3 of the users are in the suburban areas respectively. Similar to the uniform case, 125×5 users are assumed to be active in the system. Results show that the impact of beamforming on this system is identical to the uniform distribution case discussed in the previous Section. Performance for all users was improved using the optimum receiver, and the disadvantaged users in groups B and C benefitted from significant improvements using either of the beamforming receivers.

Comparing results in Table 5.2 with that of Table 5.1, we observe that the SINR performance of the users in beams (2), (4), and (5) have been slightly reduced in the non-uniform case. For users in beams (1) and (3), however, a slight improvement is observed. This is expected since, in beams (1) and (3) the suburban areas are close to the edge of the beams. The satellite antenna will receive signals from those users at a gain of around -3 dB of the maximum gain. Therefore, if more users are operating in those regions of each beam compared with the uniform case, the inter-beam interference will be reduced. This reduction in turn, results in an increase in the SINR. Similarly, since there is an increase in the concentration of users located away from the beam borders in beams (2), (4), and (5), an increase in the inter-beam interference for each of the beams is observed. As a result, the SINR for the users in those beams is reduced in the non-uniform distribution case. Comparing results in Tables 5.2 and 5.3, confirm the above remarks. Where, an increase in the concentration of users in the suburban areas has resulted in an increase in the SINR of the users in beams (1) and (3), and decrease in the SINR performance of the users in beams (2), (4), and (5).

(A) User no.	SINR (dB)		
	No beamforming	Optimum beamforming	Sub-optimum beamforming
1	8.48	8.52	8.25
2	9.08	9.17	8.74
3	7.71	7.96	7.62
4	8.28	8.57	8.08
5	8.18	8.22	7.94
6	7.99	8.28	7.90
7	7.92	8.11	7.67
8	7.58	7.70	7.22
9	8.54	8.55	8.33
10	8.16	8.32	7.91
11	7.32	7.85	7.38
12	8.56	8.61	8.36
13	8.40	8.68	8.20
14	8.07	8.12	7.71
15	7.61	8.05	7.65
16	7.43	8.27	8.01
17	7.78	8.32	8.04
18	7.69	8.72	8.33
19	7.39	7.63	7.13
20	8.37	9.04	8.66

Table 5.2: SINR for the Desired User - Non-uniform Distribution (1/3)

Users inside 3 dB beamwidth of at least one beam.

(B)	SINR (dB)		
User no.	No beamforming	Optimum beamforming	Sub-optimum beamforming
21	5.74	6.51	6.17
22	5.14	7.51	7.32
23	6.51	6.93	6.56
24	5.50	6.12	5.99
25	5.44	6.20	5.79
26	5.60	7.74	7.53
27	6.64	7.89	7.75
28	5.49	7.14	7.03
29	5.95	6.53	6.00
30	6.51	6.90	6.53
31	6.62	7.94	7.68
32	6.26	9.16	8.81

Table 5.2: SINR for the Desired User - Non-uniform Distribution (1/3) (Cont.)

Users on or just inside the beam borders.

(C)	SINR (dB)		
User no.	No beamforming	Optimum beamforming	Sub-optimum beamforming
33	4.05	6.16	5.94
34	4.44	6.82	6.60
35	4.03	5.11	4.95
36	5.02	7.72	7.36

Table 5.2: SINR for the Desired User - Non-uniform Distribution (1/3) (Cont.)

Users outside of the beams.

(A) User no.	SINR (dB)		
	No beamforming	Optimum beamforming	Sub-optimum beamforming
1	8.10	8.12	7.75
2	9.44	9.64	9.07
3	7.79	7.99	7.71
4	7.91	8.30	7.67
5	8.26	8.28	8.05
6	7.59	8.16	7.68
7	7.88	8.17	7.69
8	7.54	7.69	7.19
9	8.62	8.65	8.46
10	8.52	8.59	8.09
11	7.68	8.40	7.82
12	8.18	8.21	7.86
13	8.03	8.41	7.78
14	7.67	7.71	7.27
15	7.57	8.16	7.71
16	7.40	8.12	7.92
17	8.14	8.45	8.12
18	7.30	8.82	8.29
19	6.99	7.37	6.81
20	8.73	9.59	9.03

Table 5.3: SINR for the Desired User - Non-uniform Distribution (2/3)

Users inside 3 dB beamwidth of at least one beam.

(B)	SINR (dB)		
User no.	No beamforming	Optimum beamforming	Sub-optimum beamforming
21	6.10	6.58	6.21
22	5.11	7.69	7.46
23	6.59	6.95	6.64
24	5.12	5.62	5.45
25	5.40	6.34	5.88
26	5.57	7.62	7.47
27	6.24	7.31	7.21
28	5.10	6.56	6.48
29	5.57	6.29	5.63
30	6.59	6.92	6.61
31	6.59	8.11	7.79
32	6.62	9.56	9.04

Table 5.3: SINR for the Desired User - Non-uniform Distribution (2/3) (Cont.)

Users on or just inside the beam borders.

(C)	SINR (dB)		
User no.	No beamforming	Optimum beamforming	Sub-optimum beamforming
33	4.01	6.35	6.08
34	4.41	6.70	6.54
35	3.64	4.52	4.41
36	5.39	8.16	7.63

Table 5.3: SINR for the Desired User - Non-uniform Distribution (2/3) (Cont.)

Users outside of the beams.

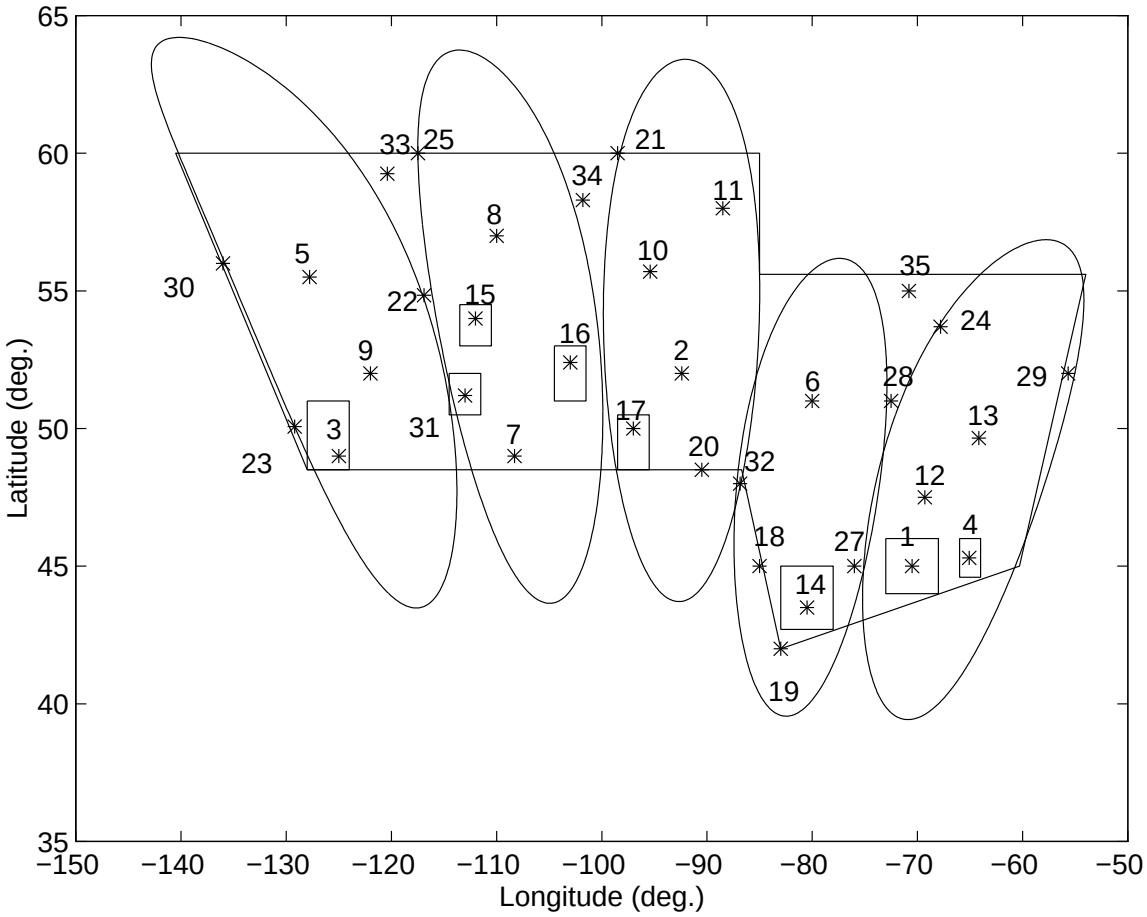

Figure 5.4: The Selected Suburban Areas in the Coverage Area
Beams are numbered (1) to (5) from left to right.

5.5.3 Shifted Feeds Arrangement

As mentioned in Section 5.2, the imaginary part of the electric field is zero if the feed is located on the focal point of the parabola. The imaginary part of the electric field reading increases as feeds move farther away from the focus. Therefore if feed placements are shifted such that none of feeds are on the focal point, and all feeds are relatively distant from the focus, the array response vectors may give more information about the location of the users. This in turn maybe useful in the beamforming receiver, which may provide more isolation between the users, and hence a reduction in multiple access interference. The drawback in moving the feed away from the focus

Coordinates	Feed no.				
	(1)	(2)	(3)	(4)	(5)
ϵ (in λ)	1.86	1.27	1.00	1.42	1.91
γ_s (deg.)	55.5	37.1	0.00	331.3	311.9

Table 5.4: Shifted Feed Coordinates

is that, there would be a loss in the general beam shape as well as the peak gain.

In order to investigate this idea, the SINR analysis was repeated for a new feed arrangement. The feed projecting the central beam was moved from the focus to $\epsilon = 1$ and $\gamma_s = 0$ on the feed plane shown in Figure 2.9 of Chapter 2. This shift was made possible by repositioning the reflector (Figure 2.5) such that the new found main beam boresight, would point towards the pre-designated centre of the central beam on earth. The coordinates of the four remaining feeds were found to satisfy the desired beam footprints using the procedure described in Section 3.2.2 of Chapter 3. The coordinates of all beam centres are given in Table 3.1 of Chapter 3. The new feed coordinates are shown in Table 5.4. Table 5.5 shows the received SINRs for the optimum beamforming, the sub-optimum beamforming, and the non-beamforming receivers. Users were assumed to be uniformly distributed in the coverage area. In order to be able to compare the results with that of the optimum beamformer in Section 5.5.2.1, the number of active users was assumed to be 625 in the system.

Results show that almost no improvement has been obtained using the new feed arrangement. Analysis show that no reduction in the multiple access interference term given by (5.59) was obtained. Other feed arrangements were also investigated and in all cases the performance either remained unchanged or depreciated compared to the original feed arrangement. The reason for the reduction in performance in some cases can be attributed to the fact that the impact of the beam shape and gain loss was stronger than the beamforming interference cancellation.

As mentioned earllier, all feeds were placed on the xy plane shown in Figure 2.5 of

Chapter 2. This plane is usually chosen since the feeds on this plane experience the least amount of phase distortion compared with any other plane. But since the phase of the received electric field is being used to isolate the users in the beamforming receiver, it may be worthwhile to investigate the system performance for cases where the feeds are on different planes.

One advantage in using the shifted feed arrangements is that the feed-blocking effects are reduced. Therefore, without resorting to the offset parabolic reflectors, the placement of the feeds can be found in such way that the projected beams would not be blocked by the feed plane on the antenna.

(A) User no.	SINR (dB)		
	No beamforming	Optimum beamforming	Sub-optimum beamforming
1	8.68	8.75	8.55
2	8.80	8.83	8.50
3	7.70	7.96	7.59
4	8.50	8.71	8.31
5	8.16	8.22	7.91
6	8.22	8.38	7.99
7	8.06	8.17	7.78
8	7.73	7.84	7.39
9	8.52	8.53	8.29
10	7.88	8.22	7.85
11	7.03	7.44	7.05
12	8.76	8.86	8.66
13	8.61	8.83	8.43
14	8.30	8.39	7.95
15	7.75	8.09	7.73
16	7.58	8.53	8.23
17	7.50	8.34	8.07
18	7.91	8.65	8.27
19	7.63	7.80	7.29
20	8.09	8.59	8.34

Table 5.5: SINR for the Desired User - Uniform Distribution

Users inside 3 dB beamwidth of at least one beam.

(B)	SINR (dB)		
User no.	No beamforming	Optimum beamforming	Sub-optimum beamforming
21	5.42	6.59	6.23
22	5.27	7.45	7.31
23	6.51	6.95	6.55
24	5.70	6.40	6.29
25	5.54	6.19	5.81
26	5.76	7.97	7.71
27	6.88	8.25	8.09
28	5.68	7.48	7.35
29	6.11	6.64	6.20
30	6.47	6.91	6.51
31	6.78	7.92	7.70
32	6.01	8.82	8.56

Table 5.5: SINR for the Desired User - Uniform Distribution (Cont.)

Users on or just inside the beam borders.

(C)	SINR (dB)		
User no.	No beamforming	Optimum beamforming	Sub-optimum beamforming
33	4.12	6.09	5.91
34	4.56	7.07	6.79
35	4.16	5.41	5.21
36	4.71	7.36	7.10

Table 5.5: SINR for the Desired User - Uniform Distribution (Cont.)

Users outside of the beams.

Chapter 6

Conclusions

In this chapter, conclusions formed in the previous chapters of this thesis are summarized and some suggestions are given for further study.

6.1 Conclusions

- A CDMA-based L-band geostationary satellite with on-board processing has been proposed to provide personal hand-held communications for users in suburban and rural areas in the southern half of Canada. Coast to coast coverage is accomplished by five spot beams. The satellite employs two multibeam reflector antennas of 8.3 and 6.7 meters in diameter for the uplink and downlink respectively. The user handsets are equipped with stub antennas of 3 dBi gain and are assumed to transmit at no more than 600 mW average power.

- When coherent demodulation on both uplink and downlink was assumed, link budget analyses showed that for a CDMA system bandwidth of 4.9 MHz, satisfactory system margins are maintained for up to a maximum of 85 and 125 simultaneous users per beam on the uplink and downlink, respectively. These results were obtained for a Rician fading environment with a K-factor of 10 dB. It was found that due to the handset's power and size limitations, uplink performance is more difficult to improve than downlink. Results showed that the

closer the user is to the centre of a spotbeam, the better are the received signal-to-interference-noise ratios on both the uplink and downlink. It was shown that the system capacity is limited by the performance of the users on the 3 dB beam borders and that the users inside the beam coverage but not within any of the beams do not meet the minimum recommended link margin and hence cannot be supported by the system. Results showed that on the uplink, intra-beam interference is much more dominant than inter-beam interference due to satellite antenna beam isolation. A hybrid CDMA/FDMA scheme with a bandwidth of 9.8 MHz was investigated and compared against a 9.8 MHz CDMA system. It was shown that the downlink capacity is the same for both systems; however, on the uplink the hybrid CDMA/FDMA system is inferior to that of CDMA.

- System performance for a non-coherent uplink scheme was investigated, and a new soft-decision Viterbi decoding scheme for the receiver was introduced. Similar to the IS-95 standard, the uplink was assumed to employ a 64-ary orthogonal modulation scheme using Walsh codes. Unlike the common maximum likelihood receiver where only the matched filter with the highest output is selected, in the proposed receiver all matched filter outputs are quantized and used in the Viterbi decoder. The Viterbi decoder was adapted to make decisions in the trellis two steps at a time as opposed to one. Using a link budget analysis, it was shown that with non-coherent uplink demodulation, the mobile-satellite system capacity in a Rician fading environment with K=10 dB will reduce from 85 to 60 users per beam. It has recently come to our attention that a similar decoding scheme with similar results appeared in a recent issue of *IEEE Transactions on Communications* [5]. The conclusions arrived at independently in this thesis agree with those of [5].

- A novel beamforming technique was proposed on the uplink. This involved adding array signal processing of multiple feeds to the uplink reflector. It was shown how to maximize beamforming network performance for each user in systems employing parabolic reflector antennas. Multi-user interference reduction

was achieved by introducing phase variation across the coverage area, traded off against signal gain maximization which is achieved by coherent focusing. It was shown that link margins are typically increased by an average of 2 dB for users in the border areas and between spot beams. Therefore, service can be provided for those users not previously supported by the system. For the beamforming analyses, a more accurate approximation for the received signal-to-interference-noise ratio was used compared to the non-beamforming case.

6.2 Suggestions for Further Research

- The beamforming technique has great potential to improve the coverage of future Ka-band systems. In this case, the improvement would be more dramatic since the beam size is smaller than in L-band systems and hence more spotbeams are required to provide the same coverage area. The antenna design algorithm given in Section 2.5 of Chapter 2 may be used to design Ka-band reflectors and hence investigate the impact of this beamforming technique on a Ka-band geostationary land-mobile satellite system.

- In this thesis, the received antenna electric field for the zero-offset reflector was used to investigate the impact of beamforming on the system performance. A study could consider the use of offset reflector electric field equations for analysis, as it gives more freedom of choice for feed locations and hence different feed arrangements such as a non-planar feed array can be investigated.

- Monte-Carlo simulations were used to determine the multiple access interference on the uplink throughout this study. A more in depth investigation is needed to determine an expression for the interference for any given user distribution in the coverage area.

- Throughout this thesis, perfect synchronization at the receiver was assumed. However, in practice this may not be attained. It has been shown that synchronization errors result in a reduction in the capacity of terrestrial CDMA systems [44]. The synchronization task in the mobile-satellite systems is an even more challenging issue than in the terrestrial systems. Due to the large distances involved, the uncertainty in the state of the received PN code is increased. Therefore, to obtain more accurate results a study can be performed where synchronization errors are taken into consideration.

Appendix A

SNR Calculation for a DS-SS System

In this appendix, the SNR for the DS-SS model disussed in Section 2.2.2.2 is calculated. Perfect synchronization and coherent demodulation are assumed. With no loss of generality, the path delay τ_i for the desired signal is assumed to be zero.

The output of the matched filter in Figure 2.2 can be written as

$$z_i = \frac{1}{T_b}\int_0^{T_b} r_i(t)c_i \cos w_o t \; dt \tag{A.1}$$

$$= \frac{2\sqrt{P_i}}{T_b}\int_0^{T_b} d_i(t)c_i(t)\cos w_o t(c_i(t)\cos w_o t)\; dt + N_i \tag{A.2}$$

where $r_i(t)$ is given by (2.3) in Chapter 2, and all other variables are described in Section 2.2.2. In (A.2), N_i is given by

$$N_i = \frac{\sqrt{2}}{T_b}\int_0^{T_b} n(t)c_i(t)\cos w_o(t)\; dt \tag{A.3}$$

It can be shown that z_i reduces to

$$z_i = \frac{1}{T_b}\int_0^{T_b} 2\sqrt{P_i}d_i(t)\cos^2 w_o t + N_i(t) = d_i(t)\sqrt{P_i} + N_i \tag{A.4}$$

where N_i represents the thermal noise and can be approximated by a zero mean Gaussian distribution with variance σ^2. The variance is given by

$$\sigma^2 = E(N_i^2) \tag{A.5}$$

$$\sigma^2 = \frac{1}{T_b^2}\int_0^{T_b}\int_0^{T_b} n(t)n(p)c_i(t)c_i(p)\cos w_o t \cos w_o p \; dtdp \tag{A.6}$$

$$\tag{A.7}$$

Since $E\{n(t)n(p)\} = \frac{N_o}{2}\delta(t-p)$, where $\delta(n-p)$ is the Dirac delta function, the above integral becomes

$$\sigma^2 = \frac{N_o}{T_b^2}\int_0^{T_b} E\{c_1^2(t)\}\{\cos^2 w_o t\}\ dt \tag{A.8}$$

$$= \frac{N_o}{2T_b} \tag{A.9}$$

Finally, the signal-to-noise ratio is given by

$$SNR = \frac{\text{signal power}}{\text{noise power}} = \frac{2P_iT_b}{N_o} = \frac{2E_b}{N_o} \tag{A.10}$$

where E_b is the received energy per data bit.

Appendix B

Evaluation of the Variance

In the following, the variance of the integral given by equation (5.22) in Chapter 5, is evaluated.

The integral, $Y(\tau_i)$ is given by

$$Y(\tau_i) = \int_0^{T_s} b_i(t-\tau_i)c_i(t-\tau_i)c_1(t)d(t) \tag{B.1}$$

The average of $Y(\tau_i)$ is zero since, data symbols and PN chips are independent and $E(b_i(t-\tau_i)) = 0$. The variance is therefore given by

$$E[Y^2(\tau_i)] = E\left\{\int_0^{T_s}\int_0^{T_s} b_i(t-\tau_i)b_i(p-\tau_i)c_i(t-\tau_i)c_i(p-\tau_i) \tag{B.2}$$

$$c_1(t)c_1(p)d(t)d(p)\Bigg\} \tag{B.3}$$

$$= \int_0^{T_s}\int_0^{T_s} E\{b_i(t-\tau_i)b_i(p-\tau_i)\}E\{c_i(t-\tau_i)c_i(p-\tau_i)\} \tag{B.4}$$

$$E\{c_1(t)c_1(p)\}d(t)d(p) \tag{B.5}$$

It is assumed that the autocorrelation function $R(\tau_i)$ for the long codes used here is given by

$$E\{c_i(t+\tau_i)c_i(t)\} = \begin{cases} 1-\frac{|\tau|}{T_c} & |\tau| \leq T_c \\ 0 & \text{elsewhere} \end{cases} \tag{B.6}$$

where T_c is the chip duration. The autocorrelation function $D(\tau_i)$ for the data symbols is also given by the above equation, where T_c is replaced by the data symbol duration

T_s. The equation (B.5) can therefore be written as

$$E[Y^2(\tau_i)] = \int_0^{T_s}\int_0^{T_s} D(t-p)R^2(t-p)dtdp \tag{B.7}$$

The Jacobian transformation can be used to evaluated the above integral. Let $k = t-p$ and $l = t+p$, the Jacobian determinant is given by

$$\frac{\partial(t,p)}{\partial(k,l)} = \begin{vmatrix} \frac{\partial t}{\partial k} & \frac{\partial t}{\partial l} \\ \frac{\partial p}{\partial k} & \frac{\partial p}{\partial l} \end{vmatrix} = \begin{vmatrix} \frac{1}{2} & \frac{1}{2} \\ -\frac{1}{2} & \frac{1}{2} \end{vmatrix} = \frac{1}{2} \tag{B.8}$$

Therefore (B.7) can be written as

$$E[Y^2(\tau_i)] = \frac{1}{2}\int_{-T_s}^{T_s} D(k)R^2(k)dk \int_k^{2T_s-k} dl \tag{B.9}$$

$$= \frac{1}{2}\int_{-T_s}^{T_s} D(k)R^2(k)(2T_s-2k)dk \tag{B.10}$$

$$= \int_{-T_s}^{T_s} D(k)R^2(k)T_s dk - \int_{-T_s}^{T_s} D(k)R^2(k)k dk \tag{B.11}$$

Using (B.6) for $R(k)$ and $D(k)$ in the above, the second integral in (B.11) will be odd and will be equal to zero. The first integral in (B.11) will be even and thus $E[Y^2(\tau_i)]$ can be written as

$$E[Y^2(\tau_i)] = 2\int_0^{T_c}(1-\frac{k}{T_s})(1-\frac{k}{T_c})^2 T_s dk \tag{B.12}$$

$$= 2(T_sT_c - \frac{1}{2}T_c^2 + \frac{1}{3}T_sT_c - \frac{1}{4}T_c^2 - T_sT_c + \frac{2}{3}T_c^2) \tag{B.13}$$

Since $T_c \ll T_s$, all terms with T_c^2 will be very small and can be neglected. Therefore,

$$E[Y^2(\tau_i)] \approx \frac{2}{3}T_sT_c. \tag{B.14}$$

References

[1] S. Arenaccio, A. Vernucci, R. Padovani, and A. Arcidiacono. "Performance, implementation & network management techniques for a european CDMA-based land-mobile satellite system". In *1990 Global Communication Conference*, pages 738–745, 1990.

[2] R. Belanger, N. Taylor, E. Bertenyi, and C. Kittiver. *MSAT Communication Payload System Overview.* American Institute of Aeronautics and Astronautics, 1993.

[3] J. Benedicto, J. Fortuny, and P. Rastrilla. "MAGSS-14: A medium-altitude global mobile satellite system for personal communications at L-band". *ESA Journal*, 16, 1992.

[4] Qi Bi. "Performance analysis of a CDMA cellular system". In *1992 IEEE Vehicular Technology Conference*, pages 43–46, 1992.

[5] L. F. Chang, F. Ling., D. D. Falconer, and N. R. Sollenberger. "Comparison of two convolutional orthogonal coding techniques for CDMA radio communications systems". *IEEE Transactions on Communications*, 43(6):2028–2037, 1995.

[6] Riccardo de Gaudenzi, carlo Elia, and Roberto Viola. "Bandlimitted quasi-synchronous CDMA: A vovel satellite access technique for mobile and personal communication systems". *IEEE Journal on Selected Areas in Communications*, 10(2):328–343, 1992.

[7] Russel J. F. Fang. "Personal handheld communications via hybris Ka- and L/S-band satellites". In *1992 Inernational Seminar Organized by Deutshce Forschungsatalt*, 1992. COMSAT Laboratories.

[8] Gilles Ferland. *Performance Analysis of Concatenated Coding Systems for Channels with Memory.* PhD thesis, Queen's University, 1992.

[9] Victor Galindo-Israel, Shung-Wu Lee, and Raj Mittra. "Synthesis of a laterally displaced cluster feed for a reflector antenna with application on multiple beams and contoured patterns". *IEEE Transactions on Antennas and Propagation*, AP-26(2):220–228, 1978.

[10] Victor Galindo-Israel and Raj Mittra. "A new series representation for the radiation integral with application to reflector antennas". *IEEE Transactions on Antennas and Propagation*, AP-25(5):631–641, 1977.

[11] A. Garcia, M. Calvo, and L. de Haro. "Design and simulation of a global system of mobile communications by satellite". In *1995 International Conference on Digital Satellite Communications*, pages 208–212, 1995.

[12] R. De Gaudenzi, C. Elia, and R. Viola. "Performance evaluation of quasi-synchronous code division multiple access (qs-cdma) for satellite mobile systms". In *1990 Global Communication Conference*, pages 1800–1804, 1990.

[13] Klein S. Gilhousen, Irwin M. Jacobs, Roberto Padovani, and Lindsay A. Weaver JR. "Increased capacity using CDMA for mobile satellite communication". *IEEE Journal on Selected Areas in Communications*, 8(4):503–514, 1990.

[14] Klein S. Gilhousen, Irwin M. Jacobs, Roberto Padovani, Andrew J. Viterbi, Jr. Lindsay A. Weaver, and Charles E. Wheatley III. "On the capacity of a cellular CDMA system". *IEEE Transactions on Vehicular Technology*, 40(2):303–312, 1991.

[15] N. Hamamoto, Y. Arimoto, Y. Hashimoto, T. Ide, and M. Sakasai. "High speed and global store and forward communication system using LEO satellites". In *1994 International Conference on Universal Personal Communications*, pages 418–422, 1994.

[16] Jerrold A. Heller and Irwin Mark Jacobs. "Viterbi decoding for satellite and space communications". *IEEE Transactions on Communications*, COM-19(5):835–848, 1971.

[17] Brima B. Ibrahim and A. Hamid Aghvami. "Direct sequence spread spectrum matched filter acquisition in frequency-selective rayleigh fading channels". *IEEE Journal on Selected Areas in Communications*, 12(5):885–890, 1994.

[18] T. Ikegami, R. Suzuki, N. Hamamoto, and N. Sato. "Experiments on a coherent matched filter receiver for spread spectrum mobile satellite communications". *IEICE Transactions*, E74(5):1130–1136, 1991.

[19] Qualcomm Inc. Mobile station-base compatibility standard for dual-mode wide-band spread system, 1993.

[20] Garrick Thomas Irvine. *Symbol-Aided Plus Decision-Direction Phase Tracking on the Shadowed Rician Fading Channel.* Master's thesis, Queen's University, 1990.

[21] Peter Jung, Paul Walter Baier, and Andreas Steil. "Advantages of CDMA and spread spectrum techniques over FDMA and TDMA in cellular mobile radio applications". *IEEE Transactions on Vehicular Technology*, 42:357–364, 1993.

[22] Joubin Karimi. *Convolutional Coding Program Notes.* Prepared for Dr. P. J. McLane, Department of Electrical and Computer Engineering, Queen's University, 1993.

[23] Joubin Karimi. *Addenda to the Convolutional Coding Program Notes.* Prepared for Dr. P. J. McLane, Department of Electrical and Computer Engineering, Queen's University, 1994.

[24] Ron W. Kerr and Vijay K. Bhargava. "4-phase DS-CDMA performance over LEOS/MEOS channels". In *1995 IEEE Pacific Rim Conference on Communications, Computers, and Signal Processing*, pages 433–436, 1995.

[25] Kyoung Il Kim. "On the error probability of a DS/SSMA system with a noncoherent m-ary orthogonal modulation". In *1992 IEEE Vehicular Technology Conference*, pages 482–485, 1992.

[26] Albert C. M. Lee and Peter J. McLane. "Convolutionally interleaved PSK and DPSK trellis codes for shadowed, fast fading mobile satellite communications channels". *IEEE Transactions on Vehicular Technology*, 39(1):37–47, 1990.

[27] Shung-Wu Lee and Yahya Rahmat-Samii. "Simple formulas for designing an offset multibeam parabolic reflector". *IEEE Transactions on Antennas and Propagation*, AP-29(3):472–478, 1981.

[28] William C. Y. Lee. *Mobile Communications Engineering.* McGraw-Hill, 1982.

[29] Shu Lin and Daniel J. Costello. *Error Control Coding: Fundamentals and Applications.* Prentice-Hall, 1983.

[30] Y. T. Lo and S. W. Lee. *Antenna Handbook.* Van Nostrand Reinhold Company, 1988.

[31] G. Maral and M. Bousquet. *Satellite Communications Systems.* John Wiley & Sons, 1993.

[32] Raj Mittra, Yahya Rahmat-Samii, Victor Galindo-Israel, and R. Norman. "An efficient technique for the computation of vector secondary patterns of offset paraboloid reflectors". *IEEE Transactions on Antennas and Propagation*, AP-27(3):294–304, 1979.

[33] Ayman F. Naguib. *Adaptive Antennas for CDMA Wireless Networks.* PhD thesis, Stanford University, 1995.

[34] Ayman F. Naguib and Arogyaswami Paulraj. "Performance of CDMA cellular networks with base-station antenna arrays". In *1994 International Zurich Seminar on Digital Communications*, 1994.

[35] Ayman F. Naguib, Arogyaswami Paulraj, and Thomas Kailath. "Capacity improvement with base-station antenna arrays in cellular CDMA". *IEEE Transactions on Vehicular Technology*, 43(3):691–698, 1994.

[36] Raymond L. Pickholtz, Donald L. Shilling, and Laurence B. Milstein. "Theory of spread-spectrum communications, a tutorial". *IEEE Transactions on Communications*, COM-30(5):855–884, 1982.

[37] Wilburn L. Pritchard, Henri G. Suyderhoud, and Robert A. Nelson. *Satellite Communication Systems Engineering.* PTR Prentice Hall, 1993.

[38] John G. Proakis. *Digital Communications.* McGraw-Hill, Inc., 1989.

[39] Stephen S. Rappaport and Donald M. Grieco. "Spread-spectrum signal acquisition: Methods and technology". *IEEE Communications Magazine*, 22(6):6–21, 1984.

[40] Allen Salmasi and Mark Epstein. CDMA common air interface (cai) standard proposed for personal communications services, 1992.

[41] D. V. Sarwate and M. B. Pursely. "Crosscorrelation properties of pseudorandom and related sequences". *Proceedings of the IEEE*, 68(5):593–619, 1980.

[42] Marvin K. Simon, Jim K. Omura, Robert A. Scholtz, and Barry K. Levitt. *Spread Spectrum Communications, Volume III.* Computer Science Press, 1985.

[43] Bruno Suard, Ayman F. Naguib, Guanghan Xu, and Arogyaswami Paulraj. "Performance of CDMA mobile communication systems using antenna arrays".

In *1993 International Conference on Acoustics, Speech, and Signal Processing*, 1993.

[44] M. O. Sunay and P. J. McLane. "Sensitivity of a DS CDMA system with long PN sequence to synchronization errors". In *1995 International Conference on Communications*, pages 1029–1035, 1995.

[45] Simon C. Swales, Mark A. Beach, David J. Edwards, and Joseph P. McGeehan. "The performance enhancement of multibeam adaptive base-station antennas for cellular land mobile radio systems". *IEEE Transactions on Vehicular Technology*, 39(1):56–67, 1990.

[46] George L. Turin. "The effects of multipath and fading on the performance of direct-sequence CDMA systems". *IEEE Journal on Selected Areas in Communications*, SAC-2(4):597–603, 1984.

[47] S. Unnikrishna. *Array Signal Processing.* Springer-Verlag, 1989.

[48] Andrew J. Viterbi, Audrey M. Viterbi, and Ephraim Zehavi. "Performance of power-controlled wideband terrestrial digital communication". *IEEE Transactions on Communications*, 41(4):559–569, 1993.

[49] Yiping Wang and J.R. Cruz. "Adaptive antenna arrays for cellular CDMA communication systems". In *1995 International Conference on Acoustics, Speech, and Signal Processing*, pages 1725–1728, 1995.

[50] John W. Woods. *Subband Image Coding.* Kluwer Academic Publishers, 1991.

[51] William W. Wu, Edward F. Miller, Wilbur L. Pritchard, and Raymond L. Pickholtz. "Mobile satellite communications". *Proceedings of the IEEE*, 82(9):1431–1448, 1994.

Vita

Joubin Karimi

EDUCATION

M.Sc. (1993–96), Electrical Engineering, Queen's University

B.Sc. (1989–93), Electrical Engineering, Queen's University

EXPERIENCE

Systems Engineer (1996), West End Systems Corp., Arnprior, ON

Research Assistant (1993-1996), Electrical & Computer Engineering, Queen's University

Teaching Assistant (1993-1995), Electrical & Computer Engineering, Queen's University

Computer Technician (Summer 1992), Technical Support Services Ltd., Kingston, ON

PUBLICATIONS

Joubin Karimi and Steven D. Blostein, "Using Array Signal Processing to Improve Rural Area Coverage in Future Personal Satellite Communication Services", submitted to *IEEE Transactions on Signal Processing*, December 1995.